AD-A083 637 HARRY DIAMOND LABS ADELPHI MD F/G 13/7
FLUERICS 40: LJARS, THE LAMINAR JET ANGULAR RATE SENSOR.(U)
DEC 79 T M DRZEWIECKI, F M MANION
UNCLASSIFIED HDL-TM-79-7 NL

1 OF 2
AD A083637

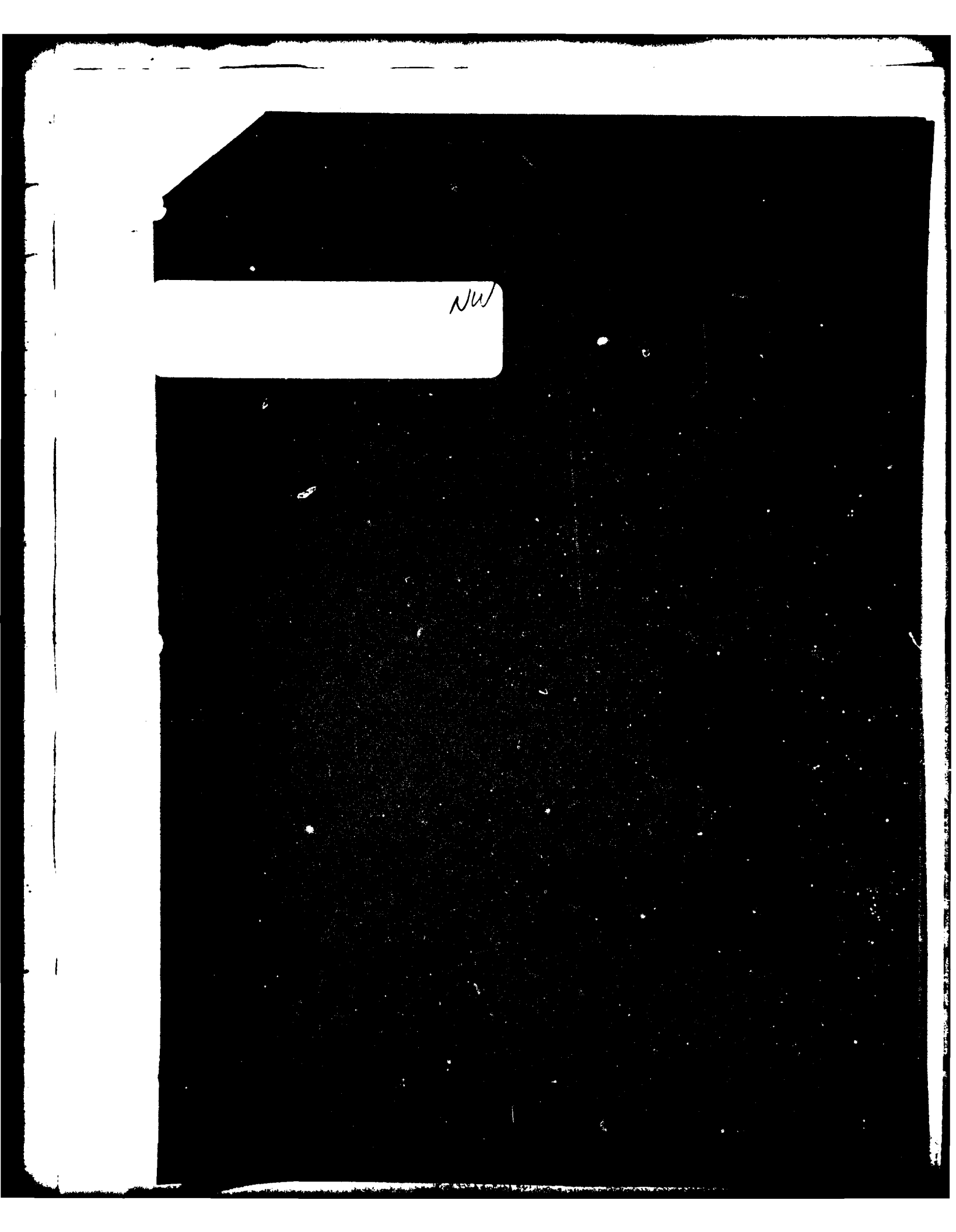
NW

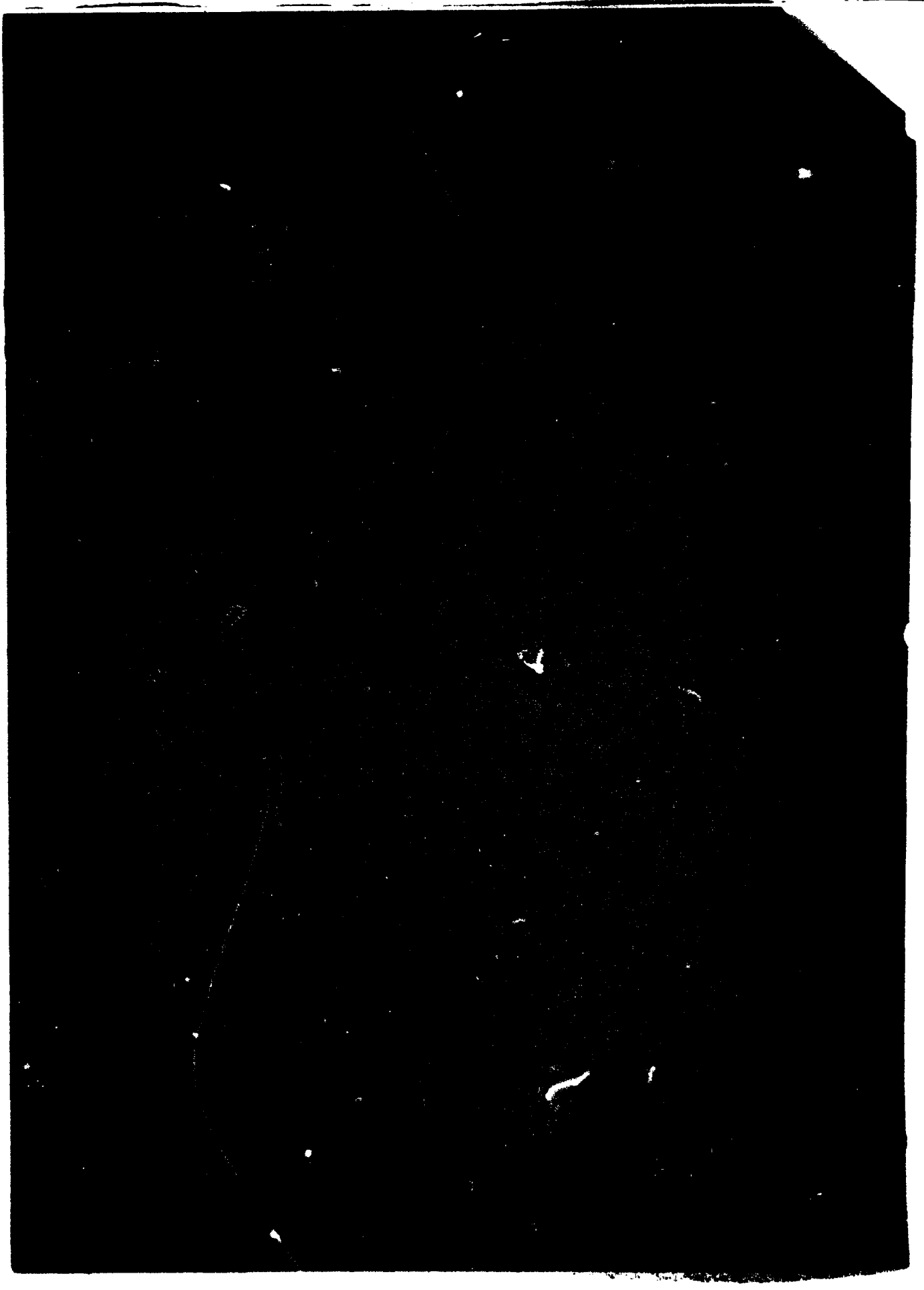

UNCLASSIFIED

SECURITY CLASSIFICATION OF THIS PAGE (When Data Entered)

REPORT DOCUMENTATION PAGE	READ INSTRUCTIONS BEFORE COMPLETING FORM
1. REPORT NUMBER: HDL-TM-79-7	2. GOVT ACCESSION NO.: AD-A083637
	3. RECIPIENT'S CATALOG NUMBER:
4. TITLE (and Subtitle): Fluerics 4: LJARS, The Laminar Jet Angular Rate Sensor	5. TYPE OF REPORT & PERIOD COVERED: Technical Memorandum
	6. PERFORMING ORG. REPORT NUMBER:
7. AUTHOR(s): Tadeusz M. Drzewiecki Francis M. Manion	8. CONTRACT OR GRANT NUMBER(s): DA: 1L161102AH44
9. PERFORMING ORGANIZATION NAME AND ADDRESS: Harry Diamond Laboratories 280 Powder Mill Road Adelphi, MD 20783	10. PROGRAM ELEMENT, PROJECT, TASK AREA & WORK UNIT NUMBERS: Program Ele: 6.11.02.A
11. CONTROLLING OFFICE NAME AND ADDRESS: U.S. Army Materiel Development & Readiness Command Alexandria, VA 22333	12. REPORT DATE: Dec 1979 13. NUMBER OF PAGES: 127
14. MONITORING AGENCY NAME & ADDRESS (if different from Controlling Office)	15. SECURITY CLASS. (of this report): Unclassified 15a. DECLASSIFICATION/DOWNGRADING SCHEDULE

16. DISTRIBUTION STATEMENT (of this Report)

Approved for public release; distribution unlimited.

17. DISTRIBUTION STATEMENT (of the abstract entered in Block 20, if different from Report)

18. SUPPLEMENTARY NOTES

HDL Project: A44934
DRCMS Code: 611102.H440011.1F-1F

19. KEY WORDS (Continue on reverse side if necessary and identify by block number)

Fluidics
Fluerics
Angular rate sensor
Inertial sensors
Rate gyroscope
Power supplies
Temperature compensation

20. ABSTRACT (Continue on reverse side if necessary and identify by block number)

This report presents an analysis and experimental data in its support for a laminar jet angular rate sensor (LJARS). An LJARS is a device in which a Coriolis force causes a jet to deflect as a function of applied angular rate. This jet deflection is sensed as a differential pressure or flow. Both the theory and the data show that the differential pressure is a linear function of applied angular rate. The report considers the fluid mechanic and fluid

DD FORM 1 JAN 73 1473 EDITION OF 1 NOV 65 IS OBSOLETE

SECURITY CLASSIFICATION OF THIS PAGE (When Data Entered)

163 050

Item 20 (Cont'd)

dynamic aspects of the device and discusses in detail such areas as jet pressure recovery, dynamic response, and transport delay. In addition, the report expands considerably on the theory by presenting numerous empirical guidelines for the design and the implementation of these devices. Included is a brief heuristic argument for the determination of the transition-to-turbulence point and methods for effecting suitable temperature and null offset compensation. Environmental temperature and pressure effects are detailed. Finally, typical LJARS characteristics are summarized and presented. The important characteristic parameters are thresholds of less than 0.1 deg/s, offsets of less than 0.5 deg/s, and sensitivities of 0.04 Pa/(deg/s). The LJARS output is easily amplified by laminar proportional amplifiers. Other desirable characteristics of the LJARS are an estimated cost of less than $100, high reliability, and instant-on performance.

FOREWORD

Since their inception in the early 1970's, the development of laminar fluidic control components has been documented almost solely with regard to the laminar proportional amplifier, yet the laminar jet angular rate sensor has been as valuable as a control component, if not more valuable. This report attempts to remedy this imbalance of technical information by compiling most of the work that has been found in laboratory notebooks of various researchers. Some data were compiled at the Harry Diamond Laboratories (HDL) by Robert Foster (formerly of HDL), Steve Tenney, Charles Paras, George Mon, and Kenji Toda; and Margaret Hackert and Kevin Hipple, former summer employees of HDL. Other data have been obtained by HDL on contract with industrial concerns: AiResearch Manufacturing Co. of Arizona; McDonnell Douglas, and TriTec, Inc. The analysis for the most part is of the authors.

It is hoped that this report will lay the technical foundation for systematic sensor design.

CONTENTS

FIGURES

FIGURES (Cont'd)

FIGURES (Cont'd)

FIGURES (Cont'd)

TABLE

1. INTRODUCTION

Fluidic angular rate sensing is older than fluidics itself. Born out of the need to replace costly and unreliable mechnical rate gyroscopes, fluidic rate sensors have carved themselves out a niche in this area. Perhaps the most familar fluidic sensor is the vortex rate sensor (VRS). This device makes use of the induced weak vortex on an inward radial flow to provide a signal as a function of applied rate.

Numerous technical papers discuss this device, but perhaps most relevant and useful are those by Ostdiek,[1] Kirshner,[2] and Hedeen.[3] The first two discuss the analytical aspects in detail, and the last describes the use of such sensors in systems. More recently, Ringwall* has described a device called the Fluidisc, which uses a flow of liquid in a helical set of passages to replace the spinning mass of a gyroscope. Rate is detected by a force balancing system on the helical flow container. This device has a moving part. Its performance is discussed by Chen and Neradka[4] in a report comparing various fluidic rate sensors.

The concept of the laminar jet angular rate sensor (LJARS)† was proposed[5] in the early 1940's, but the patents for jet angular rate sensors appeared much later (about 1970) and are held by Reader[6] and

---

[1] *A. Ostdiek, Viscous Vortex Rate Sensor, Harry Diamond Laboratories HDL-TR-1555 (November 1971).*

[2] *J. M. Kirshner, A Survey of Sensors--Part II, Proceedings of HDL Fluidic State-of-the-Art Symposium, II, Harry Diamond Laboratories (October 1974).*

[3] *J. O. Hedeen, Performance and Application of the Vortex Rate Sensor, Proceedings of HDL Fluidic State-of-the-Art Symposium, II, Harry Diamond Laboratories (October 1974).*

[4] *K. Chen and V. Neradka, Development of Critical Components, TriTec, Inc., Columbia, MD, DAAG-39-77-C-0173 (July 1978).*

[5] *H. Ziebolz, Characteristics of Hydraulic and Pneumatic Relays as Energy-Converting Devices, Instruments, 15 (September 1942).*

[6] *T. Reader, Laminar Fluidic Devices, U.S. Patent 3,662,772 (16 May 1972).*

**C. G. Ringwall, Summary Report on Single Axis Stabilization System, General Electric Co., Schenectady, NY, DAAG-39-76-C-0137 (February 1977).*

†This device is also known as LARS, for laminar angular rate sensor; however, since most high-performance vortex rate sensors also are laminar and, hence, laminar angular rate sensors, "LJARS" is used to avoid confusion.

Moore.[7] The way that this device works is that, as a jet leaves a nozzle, it tends to travel in a straight line in inertial space--yet the device structure is rotating as shown in figure 1. By the time that the particles get across the device, the structure has moved, and the jet deflection is relative to the structure. This relativity causes a pressure difference on outputs as in an LJARS or a temperature difference on thermistors as in a "Super Jet."[8] The pressure or temperature difference is related directly to angular rate.

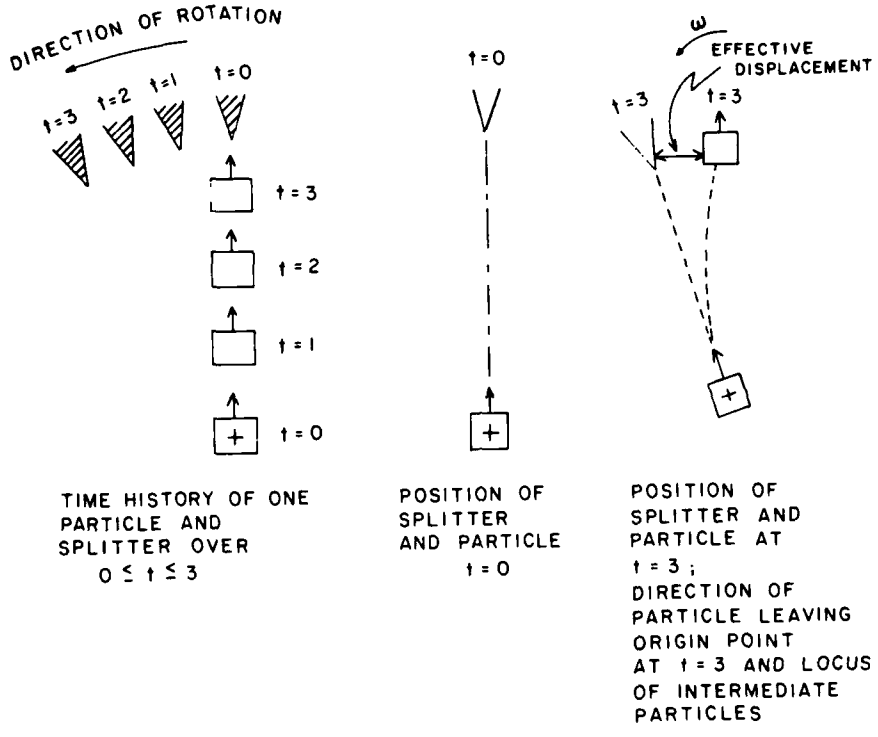

Figure 1. Coriolis jet deflection.

---

[7] *A. G. Moore, Angular Movement Sensing Device, U.S. Patent 3,500,691 (17 March 1970).*

[8] *T. M. Rankin, A. G. Moore, and W. C. Schuemann, Fluidic Angular Rate Sensor--A Replacement for Rate Gyroscopes? Johns Hopkins Applied Physics Laboratory Technical Digest (March-April 1969).*

Research on the LJARS was spurred by the limitations on the VRS, namely, the high power (or flow) consumption, the very high output impedance, and the relatively low bandwidth. The high power requirement[4] of the VRS tended to place a burden on existing power supplies, especially if hydraulic oil was used. The high output impedance effectively reduced the high sensitivity in circuits where the signal was matched to other fluidic components. Most devices exhibited output impedances one to three orders of magnitude greater than the input of a fluidic circuit; hence, the net sensitivity was decreased by the same order of magnitude. The bandwidth is limited by the time required to fill the relatively large volume of the device.

In contrast, an LJARS requires very little power to establish a rate sensitive jet, has the output impedance of a fluidic amplifier (hence, should match well), and has a bandwidth limited only by the fluid transport time across a small gap. Early attempts at analyzing and using the LJARS[9-11] led to devices shown in figure 2. A long nozzle was used because it was believed, at that time, that this length would promote a greater laminar range.[10,11] Subsequently, it was found that short nozzles appropriately designed would provide greater pressure recovery and gain in laminar amplifiers (hence, greater LJARS sensitivity) and maintain superior laminar range.[12,13] The early devices, however, did prove an important point in that they demonstrated the feasibility of laminar jet angular rate sensing and its advantages, including a remarkable (for that time) dynamic range in excess of 14,000. Dynamic range is defined as the maximum input signal (that required to saturate) divided by the threshold or smallest input. Young[11] reports an LJARS with a threshold of 0.05 deg/s and a maximum rate of 700 deg/s--hence, a dynamic range of ~14,000.

---

[4] *K. Chen and V. Neradka, Development of Critical Components, TriTec, Inc., Columbia, MD, DAAG-39-77-C-0173 (July 1978).*

[9] *T. Reader, T. Shaffer, J. Goren, and R. Kantola, Feasibility Investigation of a Laminar Rate Sensor (LARS), Phase I Report, General Electric Co. Reentry and Environmental Systems, Schenectady, NY, 69SD698 (June 1969).*

[10] *P. L. Jacobs, Theoretical Analysis of a Two-Dimensional Laminar Jet Rate Sensor, Proceedings of HDL Fluidic State-of-the-Art Symposium, II, Harry Diamond Laboratories (October 1974).*

[11] *R. Young, Development of a Laminar Angular Rate Sensor (LARS), Proceedings of HDL Fluidic State-of-the-Art Symposium, II, Harry Diamond Laboratories (October 1974).*

[12] *F. Manion and T. Drzewiecki, Analytical Design of Laminar Proportional Amplifiers, Proceedings of HDL Fluidic State-of-the-Art Symposium, I, Harry Diamond Laboratories (October 1974).*

[13] *T. M. Drzewiecki, D. N. Wormley, and F. M. Manion, Computer-Aided Design Procedure for Laminar Fluidic Systems, J. Dyn. Syst. Meas. Control, 97, Series G (December 1975).*

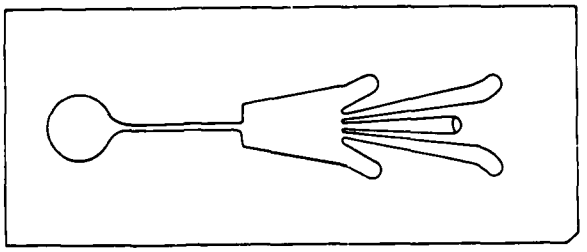

Figure 2. Early laminar jet angular rate sensor design.

Rankin et al[8] describe the axisymmetric Super Jet LJARS as a viable replacement for rate gyroscopes, quoting such performance parameters as drift of 0.001 deg/s per day and resolution of less than 0.002 deg/s. These are remarkable even for good rate gyroscopes, considering that earth rate at the equator is 0.004 deg/s.

This report lays the analytical groundwork for the coherent design of a planar LJARS. The report is divided into two sections, (1) the purely theoretical analysis verified by experimental data and (2) the design and applications guide. This second section is subdivided into critical areas that relate to the generation of a real-life system to include operating range, temperature (environmental) sensitivity, shock and vibration sensitivity, null offset, drift, dynamic range, power supply considerations, noise effects, operating fluids, fabrication, and testing. Where feasible, analytic tools are used to predict performance. Where not, rules of thumb and the experience of the authors and others are presented.

2. BASIC ANALYSIS

2.1 Free Jet Deflection in Rotating Field

The basic phenomenon of the LJARS relies on the time that it takes a particle leaving the nozzle to reach the sensing region, as illustrated in figure 1. During that time, the outputs or sensors have moved relative to their initial locations. As a result, the deflection of the jet is relative to the outputs (jet deflection due to Coriolis forces). With a rotating enclosed body like a fluidic amplifier, the field into which the jet enters is rotating with the structure due to the shear exerted on the fluid by the solid boundary planes. This rotation reduces the total jet deflection over that which would have

[8] *T. M. Rankin, A. G. Moore, and W. C. Schuemann, Fluidic Angular Rate Sensor--A Replacement for Rate Gyroscopes? Johns Hopkins Applied Physics Laboratory Technical Digest (March-April 1969).*

occurred if the field had been stationary. Consider, therefore, the net displacement of a fluid particle traveling with a velocity $u_{c\ell}$ in a radial direction (relative to the axis of rotation), with a superimposed solid body rotational velocity, as shown in figure 3.

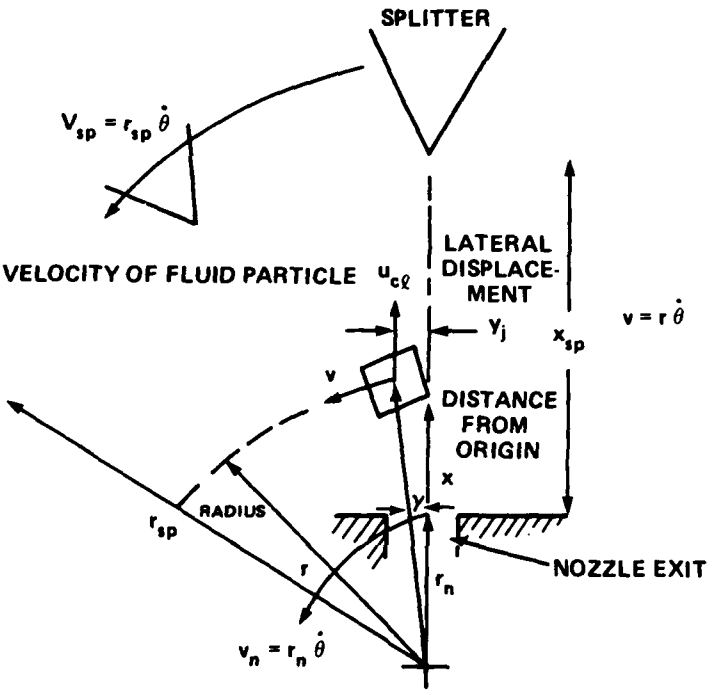

Figure 3. Geometry and coordinates for rotational deflection.

The particle displacement, y_j, at a distance, x, from the origin is the net tangential motion at tangential (lateral) velocity, v, over the period of time, τ, that it took the particle to reach x from the origin. At the average jet velocity, the lateral velocity is

$$v = r\dot{\theta} \cos \gamma \ ,$$

where the angle $\gamma = \tan^{-1} y_j/r$ so that, for transit velocities much greater than the lateral velocity, $\cos \gamma \approx 1$. Therefore, the elemental lateral displacement is

$$dy_j = r\dot{\theta}\, d\tau \ , \qquad (1)$$

and the elemental transit time, $d\tau$, is

$$d\tau = \frac{dx}{u_{c\ell}} \tag{2}$$

so that the total lateral displacement of the particle in the field is

$$y_j = \int_0^{y_j} dy = \int_{r_n}^{r_{sp}} r\dot{\theta}\,\frac{dx}{u_{c\ell}} \ . \tag{3}$$

But $r = r_n + x$ so that

$$y_j = \dot{\theta}\int_0^{x_{sp}} \frac{r_n + x}{u_{c\ell}}\,dx \ , \tag{4}$$

where x_{sp} is the distance from the nozzle to the splitter as in figure 3. The distance traversed by the splitter (or the outputs) at the tangential velocity, $r_{sp}\dot{\theta} = (r_n + x_{sp})\dot{\theta}$ in the total transit time,

$$\tau = \int_0^{x_{sp}} \frac{dx}{u_{c\ell}} \ ,$$

is

$$y_{xsp} = \left(r_n + x_{sp}\right)\dot{\theta}\int_0^{x_{sp}} \frac{dx}{u_{c\ell}} \ . \tag{5}$$

The displacement, y_r, of the jet relative to the structure is therefore the difference of these two displacements,

$$y_r = y_{xsp} - y_j = \left(r_n + x_{sp}\right)\dot{\theta}\int_0^{x_{sp}} \frac{dx}{u_{c\ell}} - \dot{\theta}\int_0^{x_{sp}} \frac{r_n + x}{u_{c\ell}}\,dx \ .$$

The terms containing the center of rotation, r_n, drop out and, hence,

$$y_r = \dot{\theta} \int_0^{x_{sp}} \frac{x_{sp} - x}{u_{c\ell}} \, dx \ . \tag{6}$$

For the high Reynolds number case where the center-line velocity is constant, equation (6) reduces to the familiar form

$$y_r = \frac{\dot{\theta} x_{sp}^2}{2u_{c\ell}} \ , \tag{7}$$

where $u_{c\ell} = \bar{u}_j = Q_s/\sigma b_s^2$, where Q_s is the jet flow rate, b_s is the nozzle width, and σ is the aspect ratio, h/b_s.

It now remains to identify the cases in which the average center-line velocity, $u_{c\ell}$, is not constant. At low Reynolds numbers, the two-dimensional laminar jet decays as the one-third power of the distance from the virtual origin so that

$$u_{c\ell} = \frac{\bar{u}_j}{\left(1 + \frac{x}{x_{vo}}\right)^{1/3}} \ . \tag{8}$$

The virtual origin, x_{vo}, is determined by matching the jet center-line velocity to that of the exit of a nozzle with fully developed (parabolic-like) flow. The reasoning behind this choice is that the parabolic profile and the hyperbolic secant profile are similar near the center, as is shown by Jacobs.[10] The actual center-line velocity is

$$u_{c\ell} = 0.4543 \left(\frac{K^2}{\nu x_{vo}}\right)^{1/3} = 2\bar{u}_j \ , \tag{9}$$

[10] *P. L. Jacobs, Theoretical Analysis of a Two-Dimensional Laminar Jet Rate Sensor, Proceedings of HDL Fluidic State-of-the-Art Symposium, II, Harry Diamond Laboratories (October 1974).*

where

$$\bar{u}_j = \frac{Q_s}{\sigma b_s^2} = c_d\left(\frac{2P_s}{\rho}\right)^{1/2}$$

and

$$K = \frac{2c_\theta b_s P_s}{\rho} ,$$

where K is the kinematic momentum flux, ν is the kinematic viscosity, Q_s is the volumetric flow rate of the supply, P_s is the supply pressure, ρ is the density, and c_θ is the momentum flux discharge coefficient. Therefore,

$$x_{vo} = \left[\frac{0.4543}{2c_d\left(\frac{2P_s}{\rho}\right)^{1/2}}\right]^3 \frac{K^2}{\nu} \qquad (10)$$

or

$$\frac{x_{vo}}{b_s} = X_{vo} = 0.01172\,\frac{c_\theta^2}{c_d^3}\,N_R ,$$

where

$$N_R = \frac{b_s\left(\frac{2P_s}{\rho}\right)^{1/2}}{\nu} ,$$

$$c_\theta = 1.15c_d^2$$

(based on a parabolic fully developed profile from a rectangular nozzle). Therefore,

$$X_{vo} = 0.0155c_dN_R . \qquad (11)$$

The center-line velocity is assumed to decay as in equation (12):

$$u_{c\ell} = \frac{\bar{u}_j}{\left(1 + \frac{x}{x_{vo}}\right)^{1/3}} = \frac{c_d\left(\frac{2P_s}{\rho}\right)^{1/2}}{\left(1 + \frac{x}{x_{vo}}\right)^{1/3}} . \qquad (12)$$

It has become obvious that three different functional relationships govern the average jet velocity, $u_{c\ell}$, in three Reynolds number regimes where the potential core (the distance over which the center-line velocity is constant) determines the velocity.

$$u_{c\ell} = \begin{cases} c_d\left(\frac{2P_s}{\rho}\right)^{1/2} , \text{ high } N_R,\ x_{core} \geq x_{sp}, \\ c_d \dfrac{\left(\frac{2P_s}{\rho}\right)^{1/2}}{\left(1 + \frac{x'}{x_{vo}}\right)^{1/3}} , \ x' = x - x_{core},\ 0 \leq x_{core} < x_{sp}, \\ c_d \dfrac{\left(\frac{2P_s}{\rho}\right)^{1/2}}{\left(1 + \frac{x}{x_{vo}}\right)^{1/3}} , \text{ low } N_R,\ x_{core} \leq 0. \end{cases} \qquad (13)$$

The core length concept is illustrated in figure 4. The core length is defined by the point where the nozzle boundary layers merge, or $\delta/b_s = 0.5$. Using this criterion and the fact that the boundary layer grows as the square root of downstream distance, we obtain

$$\frac{\left(\frac{\delta}{b_s}\right)_{exit}}{\left(\frac{\delta}{b_s}\right)_{core}} = \frac{\left(\frac{\delta}{b_s}\right)_{exit}}{0.5} = \frac{\left(x_n\right)^{1/2}}{\left(x_n + x_{core}\right)^{1/2}}$$

and

$$\left[\frac{1}{4\left(\frac{\delta}{b_s}\right)^2_{exit}} - 1\right] X_n = X_{core} \ , \qquad (14)$$

where X_n is the effective length of flat plate required to generate a nozzle exit boundary layer thickness of $\delta/b_s|_{exit}$.

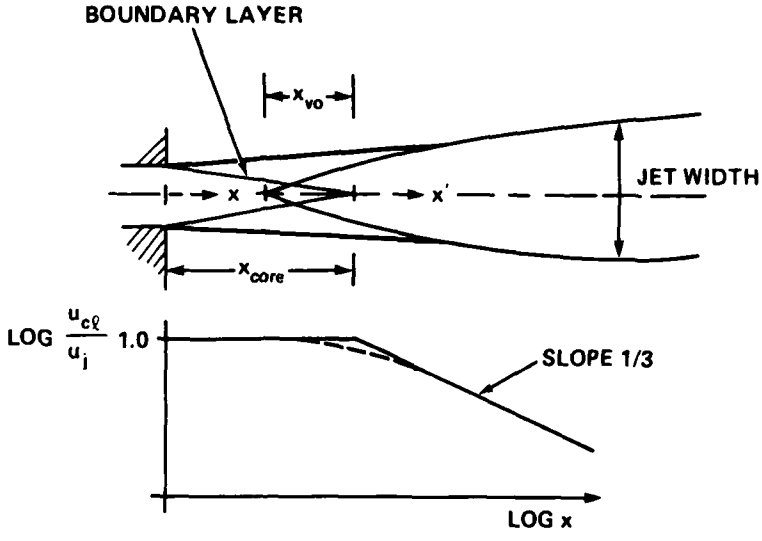

Figure 4. Physical interpretation of virtual origin and potential core.

The boundary layer thickness is related to the displacement thickness, δ^*, which is known from the discharge coefficient,[12]

$$\frac{\delta^*}{b_s} = \frac{\sigma + 1}{4} - \left[\frac{(\sigma + 1)^2}{16} - \left(1 - c_d\right)\frac{\sigma}{4}\right]^{1/2} . \qquad (15)$$

[12] *F. Manion and T. Drzewiecki, Analytical Design of Laminar Proportional Amplifiers, Proceedings of HDL Fluidic State-of-the-Art Symposium, I, Harry Diamond Laboratories (October 1974).*

For the zero pressure gradient[14,15] at the nozzle exit, $\delta/\delta^* = 10/3$ and $\delta/b_s = 5(X_n/N_R)^{1/2}$; therefore, the effective nozzle length becomes

$$X_n = \frac{x_n}{b_s} = \frac{\left(\frac{10\delta^*}{3b_s}\right)^2}{25} N_R \ . \tag{16}$$

From observations of flow visualization experiments, it is found that the core length is considerably longer than that given by equation (14), probably because the bounded jet configuration tends to reduce entrainment effects and, hence, does not degrade the center velocity as much. When one choses the fictitious conditions for boundary layer thickness at the end of the potential core as $\delta/b_s|_{core} = 1.19$ instead of 0.5 as originally assumed, the resulting equation gives good results in the overall algorithm. Hence, equation (14) becomes

$$X_{core} = \left[\frac{1.4}{\left(\frac{10\delta^*}{3b_s}\right)^2} - 1\right] X_n \ . \tag{17}$$

The general form for the jet deflection thus is

$$\frac{y_r}{b_s} = \frac{b_s\dot{\theta}}{c_d\left(\frac{2P_s}{\rho}\right)^{1/2}} \int_0^{X_{sp}} \left(X_{sp} - X\right) f(X)\, dX \ , \tag{18}$$

where X_{sp} is now the splitter distance normalized by the nozzle width and

---

[14] *T. M. Drzewiecki, Interpretation of Surface Static Pressure Distributions in Fluid Amplifier Applications, Harry Diamond Laboratories HDL-TR-1627 (July 1973).*

[15] *H. Schlichting, Boundary Layer Theory, McGraw-Hill Book Co., New York (1960).*

$$f(X) = \begin{cases} 1 \ , \ X_{core} > X_{sp}, \\ \left(1 + \dfrac{X - X_{core}}{X_{vo}}\right)^{1/3} \ , \ 0 \le X_{core} \le X_{sp} \ , \\ \left(1 + \dfrac{X}{X_{vo}}\right)^{1/3} \ , \ X_{core} \le 0 \ . \end{cases}$$

The general case when $0 \le X_{core} \le X_{sp}$ degenerates into the two other cases when at the limits; hence,

$$\frac{y_r}{b_s} = \frac{b_s \dot{\theta}}{c_d \left(\frac{2P_s}{\rho}\right)^{1/2}} \left[\int_0^{X_{core}} \left(X_{sp} - X\right) \, dX + \int_{X_{core}}^{X_{sp}} \left(X_{sp} - X\right) \left(1 + \frac{X - X_{core}}{X_{vo}}\right)^{1/3} dX \right] ,$$

and, performing the nontrivial integration,

$$\frac{y_r}{b_s} = \frac{b_s \dot{\theta}}{c_d \left(\frac{2P_s}{\rho}\right)^{1/2}} \left\{ X_{sp} X_{core} - \frac{X_{core}^2}{2} - \frac{3}{4} X_{vo} \left(X_{sp} - X_{core}\right) + \frac{9}{28} X_{vo}^2 \left[\left(1 + \frac{X_{sp} - X_{core}}{X_{vo}}\right)^{7/3} - 1 \right] \right\} , \qquad (19)$$

which reduces to

$$\left.\frac{y_r}{b_s}\right|_{(X_{core} \geq X_{sp})} = \frac{b_s\dot{\theta}}{2c_d\left(\frac{2P_s}{\rho}\right)^{1/2}} X_{sp}^2 , \tag{20}$$

which is identical with equation (7).

Equation (19) reduces to

$$\frac{y_r}{b_s} = \frac{b_s\dot{\theta}}{c_d\left(\frac{2P_s}{\rho}\right)^{1/2}} \left\{ \frac{9}{28} X_{vo}^2 \left[\left(1 + \frac{X_{sp}}{X_{vo}} \right)^{7/3} - 1 \right] - \frac{3}{4} X_{vo} X_{sp} \right\} , \tag{21}$$

for $X_{core} = 0$, that is, when there is no core length. The relationship for deflection can then be written as

$$\frac{y_r}{b_s} = \frac{b_s\dot{\theta}}{c_d\left(\frac{2P_s}{\rho}\right)^{1/2}} ZO , \tag{22}$$

where ZO represents one-half the square of the effective distance from nozzle to splitter. When the core length $x_{core} \geq x_{sp}$, $ZO = X_{sp}^2/2$. The coefficient of ZO may be rewritten as

$$\frac{b_s\dot{\theta}}{c_d\left(\frac{2P_s}{\rho}\right)^{1/2}} = \frac{b_s^2\dot{\theta}}{c_d N_R^{\upsilon}} . \tag{23}$$

Now the output pressure is related to deflection[12] by

[12] *F. Manion and T. Drzewiecki, Analytical Design of Laminar Proportional Amplifiers, Proceedings of HDL Fluidic State-of-the-Art Symposium, I, Harry Diamond Laboratories (October 1974).*

$$\frac{\left(\frac{\Delta P_o}{P_s}\right)}{\left(\frac{y}{b_s}\right)} = \frac{4C_{loss}}{B_o} = \frac{4P_{rec}}{P_s} , \tag{24}$$

where C_{loss} is the percentage of the momentum lost, B_o is the normalized width of the output channel, and P_{rec} is the jet centered recovered pressure at blocked conditions.

We define normalized sensitivity as

$$S \equiv \frac{\left(\frac{\Delta P_o}{P_s}\right)}{\left(\frac{b_s^2\dot{\theta}}{\nu}\right)} = \frac{\left(\frac{\Delta P_o}{P_s}\right)}{\left(\frac{y_r}{b_s}\right)} \frac{\left(\frac{y_r}{b_s}\right)}{\left(\frac{b_s^2\dot{\theta}}{\nu}\right)} = 4 \frac{P_{rec}}{P_s} \frac{ZO}{c_d N_R} . \tag{25}$$

To get $\Delta P_o/\dot{\theta}$ in pressure units per degree per second, we multiply S by $P_s b_s^2/57.3\nu$ so that

$$\frac{\Delta P_o}{\dot{\theta}} = \frac{2}{57.3} \frac{\mu N_R}{c_d} \frac{P_{rec}}{P_s} ZO . \tag{26}$$

Sensitivity becomes dimensionless when divided by absolute viscosity, μ. This quantity, $\Delta P_o/\mu\dot{\theta}$, is not the normalized sensitivity, but is a dimensionless sensitivity,

$$\frac{\Delta P_o}{\mu\dot{\theta}} = \frac{2}{57.3} \frac{N_R}{c_d} \frac{P_{rec}}{P_s} ZO . \tag{27}$$

To obtain sensitivity, one need only to multiply the dimensionless sensitivity by the viscosity of the fluid being used. The customary units are psi/(deg/s); SI units are Pa/(deg/s). The sensitivity of a device operating in a given medium is independent of actual size and depends only on the absolute viscosity of the fluid. The difference in operation between LJARS's of different sizes is in maximum rate since a larger device saturates before a small one due to the longer transit time.

2.2 Augmented Jet Deflection in Presence of Controls

When a jet deflection not due to a control signal occurs in a proportional amplifier configuration, a pressure difference develops across the jet and affects the jet. Apparent or real deflections occur due to misalignments, rate inputs, and geometric anomalies. In a rate sensor, therefore, the deflection can be augmented by this positive feedback, which is illustrated in figure 5.

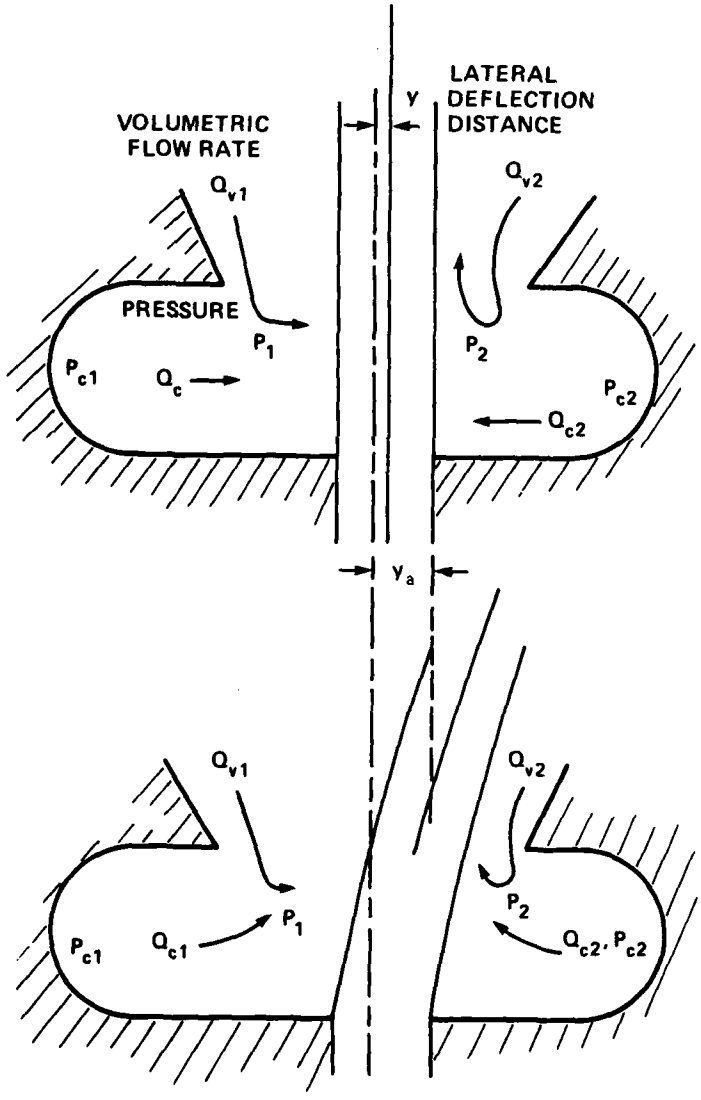

Figure 5. Deflection augmentation due to offset.

The physical explanation for this phenomenon is straightforward. Since the jet is closer to one control edge than to the other, the resistance of that clearance is higher. So more entrainment flow must be supplied from the control. Since control pressure is constant and equal on both controls, more control flow requires that the jet edge pressure be lower. Conversely, the reduced resistance of the wider side increases that pressure. This net pressure deflects the jet additionally. Deflection stops when the centripetal forces of the curving jet balance the applied pressure difference.

To compute this additional deflection, we may use the block diagram systems approach. An input deflection due to rate at the end of the control region causes a control pressure difference, which causes more deflection, which increases the deflection at the splitter (fig. 6).

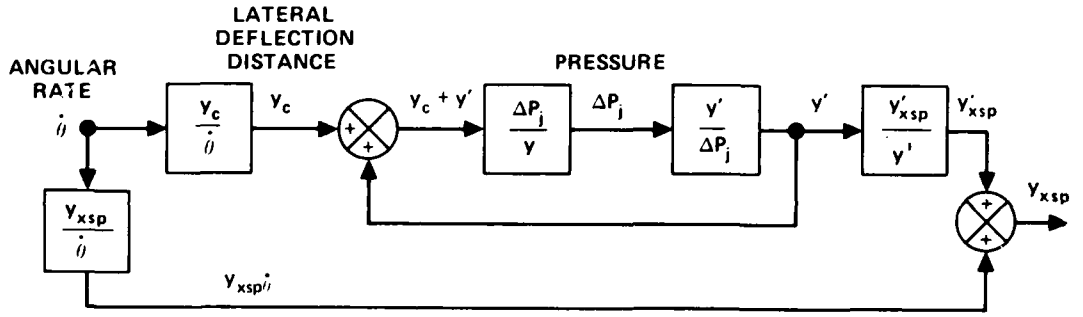

Figure 6. Positive feedback for added deflection due to presence of controls.

Section 2.1 has shown how the transfer function is determined. This section derives the transfer functions for induced pressure differential and for induced deflection.

2.2.1 Pressure Caused by Offset

In figure 7, consider the control volume near the control.[12]

The application of the incompressible continuity equation results in

[12] *F. Manion and T. Drzewiecki, Analytical Design of Laminar Proportional Amplifiers, Proceedings of HDL Fluidic State-of-the-Art Symposium, I, Harry Diamond Laboratories (October 1974).*

$$Q_{c1} + Q_{v1} + Q_y - Q_{enet} = 0 \ , \qquad (28)$$

where

Q_{c1} = control flow,

Q_{v1} = flow from vent through undeflected jet-edge space that has resistance R_v,

Q_y = flow through deflected space,

Q_{enet} = net entrained flow, that is, entrained flow, Q_e, minus spill flow, Q_{SB}. (Part of entrainment requirement is self-satisfied by spill flow.)

The control resistance, R_c, is known, as is the resistance, R_v, of the centered jet,[12,16] where resistance is defined $R = \Delta P/Q$. Equation (28) can thus be written in terms of the control volume pressure,

$$\frac{P_{c1} - P_{j1}}{R_c} + \frac{P_v - P_{j1}}{R_v} + y_{BC}h\left[\frac{2\left(P_v - P_{j1}\right)}{\rho}\right]^{1/2} - \left(Q_e - Q_{SB}\right) = 0 \ , \qquad (29)$$

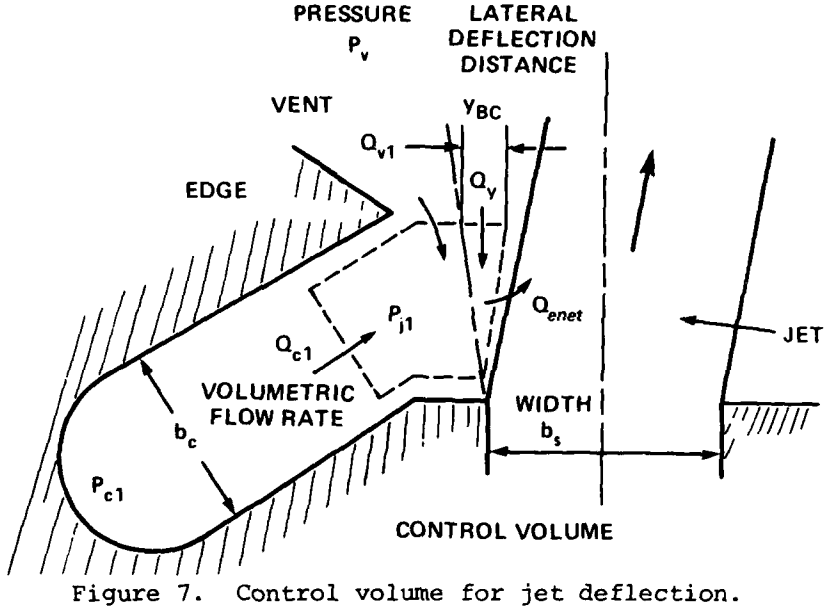

Figure 7. Control volume for jet deflection.

[12] *F. Manion and T. Drzewiecki, Analytical Design of Laminar Proportional Amplifiers, Proceedings of HDL Fluidic State-of-the-Art Symposium, I, Harry Diamond Laboratories (October 1974).*

[16] *T. M. Drzewiecki, Fluerics 38: A Computer Aided Design Analysis for the Static and Dynamic Port Characteristics of Laminar Proportional Amplifiers, Harry Diamond Laboratories HDL-TR-1758 (June 1976).*

where the flow through the deflected space is treated as an orifice flow through an area $y_{BC}h$ with unity discharge coefficient. When equation (29) is normalized by the supply jet flow $Q_s = c_d b_s h(2P_s/\rho)^{1/2}$, it becomes as shown in equation (30), in which the prime (') notation indicates quantities normalized by the corresponding supply parameter. For example, $P' = P/P_s$, $Q_e' = Q_e/Q_s$, and $R' = R/R_s$, where $R_s = P_s/Q_s$.

$$\frac{P_{c1}' - P_{j1}'}{R_c'} + \frac{P_v' - P_{j1}'}{R_v'} + \frac{y_{BC}'}{c_d}\left(P_v' - P_{j1}'\right)^{1/2} - Q_e' + Q_{SB}' = 0 \quad . \tag{30}$$

We now drop the prime notation for simplicity. To determine the change of the jet edge pressure with a change in deflection, we require the derivative of P_{j1} with respect to y_r. Thus, we differentiate equation (30) with respect to y_r and evaluate at $y_r = 0$ (the jet centered condition). For a rate sensor, the control pressure, P_{c1}, remains constant. For all cases, normally, P_v also is constant. The entrainment flow also is assumed to remain constant so that

$$\frac{\partial P_{j1}}{\partial y_r} = \frac{R_c R_v}{R_c + R_v}\left\{\frac{\left[P_v - P_j(0)\right]^{1/2}}{c_d} + \left.\frac{\partial Q_{SB}}{\partial y_r}\right|_{y=0}\right\} \quad . \tag{31}$$

Similarly for side 2, the same equation is written

$$\left.\frac{\partial P_{j2}}{\partial y_r}\right|_{y_r=0} = \frac{R_c R_v}{R_c + R_v}\left\{\frac{\left[P_v - P_j(0)\right]^{1/2}}{c_d} + \left.\frac{\partial Q_{SB}}{\partial y_r}\right|_{y=0}\right\} \quad . \tag{32}$$

Now that an expression has been obtained for the change of the jet edge pressure, it remains only to find the differential applied pressure on the jet. The pressure at the edge of the jet can be found by expanding the pressure in a Taylor series in deflection and, for small deflections, taking only the first two terms. Hence,

$$\begin{aligned} P_{j1}(y_r) &= P_{j1}(0) + y_r \left.\frac{\partial P_{j1}}{\partial y}\right|_{y=0} \quad , \\ P_{j2}(-y_r) &= P_{j2}(0) - y_r \left.\frac{\partial P_{j2}}{\partial y}\right|_{y=0} \quad . \end{aligned} \tag{33}$$

Since $P_{j1}(0) = P_{j2}(0)$,

$$P_{j1} - P_{j2} = y\left(\left.\frac{\partial P_{j1}}{\partial y}\right|_{y=0} + \left.\frac{\partial P_{j2}}{\partial y}\right|_{y=0}\right) \quad , \tag{34}$$

or the transfer function for jet edge differential pressure is

$$\frac{P_{j1} - P_{j2}}{y} = \frac{\Delta P_j}{y} = \left.\frac{\partial P_{j1}}{\partial y_r}\right|_{y=0} + \left.\frac{\partial P_{j2}}{\partial y}\right|_{y=0} = 2\left.\frac{\partial P_{j1}}{\partial y}\right|_{y=0} , \tag{35}$$

$$\frac{\Delta P_j}{y_r} = \frac{2R_cR_v}{R_c + R_v}\left\{\frac{\left[P_v - P_j(0)\right]^{1/2}}{c_d} + \left.\frac{\partial Q_{SB}}{\partial y_r}\right|_{y=0}\right\} . \tag{36}$$

Manion and Drzewiecki[12] define twice the change in spillback flow with respect to deflection as the net entrainment coefficient, a_1, which is calculated from the parameters of the problem. An improved expression is given by Drzewiecki.[16] Therefore,

$$\left.\frac{\partial Q_{SB}}{\partial y}\right|_{y=0} = -\frac{a_1}{2} . \tag{37}$$

If we consider $P_v = 0$ so that all measurements are relative to vent pressure, P_v, it then remains only to find an expression for $P_j(0)$. Manion and Drzewiecki[12] do this by applying continuity to the control leg of the device as in equation (30) at $y = 0$ so that

$$P_j(0) = \frac{R_cR_v}{R_c + R_v}\left(\frac{P_c}{R_c} - Q_{enet}\right) . \tag{38}$$

When these results are substituted into equation (36), the dc transfer function for jet pressure is

$$\frac{\Delta P_j}{y} = \frac{R_cR_v}{R_c + R_v}\left\{\frac{2}{c_d}\left[\frac{R_cR_v}{R_c + R_v}\left(Q_{enet} - \frac{P_c}{R_c}\right)\right]^{1/2} - a_1\right\} . \tag{39}$$

---

[12] *F. Manion and T. Drzewiecki, Analytical Design of Laminar Proportional Amplifiers, Proceedings of HDL Fluidic State-of-the-Art Symposium, I, Harry Diamond Laboratories (October 1974).*

[16] *T. M. Drzewiecki, Fluerics 38: A Computer Aided Design Analysis for the Static and Dynamic Port Characteristics of Laminar Proportional Amplifiers, Harry Diamond Laboratories HDL-TR-1758 (June 1976).*

One observes now from the derivation that the quantity in brackets in equation (39) must always be positive so that when the control flow, P_c/R_c, exceeds the net entrainment flow, the effect is a retarding one, as is that of the spill flow. Hence, for a rate sensor with close-in controls, the effects of the controls can be eliminated by judicious application of biasing control flow so that $\Delta P_j/y = 0$. This is an important point and is discussed further in section 3.4 on null offset compensation. Equation (39) is rewritten to accommodate an always positive radical, shown in parentheses in equation (40).

$$\frac{\Delta P_j}{y} = \frac{R_c R_v}{R_c + R_v}\left[\frac{2}{c_d}\frac{Q_{enet} - \frac{P_c}{R_c}}{\left(\left|Q_{enet} - \frac{P_c}{R_c}\right|\right)^{1/2}}\left(\frac{R_c R_v}{R_c + R_v}\right)^{1/2} - a_1\right] . \quad (40)$$

It is clear that there is a value of P_c for which $\Delta P_j/y = 0$ and that, when that value is exceeded, the effect is a net reduction in deflection.

The transfer function that determines the pressure caused by an offset is given by equation (40).

2.2.2 Augumented Deflection

As a result of the differential pressure imposed on the jet, the jet will deflect in a circular arc within the control region and have a deflection at the end of the controls as described by Manion and Mon[17] and Manion and Drzewiecki[12] and given in equation (41).

$$\frac{y'}{\Delta P_j} = \frac{B_c^2}{4C_\theta} , \quad (41)$$

where $B_c = b_c/b_s$ (the normalized control width).

---

[12] *F. Manion and T. Drzewiecki, Analytical Design of Laminar Proportional Amplifiers, Proceedings of HDL Fluidic State-of-the-Art Symposium, I, Harry Diamond Laboratories (October 1974).*

[17] *F. M. Manion and G. Mon, Fluerics 33: Design and Staging of Laminar Proportional Amplifiers, Harry Diamond Laboratories HDL-TR-1608 (September 1972).*

The net added deflection is determined by the transfer function of the positive feedback loop that has unity feedback. The gain of such a loop, G_L, is

$$G_L = \frac{G}{1 - G} = \frac{1}{\frac{1}{G} - 1} ,$$

where G is the forward gain; hence,

$$\frac{y'}{y_{BC}} = \frac{\frac{\Delta P_j}{y_{BC}} \frac{y'}{\Delta P_j}}{1 - \frac{\Delta P_j}{y_{BC}} \frac{y}{\Delta P_j}} . \tag{42}$$

When equations (40) and (41) are substituted into equation (42) and the result is rearranged, the result is

$$\frac{y'}{y_{BC}} = \frac{\frac{2\left(\frac{R_c R_v}{R_c + R_v}\right)^{1/2}\left(Q_{enet} - \frac{P_c}{R_c}\right)}{c_d\left(\left|Q_{enet} - \frac{P_c}{R_c}\right|\right)^{1/2}} - a_1}{\frac{4c_\theta\left(R_c + R_v\right)}{B_c^2 R_c R_v} - \left[\frac{2\left(\frac{R_c R_v}{R_c + R_v}\right)^{1/2}\left(Q_{enet} - \frac{P_c}{R_c}\right)}{c_d\left(\left|Q_{enet} - \frac{P_c}{R_c}\right|\right)^{1/2}} - a_1\right]} . \tag{43}$$

The jet would flow in a straight line to the splitter due only to control deflection; hence, the additional displacement at the splitter is that linear contribution from equation (43) multiplied by the geometric gain factor given by Manion and Drzewiecki.[12]

$$\frac{y_{XSP}}{y'} = \frac{2X_{sp}}{B_c} - 1 . \tag{44}$$

[12] *F. Manion and T. Drzewiecki, Analytical Design of Laminar Proportional Amplifiers, Proceedings of HDL Fluidic State-of-the-Art Symposium, I, Harry Diamond Laboratories (October 1974).*

The last transfer function required is the deflection at the control edges due to rate. For this, we use equation (20) with the control width substituted for the distance. This is reasonably accurate since right near the nozzle exit one never expects there to be much velocity decay. Thus,

$$\frac{y_{BC}}{\dot{\theta}} = \frac{b_s^2 B_c^2}{2c_d\left(\frac{2P_s}{\rho}\right)^{1/2}} \,. \tag{45}$$

The transfer function for the total dimensional deflection is therefore obtained from equations (22) and (43) to (45) as is expected from the block diagram of figure 6.

$$\frac{y_{XSP}}{\dot{\theta}} = \frac{b_s^2}{c_d\left(\frac{2P_s}{\rho}\right)^{1/2}} ZO + \underset{\text{eq (45)}}{\frac{y_{BC}}{\dot{\theta}}} \quad \underset{\text{(43)}}{\frac{y'}{y_{BC}}} \quad \underset{\text{(44)}}{\frac{y_{XSP}}{y'}}$$

or

$$\frac{\left(\frac{y_{XSP}}{b_s}\right)}{\left[\frac{b_s\dot{\theta}}{c_d\left(\frac{2P_s}{\rho}\right)^{1/2}}\right]} = ZO + \frac{B_c^2}{2}\left(\frac{2X_{sp}}{B_c} - 1\right)$$

$$\times \left[\frac{\frac{2}{c_d}\frac{\left(\frac{R_c R_v}{R_c + R_v}\right)^{1/2}\left(Q_{enet} - \frac{P_c}{R_c}\right)}{\left(\left|Q_{enet} - \frac{P_c}{R_c}\right|\right)^{1/2}} - a_1}{\frac{4c_\theta\left(R_c + R_v\right)}{B_c^2\left(R_c + R_v\right)} - \frac{2\left(\frac{R_c R_v}{R_c + R_v}\right)^{1/2}\left(Q_{enet} - \frac{P_c}{R_c}\right)}{c_d\left(\left|Q_{enet} - \frac{P_c}{R_c}\right|\right)^{1/2}} - a_1}\right] . \tag{46}$$

2.3 Loss of Momentum Due to Viscous Friction

The loss of momentum due to friction on the bounding planes has been addressed by Manion and Drzewiecki.[12] The analysis, however, overestimated these losses at low Reynolds numbers. The purpose of this section is therefore to remedy this loss in the light of possible operation of laminar devices in the low N_R region. This loss occurs most often with devices with very long nozzles as it occurred with the early LJARS. Operation with a long nozzle is usually undesirable because of the dramatically increased sensitivity to temperature changes. Nevertheless, it is of academic interest to be able to predict such performance, and it is important to be able to predict an LJARS performance over the entire laminar range. With amplifiers, one is not particularly interested in the region where the gain is less than 1, but in the LJARS there is always rate sensitivity so that all Reynolds numbers are of interest.

The net change of momentum can be estimated if the velocity distribution at two stations is known. The momentum when the jet exits from a nozzle is well known,[12] as is the velocity distribution.[14] Consider first the low Reynolds number case.

When the modified Reynolds number N_R' is less than 20, where

$$N_R' = \frac{N_R}{\left(1 + \frac{x_{th}}{b_s}\right)\left(1 + \frac{1}{\sigma}\right)^2}$$

and x_{th} is the nozzle throat length, the flow in a nozzle is fully developed. For aspect ratios near 1, the velocity profile is near parabolic, especially in the narrow dimension. When there is no effective potential core, the parabolic profile very closely approximates the two-dimensional jet profile; hence, one may expect the parabolic profile between the planes to remain parabolic, especially because there is little or no pressure gradient.

The loss coefficient is defined as the ratio of the momentum reaching the splitter, J_{XSP}, to the momentum at the nozzle exit, J_s, so

---

[12] *F. Manion and T. Drzewiecki, Analytical Design of Laminar Proportional Amplifiers, Proceedings of HDL Fluidic State-of-the-Art Symposium, I, Harry Diamond Laboratories (October 1974).*

[14] *T. M. Drzewiecki, Interpretation of Surface Static Pressure Distributions in Fluid Amplifier Applications, Harry Diamond Laboratories HDL-TR-1627 (July 1973).*

$C_{XSP} = J_{XSP}/J_s$, where the momentum flux of a parabolic profile in general is $J = (6/15)b_s h\rho u_c^2$. The ratio between two parabolic profiles is then merely the ratio of the squares of center-line velocity. From equation (8), the ratio of the velocities is

$$\frac{u_{c(x = x_{sp})}}{u_{c(x = 0)}} = \frac{1}{\left(1 + \frac{x_{sp}}{x_{vo}}\right)^{1/3}} . \tag{47}$$

Hence, the loss coefficient becomes

$$C_{XSP} = \frac{J_{XSP}}{J_s} = \left(1 + \frac{x_{sp}}{x_{vo}}\right)^{-2/3} , \; x_{core} \leq 0. \tag{48}$$

When there exists a potential core, the net loss coefficient is a product of the losses in the core region and the decaying region.

$$C_{XSP} = \frac{J_{core}}{J_s} \frac{J_{XSP}}{J_{core}} .$$

The loss coefficient in the decaying jet portion is the same as in equation (48), except that it acts over a shorter distance.

$$\frac{J_{XSP}}{J_{core}} = \left(1 + \frac{x_{sp} - x_{core}}{x_{vo}}\right)^{-2/3} . \tag{49}$$

A similar analysis is performed for the momentum loss in the potential core region, except that now the velocity profiles are not of the same form. However, the momentum in the vertical velocity profile is known when the boundary layer displacement and momentum thicknesses are known. The momentum flux in the profile per unit width is

$$\frac{J}{b_s} = \frac{J_{ideal}}{b_s} \left[1 - 2 \frac{(\delta - \delta^* - \theta)}{h}\right] . \tag{50}$$

The ratio of these momenta between any two points is therefore

$$\frac{J_{X=X2}}{J_{X=X1}} = \frac{1 - \frac{2}{\sigma}\left(\frac{\delta}{b_s} - \frac{\delta^*}{b_s} - \frac{\theta}{b_s}\right)_{X=X2}}{1 - \frac{2}{\sigma}\left(\frac{\delta}{b_s} - \frac{\delta^*}{b_s} - \frac{\theta}{b_s}\right)_{X=X1}} \quad . \tag{51}$$

For a zero pressure gradient and flow over a flat plate, momentum integral analysis[15] tells us that

$$\frac{\delta}{b_s} = 5\left(\frac{X}{N_R}\right)^{1/2} , \tag{52a}$$

$$\frac{\delta^*}{b_s} \simeq 1.729\left(\frac{X}{N_R}\right)^{1/2} , \tag{52b}$$

$$\frac{\delta^*}{\theta} = 2.61 . \tag{53}$$

When these values are substituted into equation (51) and evaluated at the core length and the nozzle exit, the result is

$$\frac{J_{Xn+Xcore}}{J_{Xn}} = \frac{1 - \frac{5.2}{\sigma}\left(\frac{X_n + X_{core}}{N_R}\right)^{1/2}}{1 - \frac{5.2}{\sigma}\left(\frac{X_n}{N_R}\right)^{1/2}} , \tag{54}$$

where X_n is the effective length of the nozzle if it were a flat plate as given in equation (16).

In general, however, one may write equation (51) as

$$\frac{J_{X=X2}}{J_{X=X1}} = \frac{1 - \frac{2\delta_2}{\sigma b_s}\left(1 - \frac{\delta^*}{\delta} - \frac{\theta}{\delta}\right)_{X=X2}}{1 - \frac{2\delta_1}{\sigma b_s}\left(1 - \frac{\delta^*}{\delta} - \frac{\theta}{\delta}\right)_{X=X1}} \quad . \tag{55}$$

---

[15] *H. Schlichting, Boundary Layer Theory, McGraw-Hill Book Co., New York (1960).*

The quantity $[1 - (\delta^*/\delta) - (\theta/\delta)]$ increases in a favorable pressure gradient and decreases in an unfavorable one. For small pressure gradients, the boundary layer thickness is roughly constant. The pressure gradient at the nozzle exit is always favorable, while downstream one would expect a slightly adverse gradient. Although there are no comprehensive data on the gradients to verify equation (55), the form of this loss equation is important. The values of $[1 - (\delta^*/\delta) - (\theta/\delta)]$ can be adjusted to give correlation of the final results with experimental data on pressure recovery. Comparison with a large number of different cases has indicated that, for aspect ratios greater than 1, there is one value and, for aspect ratios less than 1, there is another as follows:

$$\frac{J}{J_n} = \frac{1 - \frac{A}{\sigma}\left(\frac{X_n + X}{N_R}\right)^{1/2}}{1 - \frac{B}{\sigma}\left(\frac{X_n}{N_R}\right)^{1/2}} \quad , \tag{56}$$

where

$A = 4.0,\ B = 5.6,\ \sigma \geq 1,$
$A = B = 3.0,\ \sigma < 1.$

The value of X can be the core length or the splitter distance so that the loss coefficient for the case where the jet has a potential core for its entire length is

$$C_{XSP} = \frac{J_{sp}}{J_n} = \frac{1 - \frac{A}{\sigma}\left(\frac{X_n + X_{sp}}{N_R}\right)^{1/2}}{1 - \frac{B}{\sigma}\left(\frac{X_n}{N_R}\right)^{1/2}} \quad , \tag{57}$$

and the loss coefficient when a core is present is

$$C_{XSP} = \frac{J_{core}}{J_n}\frac{J_{XSP}}{J_{core}}$$

$$= \left[\frac{1 - \frac{A}{\sigma}\left(\frac{X_n + X_{core}}{N_R}\right)^{1/2}}{1 - \frac{B}{\sigma}\left(\frac{X_n}{N_R}\right)^{1/2}}\right]\left(1 + \frac{X_{sp} - X_{core}}{X_{vo}}\right)^{-2/3} \quad . \tag{58}$$

The validity of these loss coefficients is demonstrated especially well when the pressure recovery of a laminar jet device is measured, since pressure recovery is a direct measure of that coefficient as seen from equation (24), in which

$$\frac{P_{rec}}{P_s} = \frac{C_{loss}}{B_o} \quad , \tag{59}$$

where

$$C_{loss} = c_\theta C_{XSP} C_{Bsp} \quad . \tag{60}$$

Figures 8 to 10 illustrate the kind of agreement obtained with the theory and experimental data for various splitter distances, aspect ratios, and output widths. These equations and those yet to be developed have been incorporated into the numerical algorithm proposed by Drzewiecki.[16] The theoretical curves presented in figures 8 and 9 were generated by that program.

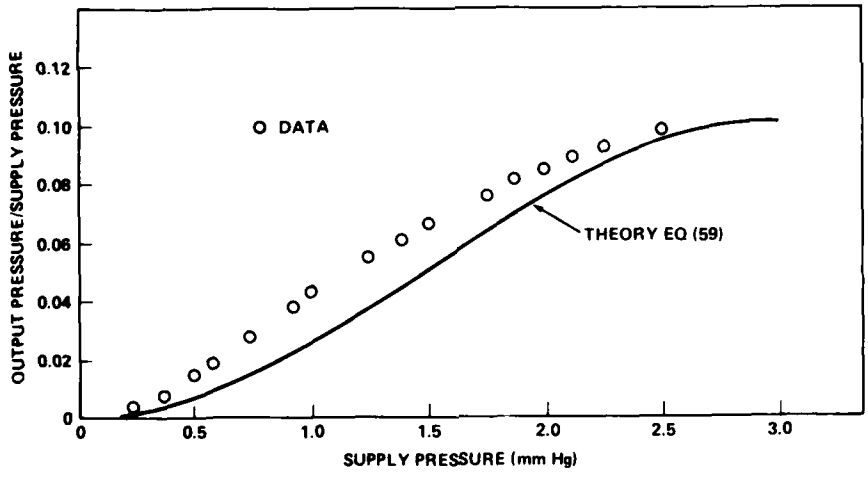

Figure 8. Pressure recovery of long, X_{th} = 40, nozzle laminar jet angular rate sensor: normalized splitter length = 20, supply width = 0.889 mm, normalized output width = 1.7, and aspect ratio = 1.1.

[16] *T. M. Drzewiecki, Fluerics 38: A Computer Aided Design Analysis for the Static and Dynamic Port Characteristics of Laminar Proportional Amplifiers, Harry Diamond Laboratories HDL-TR-1758 (June 1976).*

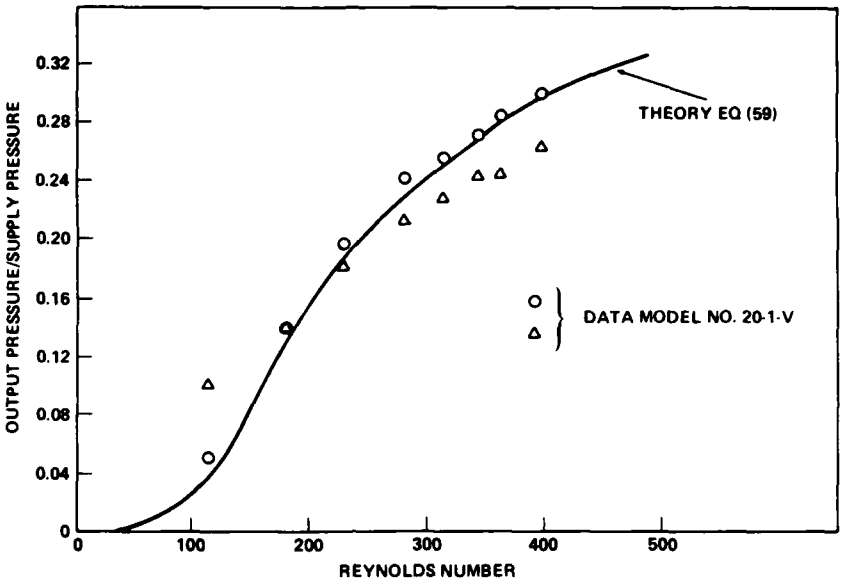

Figure 9. Pressure recovery of short nozzle laminar jet angular rate sensor: normalized splitter length = 11.11, supply width = 1.14 mm, normalized output width = 1.67, and aspect ratio = 2.77.

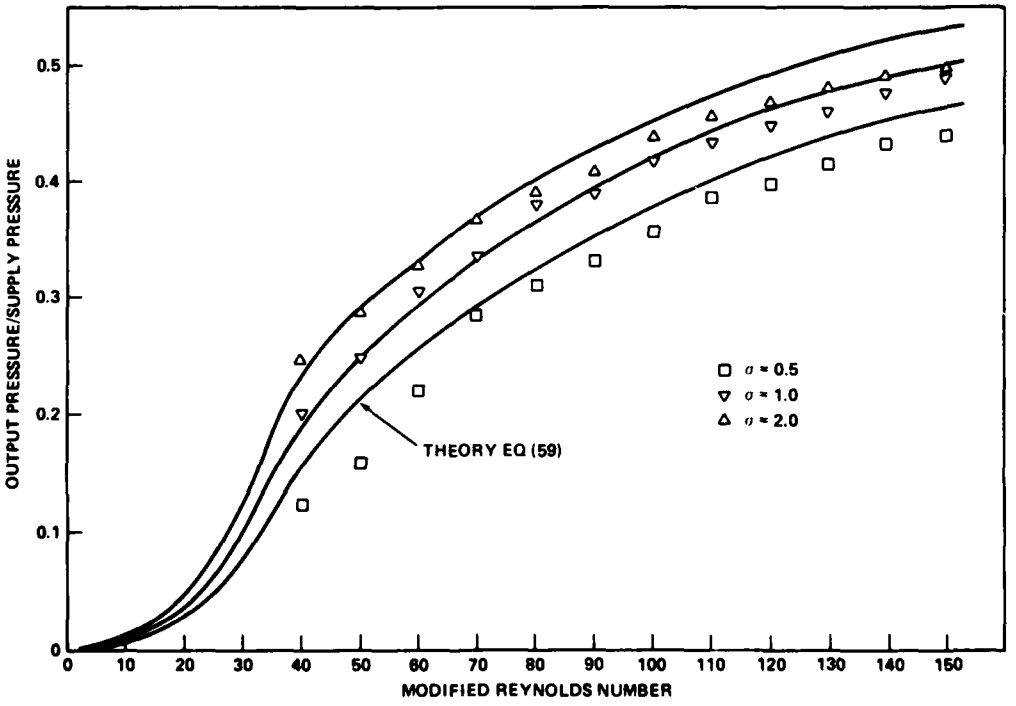

Figure 10. Pressure recovery for laminar proportional amplifiers of different aspect ratios (σ's): normalized splitter length = 8 and supply width = 0.5 mm.

An updated version of the program is given in appendix A. This program is a general laminar jet device algorithm and generates far more information than the rate sensitivity. The input and output characteristics also are available. This program now gives the rate sensitivity of amplifiers and, conversely, the gain of rate sensors.

Figures 11 and 12 allow comparison between theory and experiment for the overall sensitivity of an LJARS. The agreement is considered acceptable.

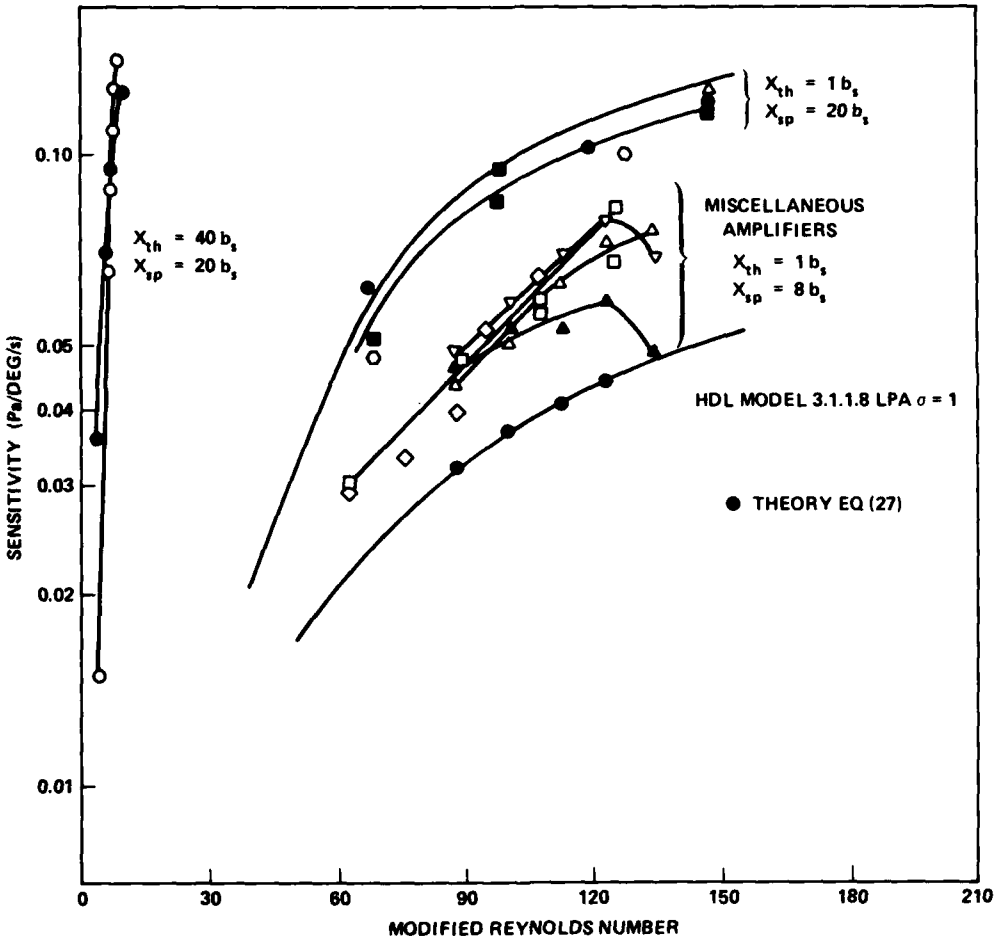

Figure 11. Sensitivity of laminar jet angular rate sensor for various configurations: X_{th} = nozzle throat length, X_{sp} = splitter length, b_s = supply width, and σ = aspect ratio.

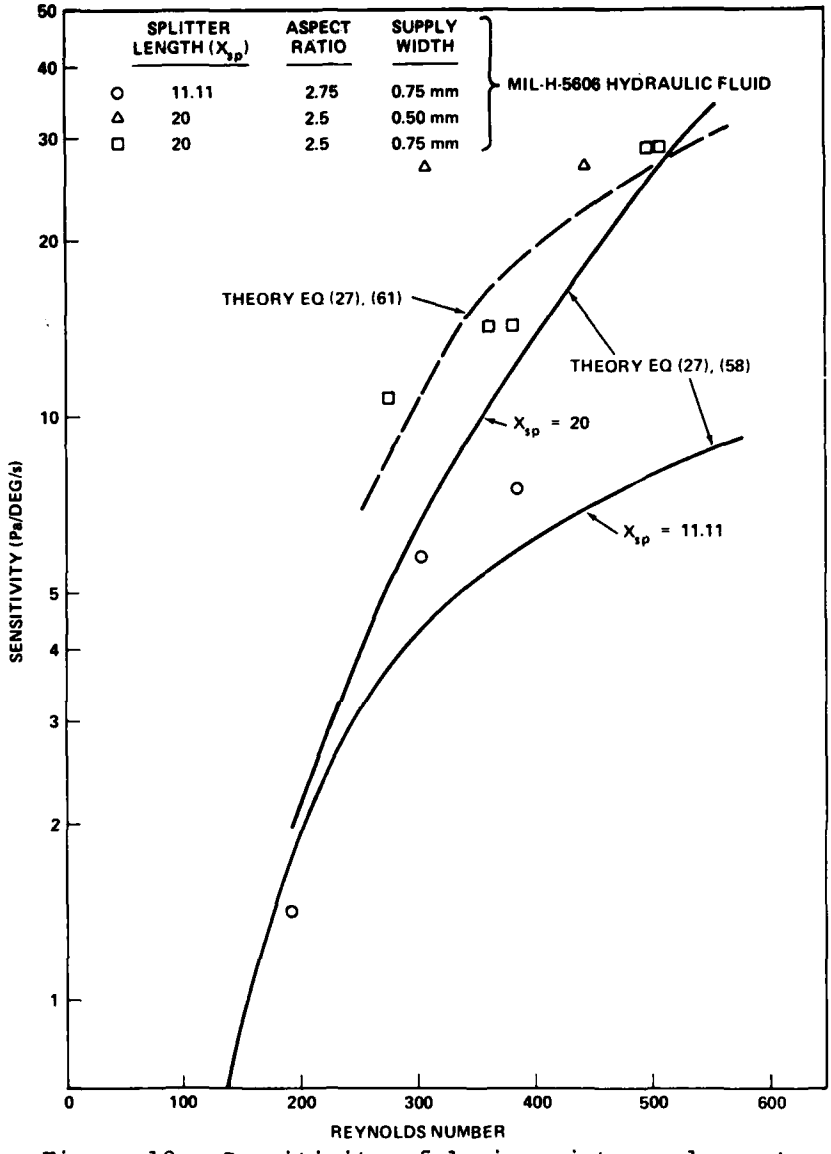

Figure 12. Sensitivity of laminar jet angular rate sensor for hydraulic operation.

For engineering purposes, the simple relation for the losses developed by Manion and Drzewiecki[12] for $N_R' > 50$ may be used without loss of accuracy. The expression for sensitivity is therefore

[12] *F. Manion and T. Drzewiecki, Analytical Design of Laminar Proportional Amplifiers, Proceedings of HDL Fluidic State-of-the-Art Symposium, I, Harry Diamond Laboratories (October 1974).*

$$\frac{\Delta P_o}{\dot{\mu\theta}} = \frac{1}{57.3} \frac{N_R}{c_d} \frac{c_\theta}{B_o} \left(1 - \frac{8X_{sp}}{c_\theta N_R \sigma^2}\right) \left[1 - \frac{1.1B_{sp}}{\left(c_d N_R \frac{B_{sp}}{2}\right)^{1/2}}\right] X_{sp}^2 \quad . \qquad (61)$$

A listing of this equation is contained in appendix A.

2.4 Dynamic Response

The response of the jet to an applied sinusoidal angular rate is complex. Ideally, with no field effects, the jet response would be governed only by the transport delay. In other words, the transfer function would be a pure delay. Such is not the case in reality. It takes the field a finite amount of time to respond to the moving of the bounding surfaces so that the device reacts like an ideal sensor for the first instant of time when subjected to a step input of rate, but then the transient of the field catches up. Figure 13 shows the output differential pressure response of an LJARS to a step in rate. There are regions that do not behave as one may have expected. For example, an initial negative spike is followed by an increasing signal, then a second but slower negative region, a second-order rise to a slight overshoot, and a settling down to a constant value. The same happens when the rate is removed.

The initial negative spike is attributable directly to the sudden acceleration of the splitter, which protrudes into the vent area and acts like a paddle. Figure 14 illustrates that, when the splitter moves upward, a stagnation (positive) pressure develops on the top side and a suction (negative) pressure develops below. This is a negative differential pressure transmitted at acoustic speed to the output ports as opposed to a final positive pressure differential at a steady rate in which the jet is lagging the structure and tends to develop a larger pressure on the lower output and a smaller pressure at the upper output. The paddle pressure signal is transmitted at the speed of sound to the output transducer.

After this spike, the jet should lag the splitter and, hence, the pressure in figure 13 rises. To explain the occurrence of the second negative part requires some analysis. However, we present only some phenomenological observations obtained from flow visualization research. Figures 15 and 16 show the instantaneous jet position as marked by a dye stream for two intermediate times. In figure 15, the time corresponds to a short time during the initial rise of the output pressure in figure 12. In figure 16, the time is at an instant just about at the minimum of the second negative portion. Qualitatively, we observe that the input disturbance at the nozzle exit travels at half

the average jet velocity. This speed is apparent when one considers a disturbance as an eddy traveling downstream like a wheel on the ground. The part of the eddy in contact with the jet has the axial velocity of the jet, yet the part in the ambient field has zero velocity; hence, the centroid of the eddy must travel half the jet velocity. Figure 17 illustrates this phenomenon.

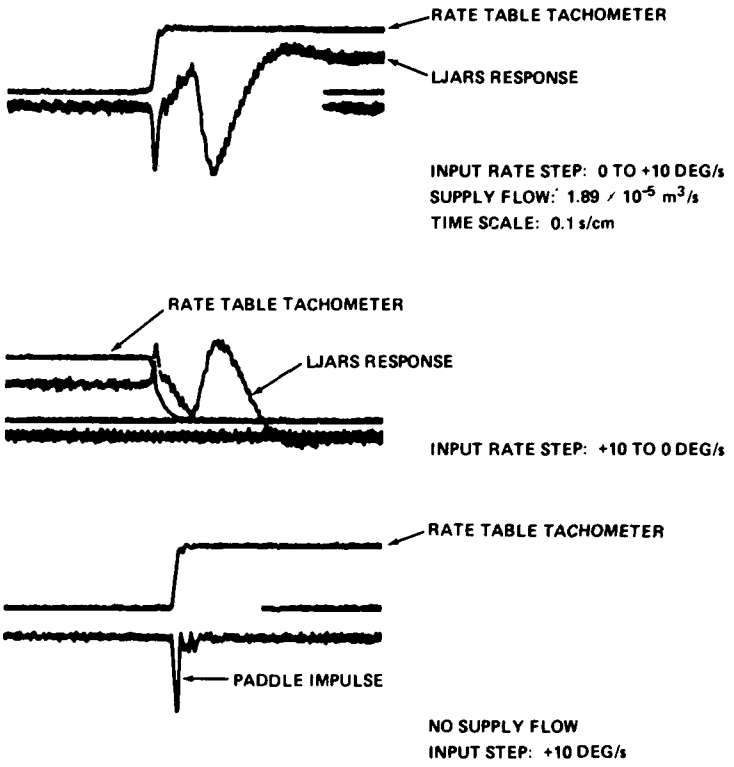

Figure 13. Oscilloscope traces of laminar jet angular rate sensor (LJARS) step response in hydraulic oil.

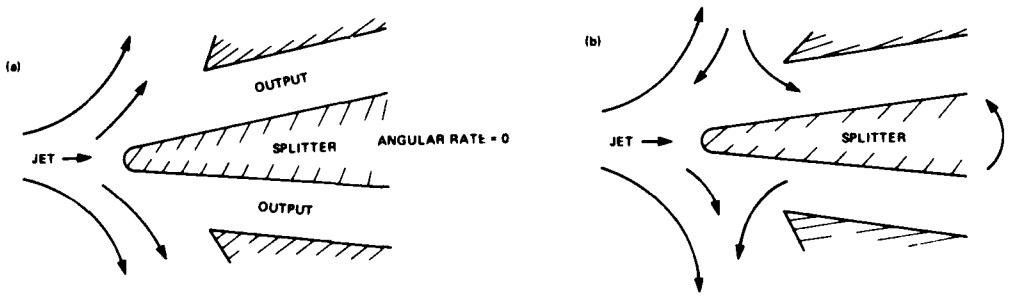

Figure 14. Paddle effect due to sudden acceleration.

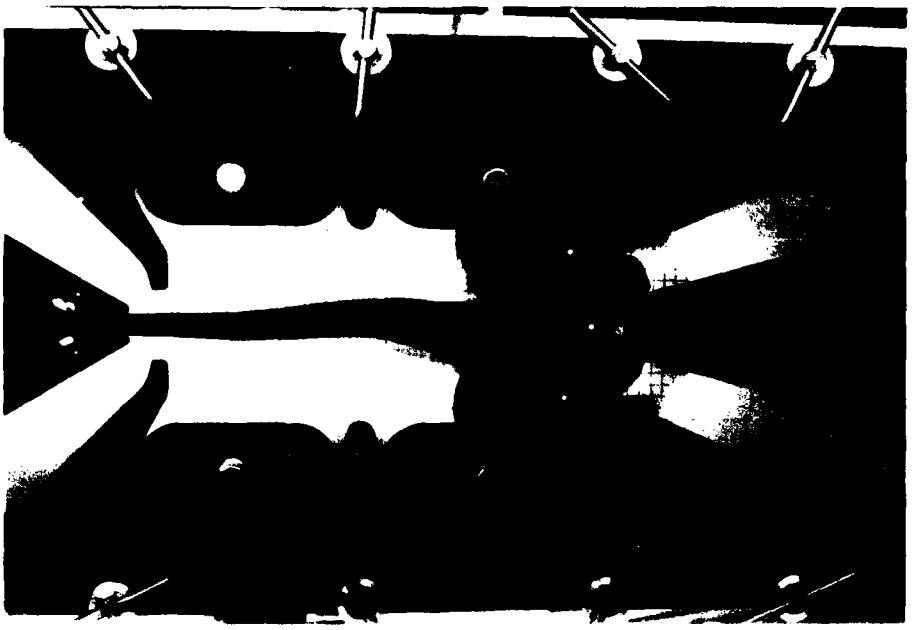

Figure 15. Step response of laminar jet angular rate sensor jet, time = 0^+.

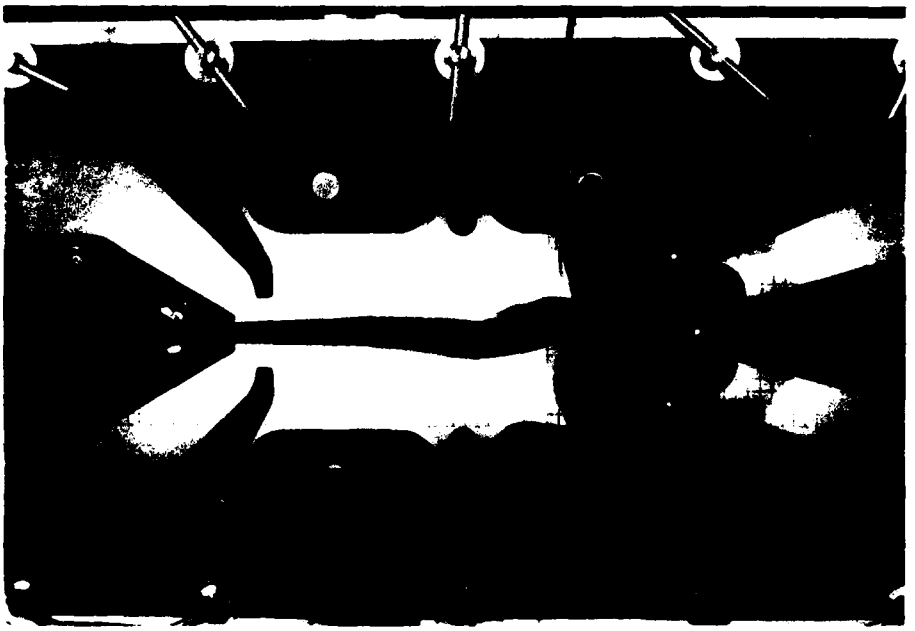

Figure 16. Step response of laminar jet angular rate sensor jet, time < steady state time.

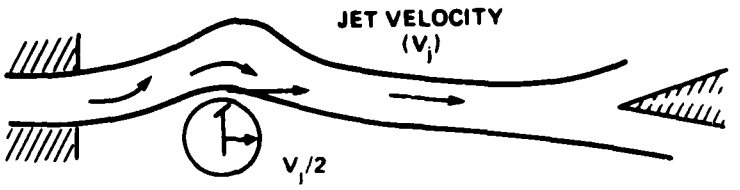

Figure 17. Convective translation of disturbance eddy.

The signal arrives at the splitter in twice the particle transport time. The disturbance as it travels to the splitter grows and causes the jet center line to deflect whiplike, causing the negative part of the output response. The jet settles out to its steady-state deflection in yet another disturbance transport time.* A steady state is achieved in two disturbance transport times or four average-particle-velocity transport times, as is evident from figure 12. We have not touched on the reason for the whiplike action of the jet. This is a topic for further research; however, we provide some rationale and direction to such research at the end of this section.

For design engineering, a delay of four times the transport time predicts a phase shift of -90 deg at a frequency far below that of the dynamic effects just stated. Since phase shift, ϕ, is defined as the ratio of delay time, τ_d, to period of oscillation, then in degrees

$$\phi = 360 \frac{\tau_d}{\lambda} , \tag{62}$$

where τ_d is four times the average transport time, and λ is the period of the frequency = 1/f, so that

$$\phi = 360 f \tau_d \tag{63}$$

and, at ϕ = 90 deg,

$$f = \frac{1}{4\tau_d} = \frac{1}{4} \left[\frac{c_d \left(\frac{2p_s}{\rho} \right)^{1/2}}{4 b_s X_{sp}} \right] . \tag{64}$$

The first edge-tone frequency occurs at a frequency roughly corresponding to twice the transport time. If, indeed, a disturbance travels to the splitter at that speed and is acoustically (virtually instantaneously) fed back, then it is reasonable that the first edge-tone frequency should be at $0.466V_s/X_{sp}$, where V_s is the supply velocity. Higher harmonics do not occur as multiples because at higher frequencies the acoustic delay becomes appreciable and changes the mode.

Remembering that

$$N_R = \frac{b_s}{\nu}\left(\frac{2P_s}{\rho}\right)^{1/2} ,$$

we have

$$f\Big|_{\phi=-90°} = \frac{c_d N_R \nu}{16 X_{sp} b_s^2} . \qquad (65)$$

From this argument, we may conclude that the frequency response of an LJARS is flat past the -90 deg phase shift point. Experimental evidence bears this out quite adequately as shown in figures 18 to 20. Figures 18 and 19 show the Bode response of an LJARS used in a tank gun stabilization system operating in hydraulic oil. It can be shown that the phase shift in figure 18 as determined from equation (65) is in excellent agreement, and consequently the point at which -90 deg occurs is well defined by the above theoretical considerations. Examination of equation (65) indicates that devices of the same size operating at the same Reynolds number have the same actual bandwidth, regardless of fluid medium, provided that the kinematic viscosity remains the same. At room temperature, the kinematic viscosities of MIL-H-5606 hydraulic fluid and air are the same. So a hydraulic rate sensor and a pneumatic rate sensor of the same size have the same response and bandwidth. This is a different effect than was found for sensitivity where sensitivity is shown to be independent of size.

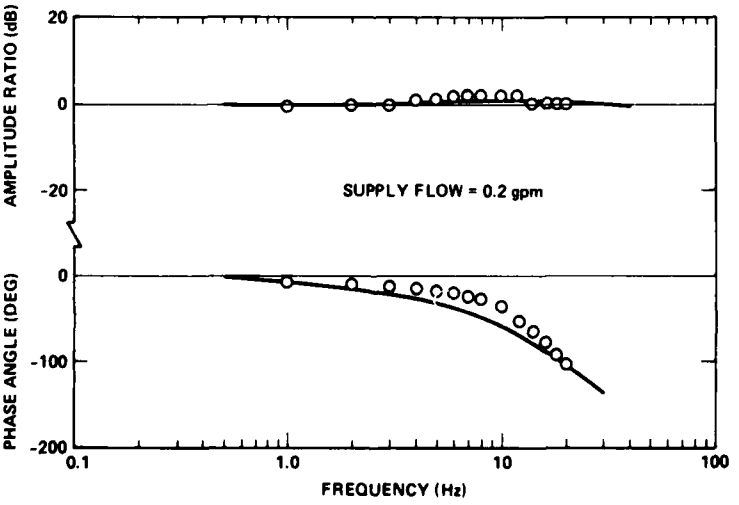

Figure 18. Dynamic response of hydraulic laminar jet angular rate sensor (from AiResearch).

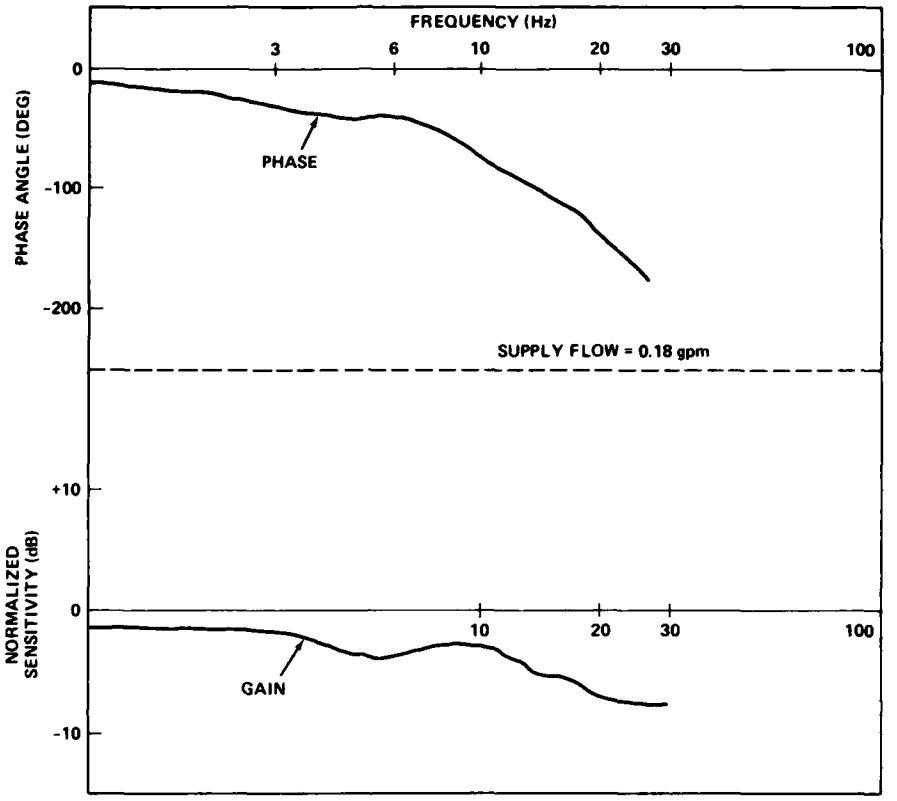

Figure 19. Dynamic response of hydraulic laminar jet angular rate sensor.

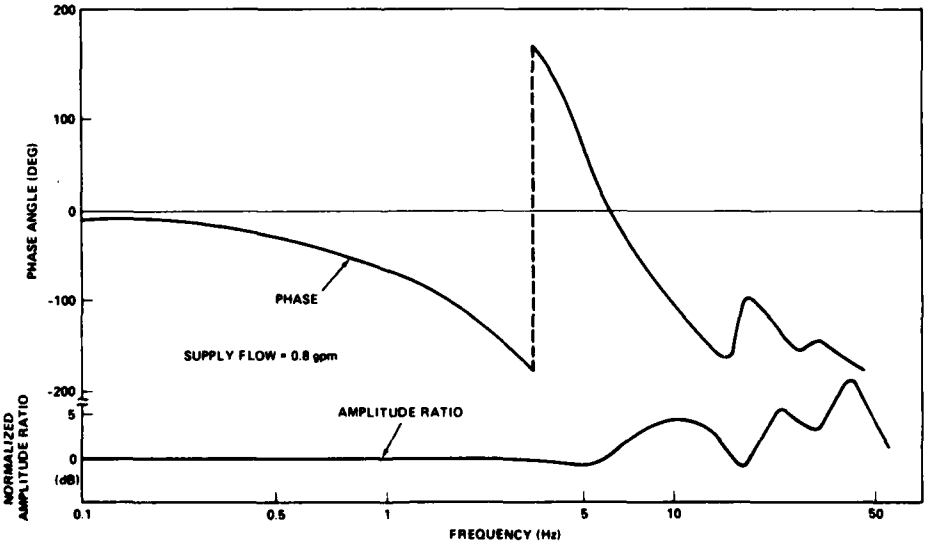

Figure 20. Dynamic response of overscale 4:1 hydraulic laminar jet angular rate sensor.

For the whiplash jet response, if it is assumed that the acceleration effects settle out before the rate sensor can respond, then the fluid in the sensor field takes on the solid body rotation of the sensor body with appropriate secondary motion as required by the governing equations. For no acceleration effect, the jet stream enters the field with a velocity relative to the field. This velocity is independent of the center of rotation of the sensor body. Experiments performed on an overscale hydraulic sensor gave the same response trace as shown in figures 13 and 15, whether the sensor was pivoted at the nozzle exit plane at the splitter or half way between the nozzle exit and the splitter. These results support the assumption that acceleration effects settle out before the sensor responds to rate input.

For this assumption, the whiplash response shown in figures 15 and 16 can be qualitatively examined. As noted in figure 3, the jet particles enter the field with a relative velocity and tend to move out of the former jet path shown in figure 21 by the dashed lines. The nozzle and the splitter also have moved in the time increment since the rate was applied.

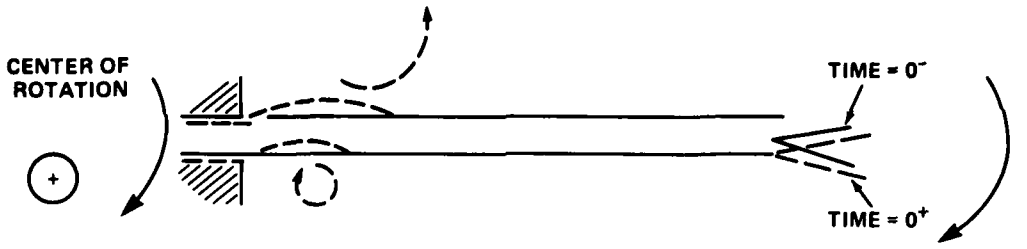

Figure 21. Transient jet particle path under step rate response; motion is frozen at time increment after step in rate was applied.

The jet stream is still continuous and includes particles that had left the nozzle before the rate was initiated. The resulting jet is as sketched in figure 21, and it gives rise to the formation of two large eddies. The leading eddy is formed as a result of the displacement of the jet in the field and is essentially a startup vortex. The law of conservation of angular momentum requires that the diameter of the eddy increase with decreasing edge velocity. Since the jet edge velocity decays downstream, it follows that the eddy increases in diameter. The starting vortex is formed on the opposite side of the jet from the signal eddy and, hence, it draws the jet particles across the instantaneous jet center line. This then accounts for the negative signal when that eddy reaches the splitter.

Considerable analysis is still required of both the amplitude dynamics and the phase dynamics of the LJARS. Correlation of step

response analysis to sinusoidal response predictions also is necessary. What is presented here is merely an engineering guide to design.

3. SENSOR DESIGN CONSIDERATIONS

This section deals with the analyses, the design guides, and the rules of thumb necessary to implement an LJARS in a system.

3.1 Operating Range

The operating range of the LJARS is determined by two limits. Primarily, the useful upper limit occurs at the onset of turbulence in the field. This has been established[12] for devices having fairly short nozzle-to-splitter distances ($8 \leq X_{sp} \leq 10$). The basic phenomenon of transistion to turbulence is complex and is buried in empiricism. However, for laminar jet devices, the phenomenon should follow the relation for the onset of instability where there exists a critical Reynolds number based on displacement thickness for each specified pressure gradient. Schlichting[15] discusses this at length, as does Hinze.[18] In principle, however, for low or almost zero pressure gradients, the result is

$$\frac{u_{max}\delta^*}{\nu} = 645 \ . \tag{66}$$

This value may be as low as 420. From equation (52b),

$$\frac{\delta^*}{b_s} \simeq 1.729 \left(\frac{X}{N_R}\right)^{1/2} \ .$$

We may thus establish a critical nozzle Reynolds number. X is the effective flat plate distance to the splitter, $X = X_{sp} + X_{eff}$ (effective length). X_{eff} is obtained from equations (15) and (16). This results in

$$XN_{R\ critical} \simeq 1.4 \times 10^5 \ . \tag{67}$$

---

[12] *F. Manion and T. Drzewiecki, Analytical Design of Laminar Proportional Amplifiers, Proceedings of HDL Fluidic State-of-the-Art Symposium, I, Harry Diamond Laboratories (October 1974).*

[15] *H. Schlichting, Boundary Layer Theory, McGraw-Hill Book Co., New York (1960).*

[18] *J. O. Hinze, Turbulence, McGraw-Hill Book Co., New York (1959).*

For $X_{sp} = 8$ and $X_{eff} = 2$, $X = 10$; this leads to a critical Reynolds number of 14,000, which is about 10 times too high. The adverse pressure gradient at the splitter should cause earlier transition. As we note from Schlichting,[15] the critical Reynolds number may easily be an order of magnitude lower in an adverse pressure gradient. Experiments have shown consistently that, for laminar devices, the relationship

$$\sigma N_{R\ critical} = 1400 \tag{68}$$

holds true with the condition that the flow entering the devices be free from noise or turbulence. (This requires a fairly smooth manifold, sect. 3.7.) For $\sigma = 1$, this would indicate that

$$XN_{R\ critical} = 1.4 \times 10^4$$

or

$$\sigma N_{R\ critical} = 1.4 \times 10^4 \frac{\sigma}{X} \quad . \tag{69}$$

σ can be replaced with an observed value for $\delta^*/b_s \simeq 0.06\sigma^{1/2}$ for $0.2 < \sigma < 4$ with equations (52b) and (69), which yields

$$\sigma N_{R\ critical} = \left[6(10^4)X_{sp}^2 + 8(10^6)\right]^{1/2} - 250X_{sp} \quad . \tag{70}$$

This is shown[19] plotted in figure 22. Now Hinze[18] states that, for Couette flow between parallel plates, the criterion for transition is

$$\frac{\bar{u}h}{\nu} = 1100 \quad . \tag{71}$$

Noting that $\bar{u} = c_d u_{max}$, $N_R = U_{max} b_s/\nu$ (where U is the mean or reference velocity), and $\sigma = h/b_s$,

$$\sigma N_R = \frac{1100}{c_d} \quad .$$

---

[15] *H. Schlichting, Boundary Layer Theory, McGraw-Hill Book Co., New York (1960).*

[18] *J. O. Hinze, Turbulence, McGraw-Hill Book Co., New York (1959).*

[19] *G. Roe, Fluidic Laminar Angular Rate Sensor Research Program, McDonnell Douglas, Titusville, FL, HDL-CR-75-020-1 (November 1975).*

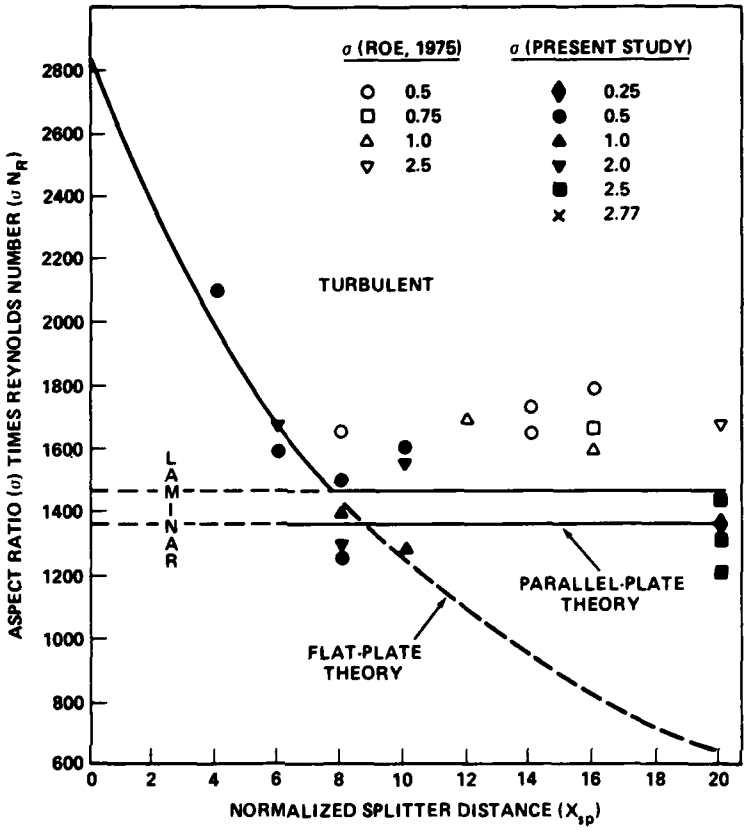

Figure 22. Critical Reynolds number as function of splitter distance.

At the point of transition, the discharge coefficient of short nozzles is on the order of 0.75 to 0.8, which leads to

$$1375 < \sigma N_R < 1470 , \tag{72}$$

which also is shown in figure 22. The flow must be stable if the Reynolds number is below the Couette flow critical number since all the flow is at or below that N_R. Hence, the flows that fall above both curves are transitional (or turbulent). For the range of interest, $X_{sp} \geq 8$, we may use the simple expression in equation (68). The rule of thumb that is used in the laboratory is

$$\sigma N_{R\ \text{transition}} = 1400 .$$

There is no effect of splitter distance until the splitter distance is less than 8; then the flow is more stable, as one might expect. The scatter of the data is due to aspect ratio variations. Recent experimental evidence correlates aspect ratio and the theoretical arguments of Manion and Drzewiecki.[12] This leads to a more universal parameter for transition wherein

$$\frac{c_d N_R}{\left(1 + \frac{1}{\sigma}\right)^2} = 200 \ .$$

Just before transition when the offset is bad, an LJARS tends to exhibit digital or erratic, albeit laminar, behavior. This clearly limits the useful range of such a device. Figure 23 shows a plot of differential output as a function of supply pressure for a device with poor offset characteristics. It is clear that the onset of turbulence occurs at about 14 in. of H_2O; however, it is undesirable to operate this device in the region where the change of output with supply pressure is so drastic and erratic. It is far more advantageous to operate on the flat portion between 8 and 10 in. of H_2O. This obviously means that the sensitivity will be lower at lower N_R. Experimental data indicate that a 30-percent backoff from critical N_R normally puts one in the range of acceptable performance. As shown in figure 23, a reduction of supply pressure by a factor of two from the transition point of 14 in. of H_2O (a 30-percent reduction in N_R) puts the device at 7 in. of H_2O, which appears to be a much better place.

For safe operation, therefore, we suggest a maximum operating Reynolds number defined by

$$\sigma N_R = 1000 \ . \qquad (73)$$

The lower limit must necessarily be defined by the user at the point below which the sensitivity is too low for use. As a rule, a 50-percent reduction of sensitivity may be acceptable. Figure 11 shows typical sensitivity as a function of Reynolds number for various devices. If the requirement for only 50-percent change in sensitivity is imposed, the device depicted by the left-most data may operate between $N_R' = 8$ and $N_R' = 7$ or a supply pressure change of only a factor of 1.3. This operation is caused primarily by the very long nozzle length, whose flow characteristics are extremely sensitive to change in N_R. On the other hand, a properly designed short nozzle configuration,

[12] *F. Manion and T. Drzewiecki, Analytical Design of Laminar Proportional Amplifiers, Proceedings of HDL Fluidic State-of-the-Art Symposium, I, Harry Diamond Laboratories (October 1974).*

while giving a similar rate sensitivity, demonstrates considerably less N_R sensitivity. Such a device may operate from as high as $N_R' = 120$ to as low as $N_R' = 75$, which is a factor of 2.56 in pressure or a good factor of 5 better in percentage than the latter case (156 versus 30 percent). This means that supply pressure regulation may not have to be as stringent a requirement.

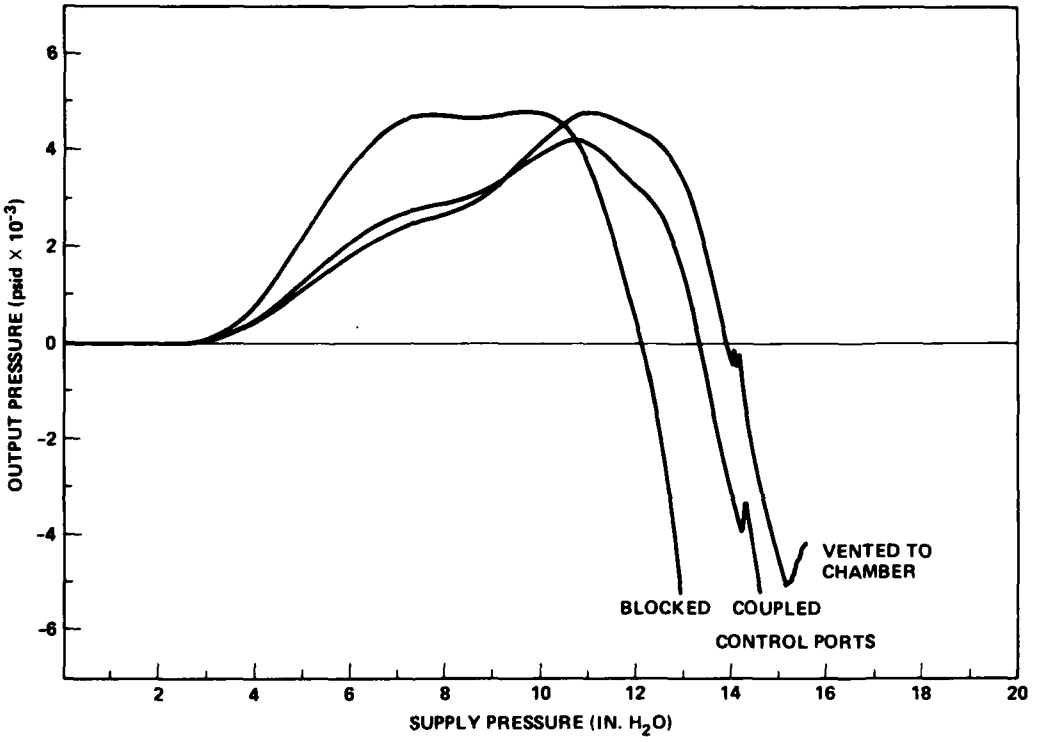

Figure 23. Null offset for early laminar jet angular rate sensor (from McDonnell Douglas (19)).

For engineering, we may allow N_R to vary by a factor of two (pressure, by a factor of four). (This incidentally corresponds to the Reynolds number change imposed when operating a pneumatic system between -55 and +80 C or -65 and +180 F.) We may thus arbitrarily define the LJARS operating range as

$$500 \leq \sigma N_R \leq 1000 , \tag{74}$$

and this is the range referred to.

3.2 Environmental Sensitivity and Compensation

Environmental sensitivity concerns itself with changes in operating characteristics due to changes in the environment. The environment consists of many different parameters such as temperature, pressure, contamination, noise, and other perturbations; this section considers only those effects that cause changes in the operating Reynolds number--temperature and pressure. The other effects are considered in later sections.

We briefly mention temperature effects in section 3.1 during the discussion of operating range. Temperature and pressure (altitude) affect the Reynolds number, $N_R = \rho b_s U_s / \mu$, through their influence on both density and viscosity. When the operating pressure or flow is held constant in an application, the Reynolds number changes due to the environmental changes. Viscosity changes with temperature, and density changes with temperature and pressure or altitude. The predominant effects are two-fold: (1) the sensitivity changes, and (2) the operating point moves with respect to the point of transition to turbulence. In any application, the limits of the Reynolds number must be determined, and the operating point must be set so that it falls within an acceptable range.

Changes in sensitivity are crucial in maintaining the stability of a feedback control system. Too much gain often is worse than not enough because the system can become unstable. Low gain prevents the system from functioning. Transition to turbulence increases the system noise, degrades the gain, and increases the threshold levels, perhaps to an undesirable point. Typically, the signal-to-noise ratio for turbulent devices may be as low as 50:1 as opposed to 10^6:1 for laminar devices.

To compensate an LJARS for temperature, one must either regulate the Reynolds number or change the gain outside the parameters of the LJARS operation.

Consider regulation of the Reynolds number when viscosity is changing. When constant mass flow, $\dot{m}$, is supplied to an orifice, $\dot{m}_o$, and a capillary, $\dot{m}_{ca}$, in parallel as shown in figure 24, the distribution of flow depends on the relative fluid viscosity and density since the resistance of the orifice depends on density only, whereas that of the capillary depends on viscosity only. As the viscosity increases (the temperature decreases in a liquid or increases in a gas), less flow passes through the capillary and, hence, more goes through the orifice. The equation for the conservation of mass is written for the resistor pair:

and

$$P = R_c \dot{m}_c = R_o \dot{m}_o = \frac{R'_o R'_c}{R'_o + R'_c} \dot{m} ,$$

so that

$$\dot{m}_o = \dot{m} - \dot{m}_c = \dot{m} - \frac{R'_o \dot{m}}{R'_o + R'_c}$$

or

$$\rho Q_o = \frac{\rho Q R'_c}{R'_o + R'_c} = \frac{\rho Q}{1 + \frac{R'_o}{R'_c}} , \qquad (75)$$

where

$$R' \equiv \Delta P / \dot{m} .$$

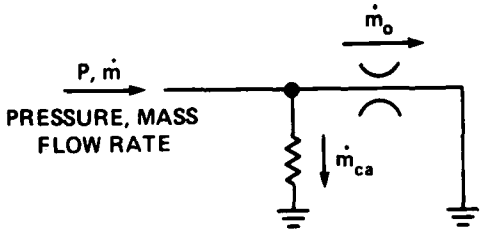

Figure 24. Parallel orifice (o)-capillary (ca) pair.

Now the orifice resistance depends on flow, $R_o = K_o \dot{m}_o$, orifice coefficient $K_o = (1/2) c_d^2 A^2 \rho$, and A is the area, so that

$$\dot{m}_o = \rho Q_o = \frac{R'_c}{K_o} \left[\left(\frac{1}{4} + \frac{K_o Q \rho}{R'_c} \right)^{1/2} - \frac{1}{2} \right] . \qquad (76)$$

As the viscosity (or R_c) increases, so does $\dot{m}_o$.

The ratio of the flow at one viscosity to that at another viscosity is

$$\frac{\dot{m}_{o1}}{\dot{m}_{o2}} = \frac{R_{c1}}{R_{c2}} \frac{\left(\frac{1}{4} + \frac{K_o Q\rho}{R'_{c1}}\right)^{1/2} - \frac{1}{2}}{\left(\frac{1}{4} + \frac{K_o Q\rho}{R'_{c2}}\right)^{1/2} - \frac{1}{2}} \quad . \tag{77}$$

In the limit as the capillary resistance becomes very small (one bypasses a large amount of flow around the orifice), $R_c << K_o \dot{m}$,

$$\frac{\dot{m}_{o1}}{\dot{m}_{o2}} = \left(\frac{R'_{c1}}{R'_{c2}}\right)^{1/2} \quad . \tag{78}$$

Capillary resistance is directly related to viscosity; hence,

$$\frac{\dot{m}_{o1}}{\dot{m}_{o2}} = \left(\frac{\nu_1}{\nu_2}\right)^{1/2} \quad . \tag{79}$$

Now the flow Reynolds number is defined as $\bar{N}_R = \dot{m}/h\mu$; hence, the ratio of two orifice Reynolds numbers is

$$\frac{\bar{N}_{R1}}{\bar{N}_{R2}} = \frac{\dot{m}_{o1}}{\dot{m}_{o2}} \frac{\mu_2}{\mu_1} \quad . \tag{80}$$

Substituting equation (79) into equation (80), therefore, yields

$$\frac{\bar{N}_{R1}}{\bar{N}_{R2}} = \left(\frac{\mu_2}{\mu_1}\right)^{1/2} \quad . \tag{81}$$

This result clearly indicates that, as viscosity increases, the Reynolds number still decreases; however, instead of decreasing linearly with the reciprocal of viscosity, it now decreases as the square root of that quantity. For a change in viscosity of a factor of four, the Reynolds number changes only a factor of two under this condition.

One cannot pay the penalty of infinite flow bypass, so that equation (82) must be used.

$$\frac{\bar{N}_{R1}}{\bar{N}_{R2}} = \left[\frac{\left(\frac{1}{4} + \frac{\dot{m}K_o}{R'_{c1}}\right)^{1/2} - \frac{1}{2}}{\left(\frac{1}{4} + \frac{\dot{m}K_o}{R'_{c2}}\right)^{1/2} - \frac{1}{2}}\right] \left(\frac{\rho_2}{\rho_1}\right) \quad . \tag{82}$$

We now recall equation (26) for the rate sensitivity of the LJARS that has an orifice-like supply nozzle,

$$S = \frac{2}{57.3} \frac{N_R}{c_d} \frac{P_{rec}}{P_s} ZO\mu \ ,$$

and we observe the ratio of two sensitivities at two viscosities,

$$\frac{S_1}{S_2} = \frac{N_{R1}}{N_{R2}} \frac{\left(\frac{P_{rec}}{P_s}\right)_1}{\left(\frac{P_{rec}}{P_s}\right)_2} \frac{ZO_1}{ZO_2} \frac{\mu_1}{\mu_2} \quad . \tag{83}$$

If we linearly approximate the pressure recovery in terms of Reynolds number (fig. 9) so that $P_{rec}/P_s = kN_R$, where k is a constant and assume that $ZO_1 = ZO_2$, then

$$\frac{S_1}{S_2} = \frac{N_{R1}^2}{N_{R2}^2} \frac{\mu_1}{\mu_2} = \left.\frac{\nu_2}{\nu_1}\right| \text{ no compensation} \quad . \tag{84}$$

In the best compensated case, equation (81), we substitute for $\bar{N}_{R1}/\bar{N}_{R2}$ (noting that $\bar{N}_R = c_d N_R$)

$$\frac{S_1}{S_2} = \left[\left(\frac{\mu_2}{\mu_1}\right)^{1/2} \frac{c_{d2}}{c_{d1}}\right]^2 \frac{\mu_1}{\mu_2} = \left(\frac{c_{d2}}{c_{d1}}\right)^2 \quad .$$

This says that, as the Reynolds number increases (c_d increases with N_R), sensitivity decreases. Since we have seen that a temperature-related Reynolds number increase cannot be halted entirely, then sensitivity can decrease. Without compensation, the sensitivity increases with increasing Reynolds number (increasing c_d). When one considers, however, that the supply nozzle of a sensor is not a pure orifice, that a shunt capillary is not a pure linear resistor, and that one cannot afford to shunt

an infinite amount of flow, then the amount of compensation is considerably reduced. This reduced compensation can be determined by solving the complete equation for the flow, equation (76). One can rewrite equation (76) for the Reynolds number, $N_R = \dot{m}_o/c_d h\mu$, and define ratios of viscosity, resistance, and discharge coefficient relative to some nominal conditions identified by subscript "o." Also, the total flow is held constant so that

$$\dot{m} = N_{Ro} c_{do} \mu_o h_o \left(\frac{R_o\big|_o}{R_c\big|_o} + 1 \right) ,$$

where

$$R_o\big|_o = K_o \dot{m}_o\big|_o .$$

We further define the ratio of nozzle resistance to shunt resistance at the nominal point $R_o/R_c\big|_o$. After considerable manipulation, equation (76) becomes

$$\frac{N_R}{N_{Ro}} = \left(\frac{R_c'}{R_o'} \right) \frac{c_d}{c_{do}} \left(\left\{ \frac{1}{4} + \frac{\mu_o}{\mu} \left(\frac{R_o'}{R_c'} \right)_o \left[\left(\frac{R_o'}{R_c'} \right)_o + 1 \right] \frac{c_{do}^2}{c_d^2} \right\}^{1/2} - \frac{1}{2} \right) . \qquad (85)$$

The universal equation for the discharge coefficient is given as equation (86) and shown in figure 25,

$$N_R' = \frac{2.667}{c_d} \left[\exp \left(6.6 c_d^2 \right) - 1 \right] , \qquad (86)$$

so that these two equations may be successfully iterated. An iterative computer program is given in appendix A. The result is perfectly general for all linear shunts (capillaries). Figure 26 shows the results generated from equations (85) and (86) for a nozzle with a high discharge coefficient, meaning that the linear portion is small. The efficacy of such a scheme can be observed. However, this compensation scheme is of no value when the nominal operating modified Reynolds number is low for a very long nozzle, such as 40 nozzle lengths. Figure 27 shows the nozzle Reynolds number as a function of shunt resistance, illustrating the futility of shunting in such a case. Even on an

expanded scale, little change is observed. (Merely using a constant flow source in itself compensates a little for viscosity changes. If pressure is held constant, when viscosity changes by a factor of five, so does the Reynolds number; however, at a constant flow, the same factor of five yields only a factor of four, as shown in figure 26. It does so due to a slight increase in supply pressure with increasing viscosity for constant flow due to an increased overall resistance.

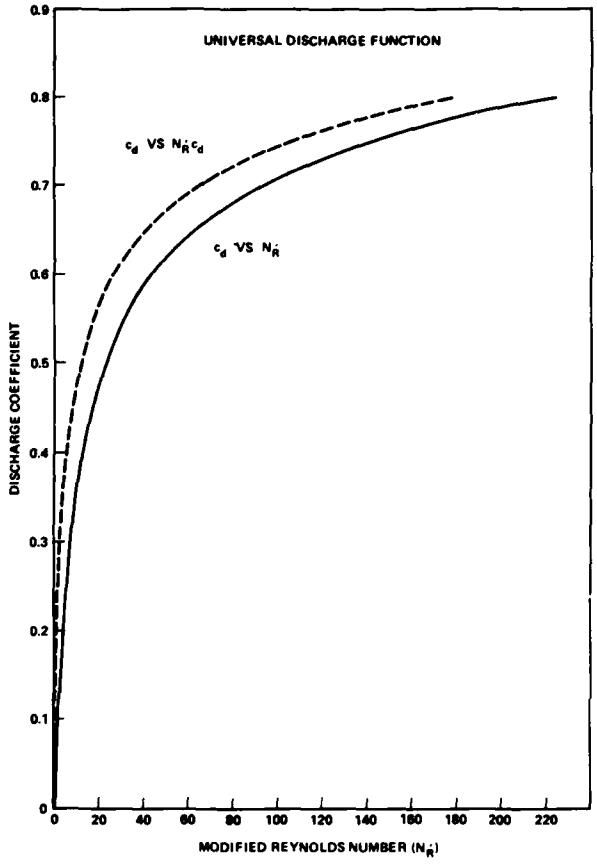

Figure 25. Universal discharge coefficient (c_d) function.

Figure 28 shows how kinematic viscosity changes for air and two types of hydraulic fluid. Hydraulic fluid dramatically changes in viscosity over a typical vehicular temperature range (6:1 to 17:1), whereas air changes less than a factor of two over the same range. When the rule of thumb is applied that the Reynolds number excursion can be kept to half the viscosity excursion, hydraulic fluid may still change from 3:1 to 8:1. In this manner, by compensating for viscosity changes, we compensate for changes in temperature.

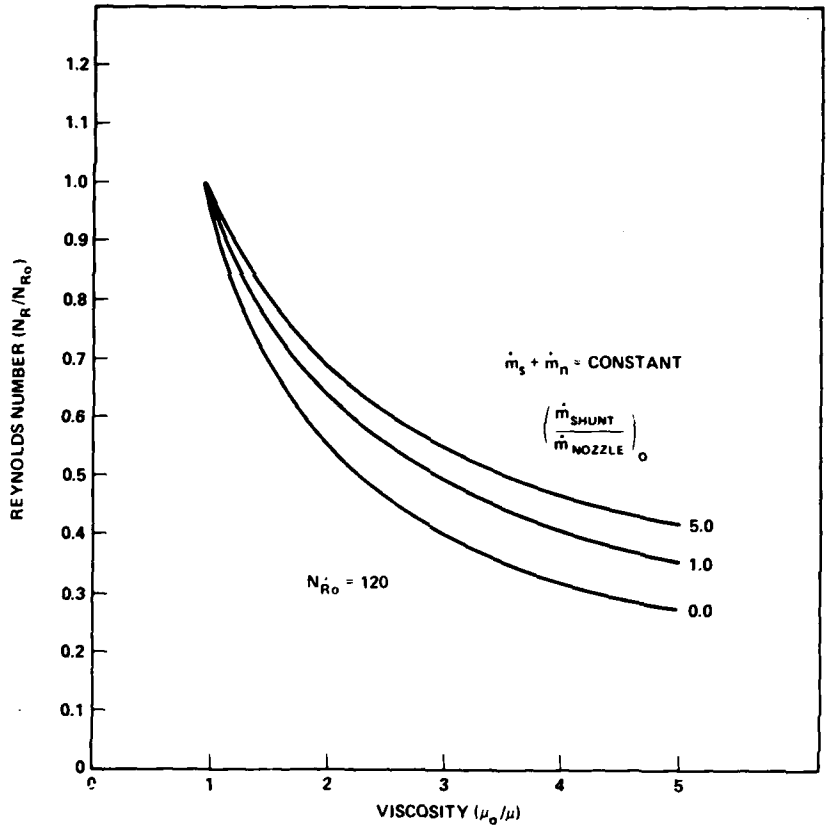

Figure 26. Change of Reynolds number (N_R/N_{Ro}) with viscosity (μ_o/μ) for different shunt resistances.

In figure 29, data show the amount of compensation possible with a shunt resistor roughly equal to seven times the room temperature nozzle resistance. When the flow and the temperature are high, the sensitivity can be reversed as predicted. In this case, at about 47 C, the shunt resistance is roughly equal to the nozzle resistance so that, above that temperature, reversal compensation occurs.

When viscosity decreases, LJARS sensitivity may be made to decrease. Also, among the typical gain characteristics of fluidic amplifiers, the gain increases with decreasing viscosity (an increasing modified Reynolds number) as shown in figure 30. It is therefore possible to achieve a flat or compensated net sensor-gain-block rate sensitivity over a wide band of temperatures.

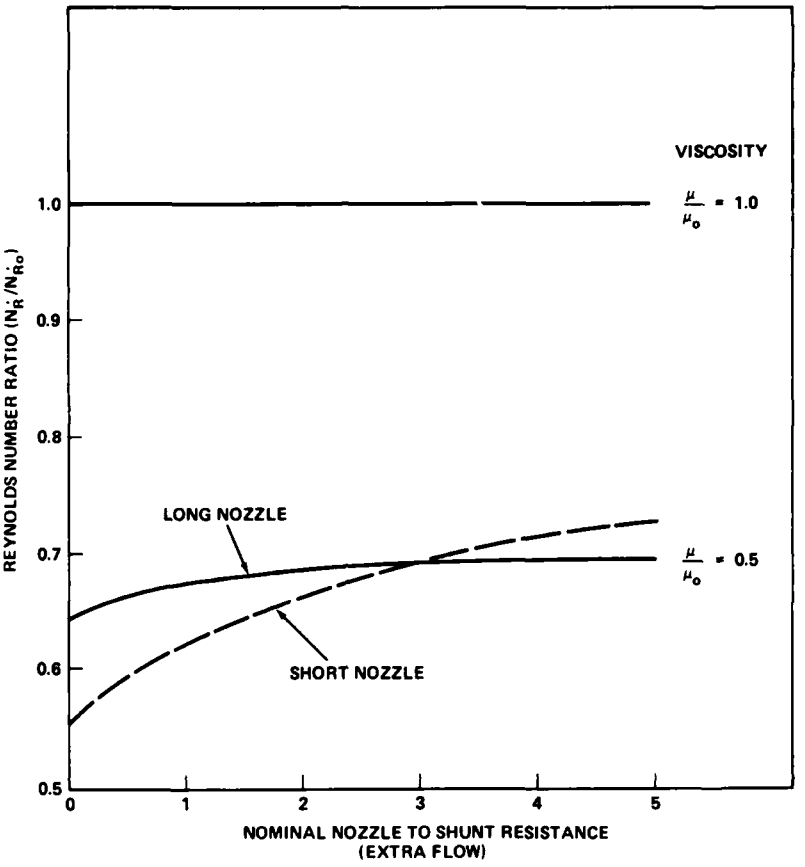

Figure 27. Effect of shunt temperature compensation on long nozzle.

In figure 31, a composite gain or sensitivity graph is determined from the gain data of figure 30 and compensated sensitivity from equation (84) and figure 26. The sensitivity of a pneumatic rate sensor is superimposed on (multiplied by) the gain of a three-stage gain block. As is evident, the range for a ±10 percent variation of an uncompensated system would be unacceptable; however, when the LJARS is compensated by using shunt flow, the system can operate over a ±60 C range (the military environment range) with less than a ±10 percent sensitivity variation. This type of design guide can be generated from the following rules of thumb:

a. The gain decreases are within 10 percent per stage if the Reynolds number decreases less than 50 percent from maximum for standard laminar proportional amplifiers (LPA's) (configuration in app A). (The gain increases 10 percent when the Reynolds number increases 100 percent from midrange.)

b. The net staged gain change is the product of the number of stages with the per-stage gain change.

c. The Reynolds number changes inversely with viscosity.

d. The military temperature range corresponds to a factor of two in viscosity for pneumatic systems.

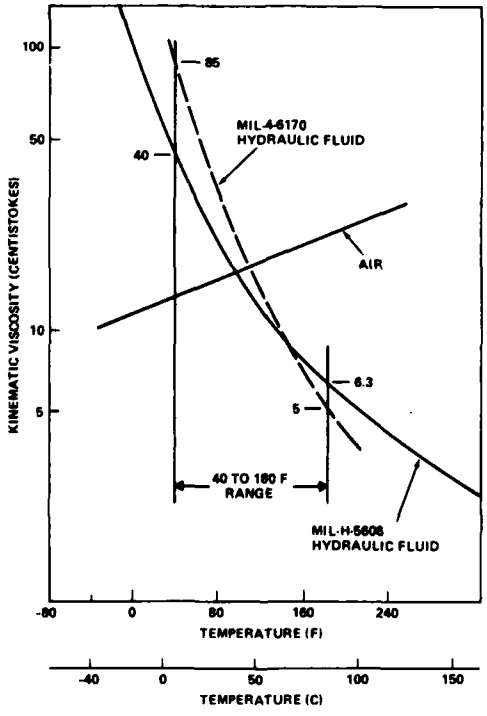

Figure 28. Viscosity versus temperature for various fluids.

It is of considerable benefit to have sensors and amplifiers that exhibit good orifice characteristics, not only from the standpoint of compensation, but also because they inherently are less sensitive to temperature change and have higher gain and better overall performance.

In conclusion of this section on temperature compensation, there are other methods to control the Reynolds number. Drzewiecki[20] reports a bimetallic resistive element designed to keep the Reynolds

[20] *T. M. Drzewiecki, Fluidic Resistive Element, U.S. Patent 3,980,103 (14 September 1976).*

number constant. Also, classical in gaseous systems is the use of a parallel orifice-capillary pair. The orifice resistance depends only on density, which decreases with temperature, and the capillary resistance depends on viscosity, which increases with temperature. In such a manner, there exists a region of temperatures in which the net parallel resistance is constant. Such passive compensation componentry is necessary when bridges and other ancillary circuitry are used with the LJARS and the LPA. Compensation of LPA's may be achieved by using operational amplifiers where the system gain depends on the ratios of feedback to input resistors (provided that there is sufficient forward gain). When these resistors both are of the same type, there is no compensation. When the feedback resistor depends on viscosity and the input depends on density, the gain varies with kinematic viscosity (increases with temperature in air). This gain may be shaped by appropriate selection of combinations of resistors. Mon[21] has demonstrated a constant gain (to ±10 percent) from modified Reynolds numbers of 20 to above 100 or a range of 5 to 1. The penalty to be paid here is the large number of amplifiers required to get the desired gain and, hence, increased complexity, size, and flow. Available on the market are temperature compensated flow controllers. Mechanical devices such as pressure and flow regulators may have their characteristics adjusted to provide some Reynolds number regulation. Mechanical, less reliable devices may have to be resorted to in the extreme cases of hydraulic fluid operation of from -40 to +80 C, for example. In such an event, the system reliability would be limited by such a device.

Changes in density may be compensated for by enclosing the system, pressurizing it, and allowing it to bleed to ambient conditions through a sonic orifice as suggested by the work at McDonnell Douglas.[19,22] In this manner, any pressure disturbances outside are not able to propagate into the system. This also successfully isolates the system from outside noise in addition to altitude changes. Care must be exercised, however, to insure that the sonic orifice does not itself generate noise due to turbulent flow upstream of the throat.

---

[19]*G. Roe, Fluidic Laminar Angular Rate Sensor Research Program, McDonnell Douglas, Titusville, FL, HDL-CR-75-020-1 (November 1975).*

[21]*George Mon, Flueric Laminar Gain Blocks and an Operational Amplifier Scaler, Harry Diamond Laboratories HDL-TR-1730 (December 1975).*

[22]*W. J. Westerman and R. E. Wright, Evaluation Program--Fluidic Laminar Rate Sensor--Final Report, McDonnell Douglas, Titusville, FL, NAVAIR LO252 (8 March 1974).*

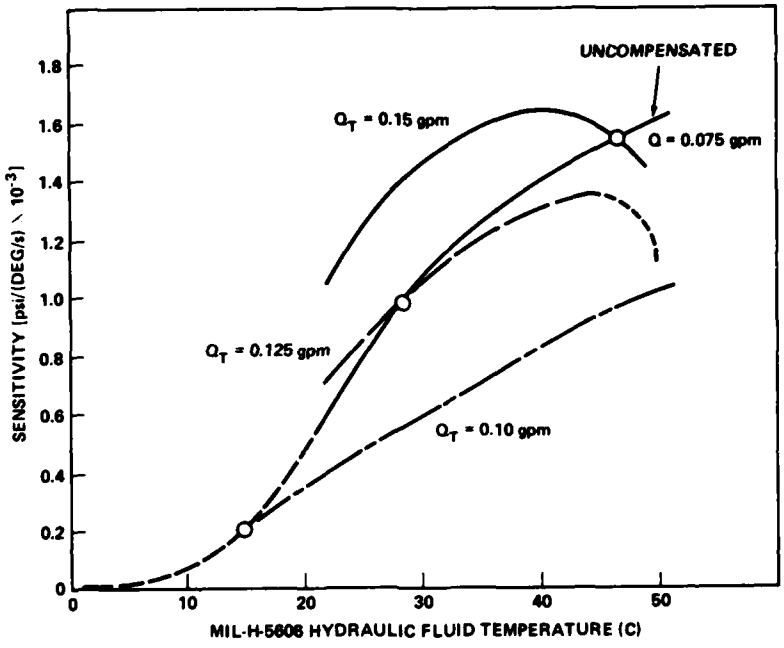

Figure 29. Temperature compensation of laminar jet angular rate sensor (LJARS): normalized splitter length = 20, supply width = 0.75 mm, aspect ratio = 2.5, and shunt resistance = 7 × LJARS supply resistance.

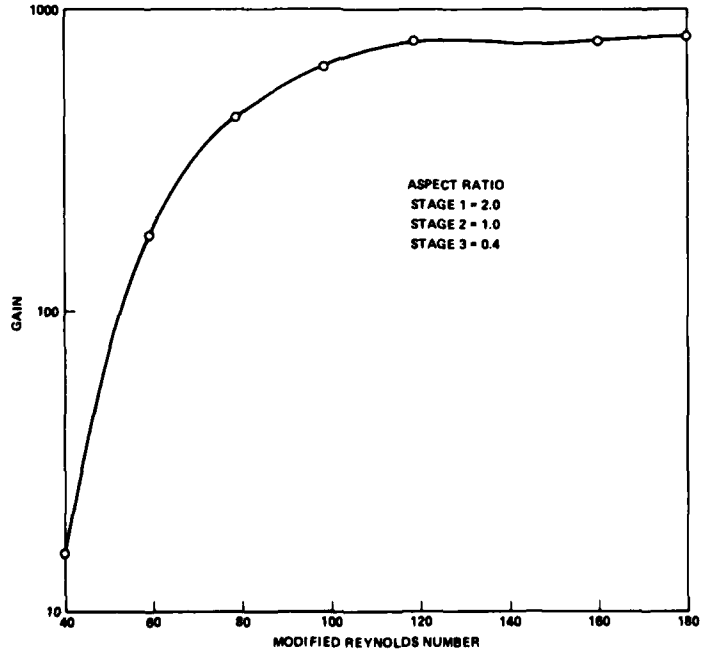

Figure 30. Three-stage amplifier gain.

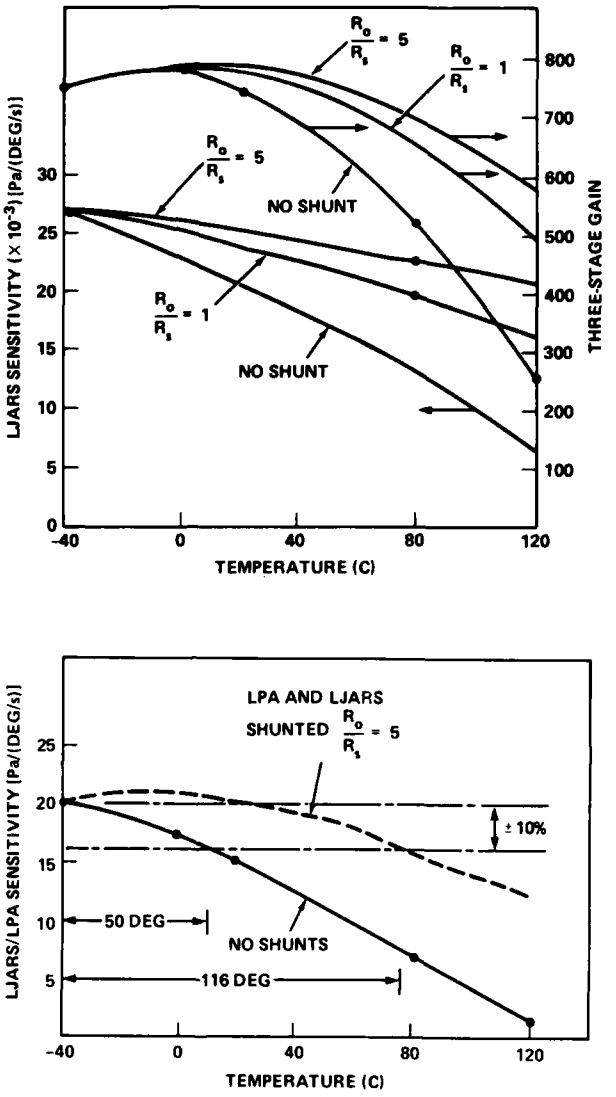

Figure 31. Temperature compensation by capillary shunt resistance of subsystem of laminar jet angular rate sensor (LJARS) and laminar proportional amplifier (LPA).

3.3 Shock and Vibration Sensitivity

As a follow on to environmental sensitivity, it is of interest to consider the effects of shock and vibration.

From a theoretical standpoint, shock and vibration constitute accelerations in axes perpendicular and parallel to the laminar jet. They act equally on all fluid particles in the region. As long as there exist no density gradients, the body forces produced act equally on all particles; thus, no net forces act on the jet. In addition, those accelerations along the jet axis and those perpendicular to the bounding planes produce body forces that are in the common mode to the outputs. They would not contribute any differential signal if the common mode rejection ratio (CMRR) were infinite. They may add some signal in the real case; however, since these forces do not move the jet, the CMRR for such a phenomenon is extremely high. In the cross axis, there exists the possibility of jet movement; however, since the structure, the field, and the jet move together again, no differential signals should appear. Rotational accelerations that are within the bandwidth of the device will be detected. In section 2.4, the bandwidth is discussed. From the typical frequency response of figure 20 and the analysis, we can estimate the bandwidth to be at least twice the -90 deg of phase shift frequency, probably more like 10 times. Since the LJARS measures rotational rate, however, it is reasonable that rotational shocks and vibrations should pass through. Alternatively, one can assume that noise or signals come from angular disturbances only.

As further demonstration that LJARS characteristics remain unchanged in vibrational environments, experiments were conducted at AiResearch[23] on pneumatic devices in the frequency range of 5 to 1000 Hz at an amplitude of 10 g, in all three orthogonal axes. These experiments showed no increase in noise whatever (as monitored on oscilloscopes) and no effect on gain. Analysis and experiments on an early design LJARS at General Electric[24] coupled with laminar amplifiers indicate no vibration sensitivity at 5 g from 5 to 2000 Hz. Shock loading of 12,500 g (nonoperational) did not alter characteristics of or damage the LJARS. The most susceptible regions are internal cavities that are excited by outside perturbations. In general, in both pneumatic and hydraulic operations, these resonances are at very high frequencies, greater than 5 kHz for devices with nozzle dimensions on the order of 1 mm.

---

[23] *M. Cycon, T. Sutton, and H. Gamble, Environmental Test Program for the Evaluation of Fluidic Elements, AiResearch Manufacturing Co. of Arizona, Phoenix, AZ, HDL-CR-75-187-1 (12 December 1975).*

[24] *V. Bravo, Feasibility Investigation of a Laminar Rate Sensor (LARS), Phase III Report, General Electric Co, Schenectady, NY, 71SD2118 (December 1971).*

3.4 Null Offset and Null Offset Compensation

Perhaps the most trying aspect of fluidics is the persistent presence of null offset as shown in figure 23. In an LJARS, this is a false rate signal. The primary causes of null offset are geometric asymmetries. If the jet is displaced relative to the outputs, there exists a differential output pressure. This displacement may be due to a misalignment of the splitter with the nozzle, or it may be due to an angular error of alignment of the nozzle axis with that of the splitter. From equation (59), it is apparent also that the recovered pressure depends on the output width. If the two outputs differ in area, then a pressure difference exists with no jet deflection. Unequal control resistance or edges lead to a differential pressure across the jet, which causes it to deflect. This deflection depends on gain, so that at low Reynolds numbers there is little deflection, and at high Reynolds numbers there is large deflection.

Deflection is caused also by asymmetric separation off uneven nozzle exit corners as described by Manion and Drzewiecki.[12] Composite diagrams of these effects are shown in figures 32 and 33. One may estimate the amount of offset by knowing such things as the percentage of the difference in output areas. From equation (59), it follows that there is a one-to-one relationship. The percentge of the difference in areas gives the percentage of the difference in recovered pressures.

It is not so simple with deflection, however. Consider that for an LJARS with $X_{sp} = 20$, full saturation occurs when the jet deflects $0.5b_s$ at the splitter; hence, a jet angle of 1/40 radians or 1.4 deg causes a pressure differential of twice the pressure recovery. Typical null offsets are 2 percent. Hence, the jet deflection is of the order of 0.03 deg or 0.5 mr. Such large null offsets in a high gain system can easily cause saturation in one or two stages.

For example, if the gain is 10^6 and the output saturation is 20 kPa, then an input of 2.0×10^{-5} kPa (0.02 Pa) causes saturation. A rate sensor operating typically at 50 Pa recovers at saturation about 20 Pa, but 0.02 Pa output saturates the gain block. Since this pressure of 0.02 Pa represents 1/1000 of the saturation pressure, a 0.1-percent offset is intolerable. So one needs an offset of less than at least 0.01 percent or 200 times less than normal offset. This is a jet deflection or a geometric alignment of less than 0.00015 deg or a displacement of the splitter of $0.0001b_s$ relative to the nozzle. For $b_s = 0.5$ mm, this represents the physically impossible tolerance requirement of 50 μm (2×10^{-6} in.).

---

[12] *F. Manion and T. Drzewiecki, Analytical Design of Laminar Proportional Amplifiers, Proceedings of HDL Fluidic State-of-the-Art Symposium, I, Harry Diamond Laboratories (October 1974).*

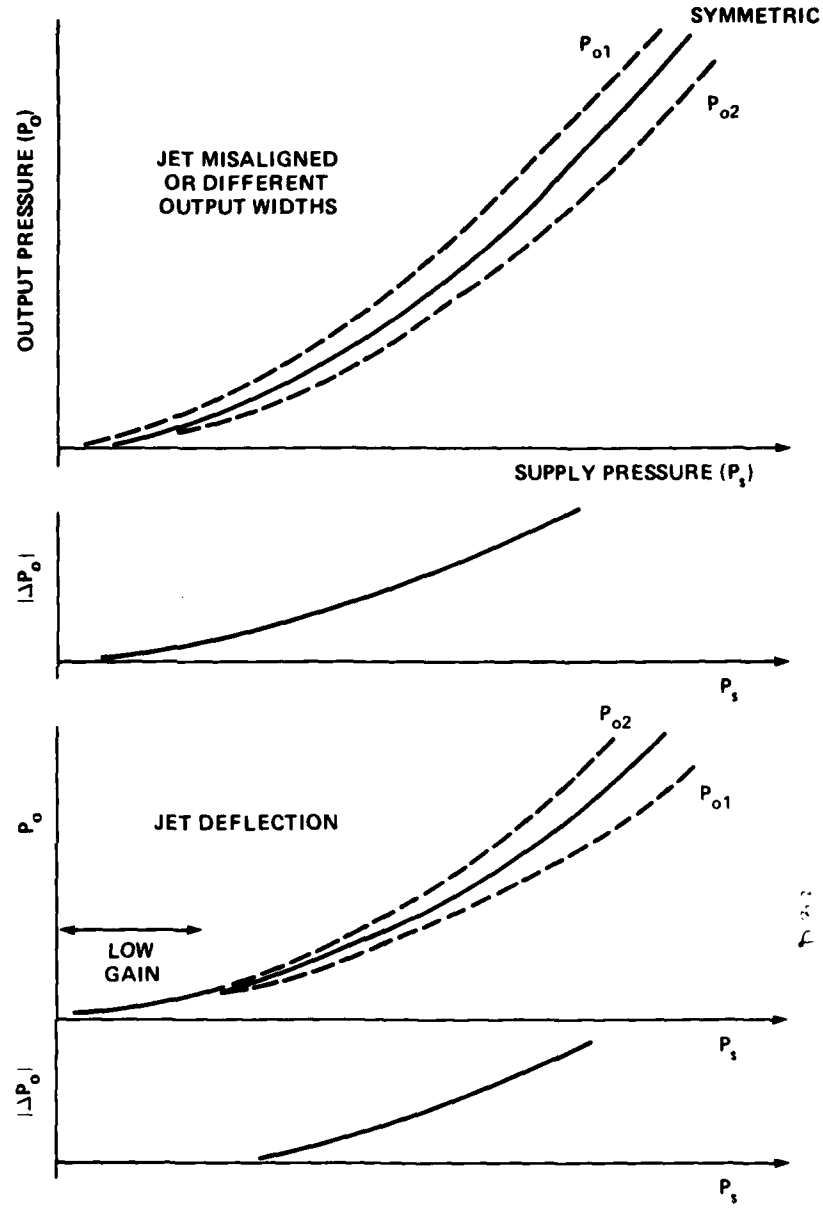

Figure 32. Typical output pressure versus supply pressure for separate causes of offset.

Many manufacturers have tried to make the devices symmetric. Standard format devices can be manufactured by exacting techniques such

as fine blanking[25] and, for large production runs, this appears to be a reasonable method. Since alignment of the nozzle and the splitter is crucial, vertically laminated devices as shown in figure 34 would aid symmetry. Capillary shunts are provided in one of the laminates to give temperature compensation. This method of fabrication closely follows that of O'Neal,[26] who proposed the stacked port amplifiers shown in figure 35. The improvement in null offset is nominally an order of magnitude, as shown in figure 36, where the null is referenced to the relative rate.

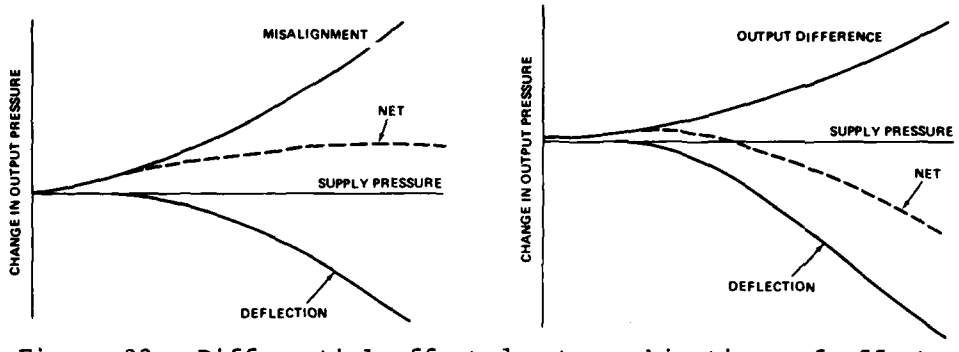

Figure 33. Differential offset due to combinations of effects.

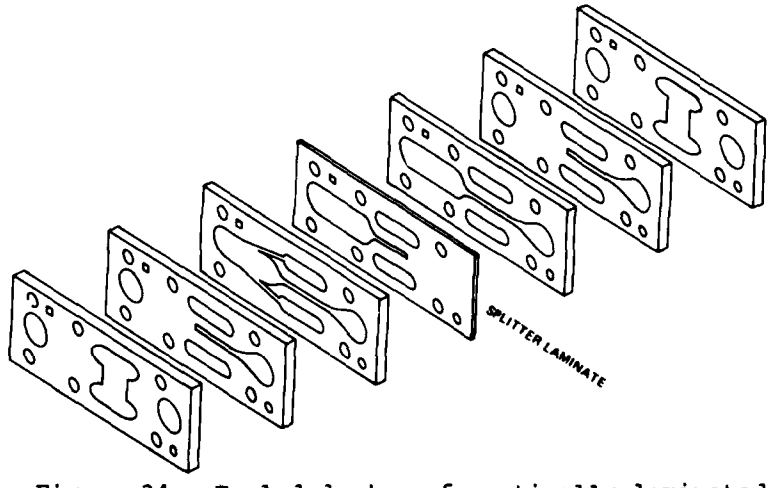

Figure 34. Exploded view of vertically laminated laminar jet angular rate sensor.

---

[25] *R. M. Phillippi, A Study of Fineblanking for the Manufacture of Flueric Laminar Proportional Amplifiers, Harry Diamond Laboratories HDL-TM-77-8 (May 1977).*

[26] *C. D. O'Neal, Stacked Port Fluidic Amplifier, U.S. Patent 3,468,331 (23 September 1969).*

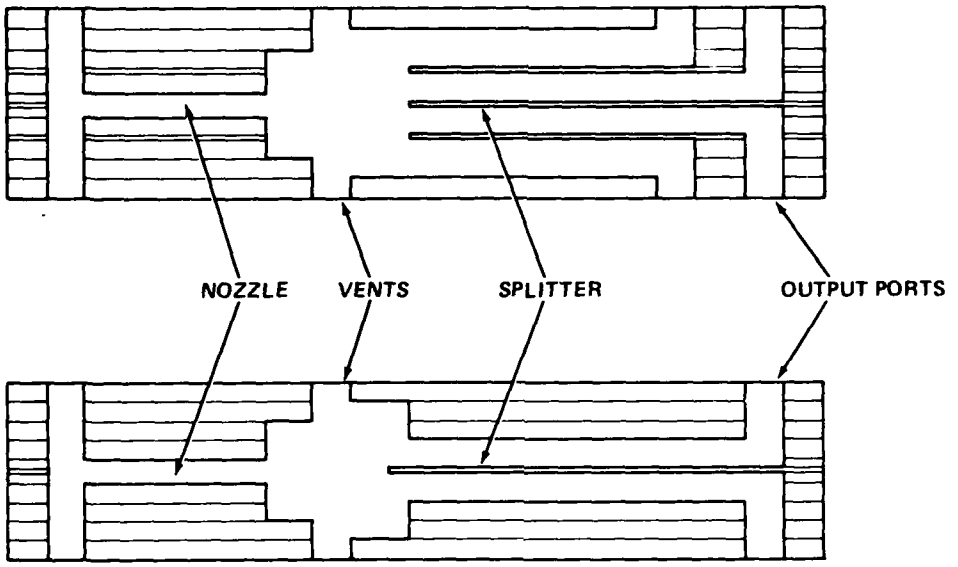

Figure 35. Vertically laminated fluidic amplifiers (after C. D. O'Neal, U.S. Patent 3,468,331, 23 September 1969).

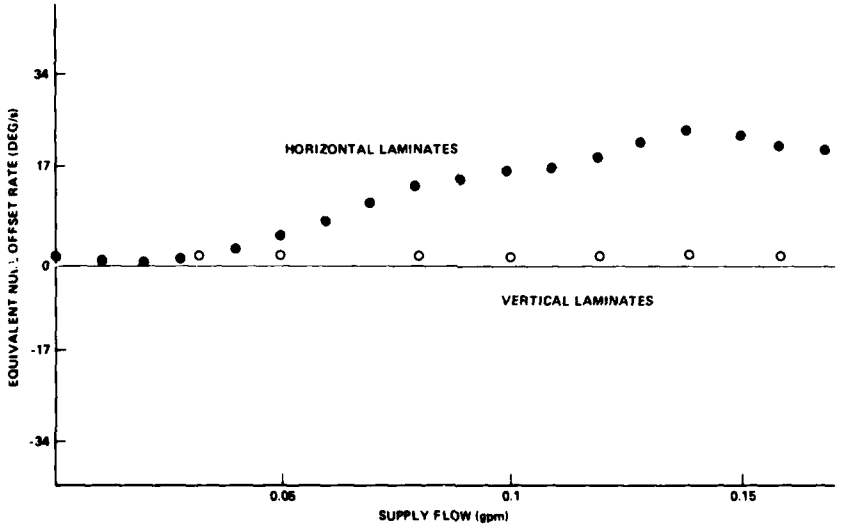

Figure 36. Horizontal and vertical laminate construction for null offset versus supply flow: MIL-H-5606 hydraulic fluid, saturation rate 900 deg/s, and threshold less than 0.1 deg/s.

More recently, another approach was tried. Recognizing that an output error exists, we fed this signal back through a resistive circuit to the inputs (negative feedback) and used the jet deflection gain to achieve a net attenuation. At about the same time, we tried a second approach that uses the flow difference generated between an orifice and a capillary to deflect the jet in a direction opposite to its null deflection (fig. 37). This technique requires matching resistors to the particular null characteristic at hand, although variable orifices (valves) and variable capillaries can be used to provide adjustments.

In yet another technique, we used the jet deflection augmentation principle. Equation (43) relates additional jet deflection to an initial displacement in the presence of control edges. When the bias control pressure is some positive value, the transfer function is less than unity. More simply, equal bias acts as a suppressor of jet deflection. This is intuitively obvious when one recognizes that deflection gain decreases with increasing bias. Bias flow straightens the jet out between the control edges and gives dramatic feedback results.

O'Keeffe[27] considered the problem of multistage fluidic elements. The offset of the first stage dominates in that it is multiplied by the gain of the later stages. By use of high resistance feedback in only the first stage (to prevent overall loss of gain), O'Keeffe reduced overall three-stage LPA offsets of 40 percent to less than 2 percent. More important, the absolute offset was kept constant with supply pressure as shown in figure 38. As a side benefit, the range of constant gain was improved by a factor of two. In figure 39, the original gain change is over 30 percent for a Reynolds number change of a factor of two (140:70), as is expected by application of the first rule of thumb in section 3.2. With null compensation, the gain change is less than 15 percent over the same 100-percent Reynolds number range. The useful range of a 10-percent change in gain is extended for the gain block from N_R' of 110 to 140 to N_R' of 85 to 140. This latter is the same change in the Reynolds number that one would expect of an uncompensated nozzle in pneumatic operation over a temperature range of -40 to +80 C. Performance is considerably superior at higher aspect ratios, that is, $\sigma > 1$. The amount of null attenuation by error feedback is minimal. The basic effects are those of the bias level and the induced differential flow through unequal feedback resistances. (See fig. 39, p. 71.)

The important contribution of this research is that there exist a temperature and a null compensation with a single circuit that do not consume any additional flow or power and that do not depend on power supply.

---

[27] *D. O'Keeffe, Null Offset Compensation of Fluidic Amplifiers Using External Negative Feedback, Proceedings of HDL Student Technical Symposium, Harry Diamond Laboratories (August 1978).*

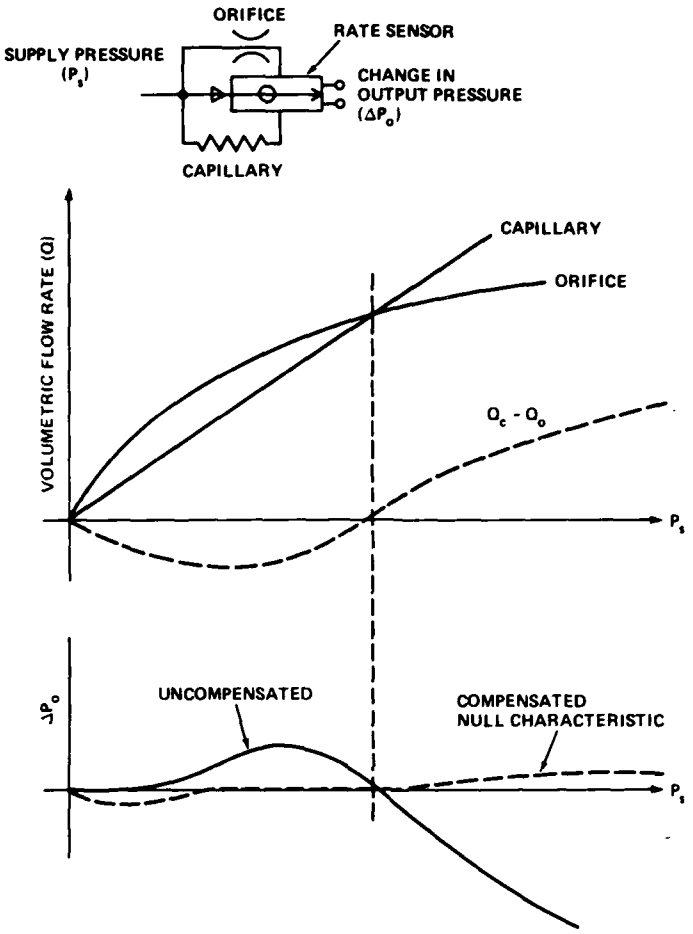

Figure 37. Null offset compensation of laminar jet angular rate sensor by orifice-capillary control bias.

Other techniques that have been tried include bending, vanes in the supply, movable obstructions in the jet, and variable in-line resistors between the sensor and the gain block.

In conclusion, circuit techniques such as bias control and feedback have the best chance of universal application due to their simplicity and performance. The mechanical techniques may tend to be susceptible to vibration environments and be less reliable due to moving parts. Bending in itself has shown to be susceptible to thermal stressing due to gradients. In-line resistors yield unequal response in different directions. With better fabrication techniques, null is not an insurmountable problem.

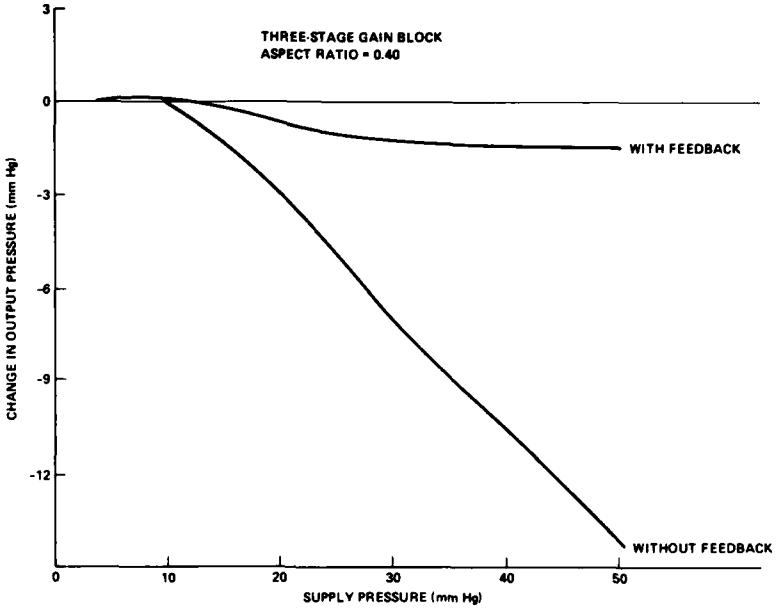

Figure 38. Effect of feedback compensation on null offset.

3.5 Drift and Drift Compensation

Drift is closely related to variation of null offset (sect. 3.4). Drift is essentially the change of output level as a function of time. The time rate of change of output, therefore, is the critical parameter. Since output can change with other variables, we write the total derivative as

$$\frac{d\Delta P_o}{dt} = \frac{\partial \Delta P_o}{\partial P_s}\frac{dP_s}{dt} + \frac{\partial \Delta P_o}{\partial T}\frac{dT}{dt} + \frac{\partial \Delta P_o}{\partial Q_s}\frac{dQ_s}{dt} + \frac{\partial \Delta P_o}{\partial \chi}\frac{d\chi}{dt} \quad , \tag{87}$$

where the offset depends on supply pressure, flow, temperature (T), and other causes, χ. All these effects are Reynolds number effects; hence, each term can be written in terms of the Reynolds number as

$$\frac{d\Delta P_o}{dt} = \frac{\partial \Delta P_o}{\partial N_R}\left(\frac{\partial N_R}{\partial P_s}\frac{dP_s}{dt} + \frac{\partial N_R}{\partial Q_s}\frac{dQ_s}{dt} + \frac{\partial N_R}{\partial T}\frac{dT}{dt} + \frac{\partial N_R}{\partial \chi}\frac{d\chi}{dt}\right). \tag{88}$$

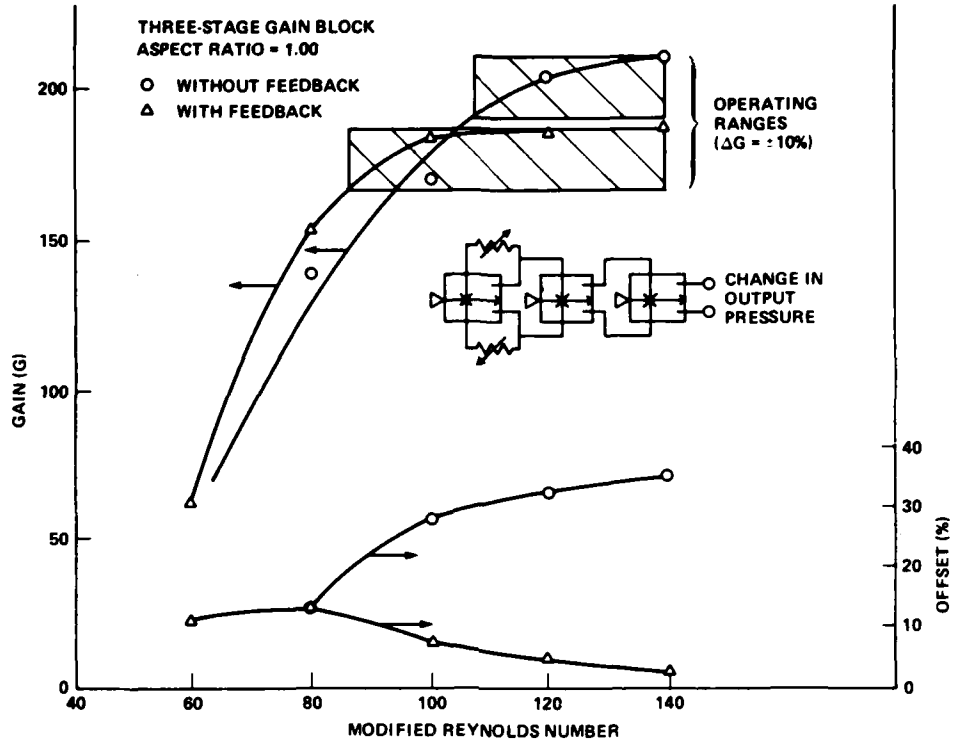

Figure 39. Effect of feedback compensation on laminar proportional amplifier gain and percentage of null offset.

When N_R varies with T due to $\mu(T)$ and $\rho(T)$, then

$$\frac{d\Delta P_o}{dt} = \frac{\partial \Delta P_o}{\partial N_R}\left\{\frac{b_s}{2\mu}\left(\frac{2\rho}{P_s}\right)^{1/2}\frac{dP_s}{dt} + \left(\frac{1}{c_d h\nu} - \frac{Q_s}{c_d^2 h\nu}\frac{dc_d}{dQ_s}\right)\frac{dQ_s}{dt}\right.$$

$$\left. + \left[-\frac{b_s}{\mu^2}\left(2P_s\rho\right)^{1/2}\frac{d\mu}{dT} + \frac{b_s}{2\mu}\left(\frac{2P_s}{\rho}\right)^{1/2}\frac{d\rho}{dT}\right]\frac{dT}{dt} + \frac{\partial N_R}{\partial \chi}\frac{d\chi}{dt}\right\}. \quad (89)$$

If the supply pressure or the flow is held constant (by regulation, etc.), then the drift reduces to a problem in temperature compensation. It can be reduced by temperature regulation or by minimization of offset as before. Figures 38 and 39 show what can be

achieved in the way of offset reduction so that, if offset is reduced to a constant, no drift occurs, and a circuit needs only a constant additive term to compensate it. Operating with fluid with small thermal changes in properties, such as air, may be advantageous. However, if the LJARS output is amplified by n stages of amplifiers of equal gain, G_{po}, then

$$\Delta P_o = nG_{po}\Delta P_{o\ LJARS} \cdot \tag{90}$$

The rate sensitivity of a hydraulic LJARS is higher than that of a pneumatic LJARS by the ratio of absolute viscosities (which is about 1000). So a pneumatic LJARS requires 1000 times more gain to drive the same load. If the percentage of offset, $\Delta P_o/P_s$, is the same out of each LJARS, then

$$\frac{\Delta P_{o\ oil}}{\Delta P_{o\ air}} = \frac{G_{p\ oil}}{G_{p\ air}} \frac{\Delta P_{o\ LJARS\ oil}}{\Delta P_{o\ LJARS\ air}} = \frac{G_{p\ oil}}{G_{p\ air}} \frac{\left(\frac{\Delta P_o}{P_s}\right)_{oil}}{\left(\frac{\Delta P_o}{P_s}\right)_{air}} \frac{P_{s\ oil}}{P_{s\ air}} \tag{91}$$

or

$$\frac{\Delta P_{o\ oil}}{\Delta P_{o\ air}} = \frac{G_{p\ oil}}{G_{p\ air}} \frac{P_{s\ oil}}{P_{s\ air}} \cdot \tag{92}$$

When both are operated at the same modified Reynolds number,

$$\frac{P_{s\ oil}}{P_{s\ air}} = \frac{\rho_{air}}{\rho_{oil}} \left(\frac{\mu_{oil}}{\mu_{air}}\right)^2 \left(\frac{b_{s\ air}}{b_{s\ oil}}\right)^2 \cdot \tag{93}$$

Typically, one uses the same size devices; hence, $b_{s\ oil}/b_{s\ oil} = 1$. Since $G_{p\ oil}/G_{p\ air} = \mu_{air}/\mu_{oil} \sim 1/870$, then

$$\frac{\Delta P_{o\ oil}}{\Delta P_{o\ air}} = \frac{\mu_{oil}}{\mu_{air}} \frac{\rho_{air}}{\rho_{oil}} = \frac{\nu_{oil}}{\nu_{air}} \cdot \tag{94}$$

If the kinematic viscosities are the same, there is no difference in net offset. The design rule, therefore, is not to introduce more gain than necessary to overcome the difference in absolute viscosity.

Typically, an LJARS may exhibit an offset of 2 percent at 100 percent of operating pressure or $\partial\Delta P_o/\partial P_s \approx 0.02$. If a typical regulator can hold only ±2 percent of a set pressure, then $\partial P_s/\partial t = 0.02/\tau$. This value of $\partial\Delta P_o/\partial P_s$ is related only to the inverse of the CMRR where

$$\text{CMRR} = \frac{\left(\frac{\partial\Delta P_o}{\partial\Delta P_c}\right)}{\left(\frac{\partial\Delta P_o}{\partial P_c}\right)} = \frac{G_p}{\left(\frac{\partial\Delta P_o}{\partial P_c}\right)} \quad .$$

Change of P_c at a constant supply has the same effect as holding the control constant and changing the supply or

$$\frac{\partial\Delta P_o}{\partial P_c} \approx \frac{-\partial\Delta P_o}{\partial P_s} \quad ,$$

since it is merely a change of bias.

Therefore, there are two basic means of controlling drift: reduction of offset and reduction of supply variations. The reduction of offset has already been considered. The reduction of supply variations is not within the scope of this project; however, typical solutions use multiple regulators in series, bottled gas, precisely controlled electric motor driven pumps, and feedback controllers.

3.6 Dynamic Range and Maximum Rate

The dynamic range of a device is defined by the ratio of the input signal that causes saturation or maximum output to the input signal that causes the first perceptible output signal. For a device with a constant gain, this is the same as the ratio of saturation output level to output noise level. Ever since the inception of laminar fluidic devices, the concept of noise has been of concern. Theoretically, a laminar flow has no noise in and of itself; hence, the theoretical dynamic range limit for an LJARS or an LPA is infinite. Laboratory experiments during this project have shown that an LPA can have dynamic ranges in excess of 10^6. However, to meaningfully establish the dynamic

range of an LJARS, one must be able to predict its maximum rate and noise.

The maximum rate that can be sensed by an LJARS is that which produces a jet deflection at the splitter that gives a maximum recovered pressure. Drzewiecki[16] has shown that the maximum output of one port is twice the jet centered pressure recovery; hence, the maximum differential pressure in one direction is two times the jet centered pressure recovery for one output port.

$$\Delta P_{o\ max} = 2P_{rec} \quad . \tag{95}$$

The rate sensitivity is defined as

$$S = \frac{\Delta P_o}{\dot{\theta}} \quad .$$

Hence, the rate at which maximum recovery is attained is

$$\dot{\theta}_{max} = \frac{2P_{rec}}{S} \quad . \tag{96}$$

When the result from equation (26) is substituted into equation (96), the result is (in degrees per second)

$$\dot{\theta}_{max} = \frac{57.3 c_d \nu N_R}{2 b_s^2 ZO} \quad . \tag{97}$$

When $ZO = X_{sp}^2/2$ (an efficient nozzle at a high Reynolds number), we use the result of the frequency at a phase shift of -90 deg from equation (65) so that

$$\dot{\theta}_{max} = \frac{16(57.3)}{X_{sp}} f_{90} \quad . \tag{98}$$

This result indicates that the maximum rate is directly related to the frequency response.

---

[16] *T. M. Drzewiecki, Fluerics 38: A Computer Aided Design Analysis for the Static and Dynamic Port Characteristics of Laminar Proportional Amplifiers, Harry Diamond Laboratories HDL-TR-1758 (June 1976).*

For the LJARS considered in figure 12, operating in hydraulic fluid, an operating rate sensitivity is 2×10^{-3} psi/(deg/s). That same device exhibits a bandwidth $f_{90} \sim 12$ Hz as shown in figure 19 and computed from equation (65) when $X_{sp} = 20$, $b_s = 0.9$ mm, $N_R = 400$, $c_d = 0.5$, and $\nu = 1.8 \times 10^{-5}$ m^2 s. Therefore, the maximum rate that can be observed is 550 deg/s if the device is linear up to saturation. Figure 40 shows the output signal and corresponding noise levels for the same LJARS in response to various levels of rate input. The output is significantly identifiable when the input rate is as low as 0.1 deg/s. The noise level is roughly one-third that output; hence, one should be able to discriminate a signal of one-sixth the input or about 0.02 deg/s. This signal results in a dynamic range of 27,500 and is of the same order of the dynamic range of 14,000 reported by Young.[11]

Most noise cancels out in the differential mode by virtue of the CMRR of a device. If the outputs are close together, then the noise of the system is imposed simultaneously on both and causes a zero differential signal. However, there exists a finite CMRR and also a nonzero gradient of output differential pressure with supply pressure. Typical values of $\partial \Delta P_o / \partial P_s = 0.02$ are discussed in section 3.5. Noise can be at any point of the frequency spectrum; hence, drift may be merely the low-frequency component due to supply noise. It follows that the minimum signal that can be discerned is half the noise level divided by the sensitivity (or the equivalent rate of half the noise).

$$\dot{\theta}_{min} = \frac{0.5 \Delta P_o \big|_{noise}}{S} \quad . \tag{99}$$

The noise level due to a fluctuating supply is approximately

$$\Delta P_o \big|_{noise} \approx \frac{\partial \Delta P_o}{\partial P_s} \Delta P_s \quad ,$$

where ΔP_s is the amplitude of the change of the supply or the degree to which one can regulate the supply pressure or flow. Therefore, the dynamic range, D_R, is

$$D_R = \frac{\dot{\theta}_{max}}{\dot{\theta}_{min}} = \frac{16(57.3) f_{90} S}{X_{sp} 0.5 \frac{\partial \Delta P_o}{\partial P_s} \Delta P_s}$$

[11] *R. Young, Development of a Laminar Angular Rate Sensor (LARS), Proceedings of HDL Fluidic State-of-the-Art Symposium, II, Harry Diamond Laboratories (October 1974).*

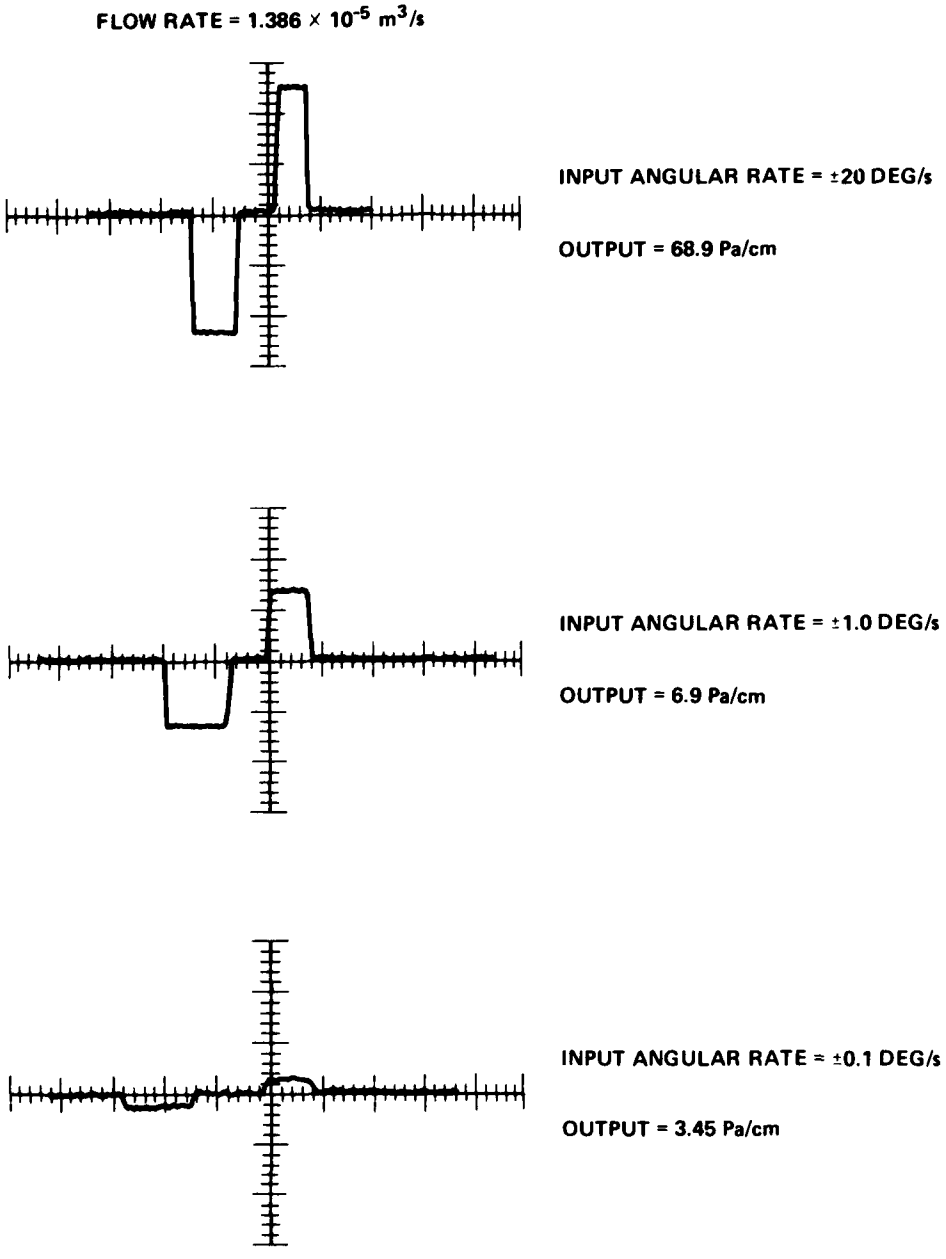

Figure 40. Oscilloscope traces of output of hydraulic laminar jet angular rate sensor in response to different angle rates.

or

$$D_R = \frac{1835 f_{90} S}{X_{sp} \frac{\partial \Delta P_o}{\partial P_s} \Delta P_s} \quad . \tag{100}$$

But the CMRR is merely the pressure gain divided by the supply sensitivity (sect. 3.5); hence,

$$D_R = \frac{1835 f_{90} S(CMRR)}{X_{sp} G_p \Delta P_s}$$

or

$$D_R = 4 \left(\frac{P_{rec}}{P_s} \right) \left(\frac{P_s}{\Delta P_s} \right) \frac{CMRR}{G_p} \quad . \tag{101}$$

For the above problem, $f_{90} = 12$ Hz, $S = 2 \times 10^{-3}$, $X_{sp} = 20$, CMRR ~ 400,[23] $G_p \sim 10$, $\Delta P_s = 0.005$ psi, and $D_R = 1.75 \times 10^4$. The supply pressure is about 5 psi; hence, the regulation requirement is ±0.1 percent to maintain dynamic range. The amount of noise suppression or supply regulation required for a given dynamic range can be determined from equation (101) so that

$$\frac{\Delta P_s}{P_s} = \frac{1835 f_{90} S(CMRR)}{X_{sp} G_p D_R P_s} = \frac{4}{D_R} \left(\frac{P_{rec}}{P_s} \right) \frac{CMRR}{G_p} \quad . \tag{102}$$

For example, to obtain a dynamic range of 10^6 as in the LPA experiments, three regulators and a very large tank are used in series to supply the device. From equation (102), for a typical LJARS to have the same $D_R = 10^6$, $\Delta P_s/P_s = 1.5 \times 10^{-5}$ or a regulation to ±0.0015 percent of nominal supply pressure over the entire bandwidth of amplitude response or roughly 120 Hz in this case. A tank or an accumulator can be tuned as a low pass filter to a low enough frequency to take out all high frequencies. The regulators act to take out low-frequency components if they are good enough.

Most mechanical regulators have a typical suppression ratio of about 1000. For example, a 100-kPa change in upstream pressure results in a change of only 0.1 kPa at the load. Hence, two in series cause a suppression of 10^6. Thus, changes at the compressor, the pump, or another supply can virtually be eliminated. Typically, when the load

[23] M. Cycon, T. Sutton, and H. Gamble, *Environmental Test Program for the Evaluation of Fluidic Elements, AiResearch Manufacturing Co. of Arizona, Phoenix, AZ, HDL-CR-75-187-1 (12 December 1975).*

resistance changes, as when the temperature changes, pneumatic regulators do not respond until a ±0.2-mm-Hg change occurs at best. Consequently, the regulator appears as a resistance in series with a variable resistance. If the load is predominantly an orifice, as is the regulator, then there is little relative change in resistance ratio and the supply pressure is unaffected. If, on the other hand, the load is predominantly a viscous restriction, then there can be appreciable variation in the pressure division and the supply pressure to the load. Typically, however, most LPA's and LJARS's may be considered as orifices; hence, changes with temperature should not change the supply pressure significantly. One can see the difficulty of using long-nozzle devices.

In most mechanical regulators, an absolute value of pressure is required to overcome friction, which is about ±0.2 mm Hg regardless of the pressure regulated. The higher the nominal pressure, the better the percentage of regulation. The pneumatic rate sensor and the amplifier described in figures 30 and 31 require a minimum supply pressure of 0.5 mm Hg to the rate sensor and a maximum of 20 mm Hg to the last amplifier stage. The pressure regulation can be kept to ±0.2 mm Hg so that the rate sensor supply varies at most 0.005 mm Hg when the pressure is divided through a series of resistors. The dynamic range from equation (101) therefore is greater than 1.75×10^3 when CMRR = 400 and the regulation is 1 percent. For a regulation to ±0.1 percent and an increase in the CMRR to 4000, the dynamic range exceeds 1.75×10^5. Such regulation and CMRR are not too difficult to achieve with present techniques.

To improve the response or the sensitivity by elimination of friction due to moving parts of a regulator, one may use a fluidic regulator. This is a high-gain amplifier with negative feedback. The regulation is limited by the available forward gain. An operational amplifier saturated to one side may be used to deliver constant pressure. The penalty for such operation is flow consumption. In an air-driven system, flow may not be a problem whereas, in a hydraulic system, flow is generally at a premium.

3.7 Power Supply Considerations

We have already discussed power supply requirements in the sections dealing with environmental effects, offset, drift, and dynamic range. It remains only to discuss contamination and the implementation of the required power supplies. Unfortunately, the design of fluidic power supplies has been generally neglected. Fluidic circuits have been expected to operate and have operated in near-impossible conditions such as, for example, the DC-10 aircraft thrust reverser control that operates off compressor bleed air in the jet engine environment.[28] However,

[28] *T. Sutton and W. Anderson, Aerospace Fluidics Applications and Circuit Manufacture, Proceedings of HDL Fluidic State-of-the-Art Symposium, V, Harry Diamond Laboratories (October 1974).*

when one must operate a precision control circuit, as with a platform stabilization system, attention must be paid to the power supply. Considerable attention has been paid to contamination effects and means of control.[29-32] The basic conclusion that can be drawn from these reports is that a laminar fluidic circuit operating on well-filtered air has a mean time to failure (MTTF) of about 25,000 hr; a hydraulic circuit has about 50,000 hr. This is equivalent to over 3 years of continuous duty and 30 years on a 10-percent duty cycle. Failures are nearly all attributable to clogging[33-35] and, hence, are reversible.

In general, power supplies are categorized as mechanical, chemical, and storage.[36] Mechanical devices are all manners of pumps, compressors, fans, and engine bleed. These are the typical sources of fluidic power for continuous duty fluidic systems. Chemical supplies require a reaction of sorts, and the gaseous products of combustion or reaction are used as the working fluid. These are generally one-shot supplies. Storage supplies are in effect fluidic rechargeable batteries. These include bottled gas, liquefied gas, and pneumatically pressurized hydraulic accumulators. These storage power supplies provide the most uniform quiet flow and are well suited to precision work. Used with a mechanical device to provide intermittent recharging, these supplies offer the best solution to long-time power supply for sophisticated circuitry, provided that the flow consumption is not excessive.

---

[29]*W. Westerman and R. Wright, Fluidic Reliability Program, McDonnell Douglas, Titusville, FL, LO242 (21 December 1973).*

[30]*W. Westerman, R. Wright, and G. Roe, Investigation of the Effectiveness of Cyclone Separators on Fluidic Power Supplies, McDonnell Douglas, Titusville, FL, LO243 (21 December 1973).*

[31]*L. Banaszak and W. Posingies, Hydrofluidic Stability Augmentation System (HYSAS) Operational Suitability Demonstration, Honeywell, Minneapolis, MN, USAAMRDL-TR-77-31 (October 1977).*

[32]*W. Westerman and R. Wright, Reliability Testing of Laminar Jet Fluidic Elements, McDonnell Douglas, Titusville, FL, LO266 (1 June 1974).*

[33]*R. Comparin, H. Moses, and E. Rowell, Contamination Effects in a Laminar Proportional Amplifier, Virginia Polytechnic Institute, Blacksburg, VA, HDL-TR-74-175-1 (June 1974).*

[34]*H. Moses and E. Sancaktar, The Effect of Geometric Changes Due to Contamination on Fluid Amplifier Performance, Virginia Polytechnic Institute, Blacksburg, VA, HDL-CR-75-192-1 (November 1975).*

[35]*R. Martin, J. Denneny, and T. Sutton, Three-Phase Program to Define Requirements for Operation of Fluidics on Compressor Bleed Air, AiResearch Manufacturing Co. of Arizona, Phoenix, AZ, 76-411328 (August 1976).*

[36]*W. Westerman and G. Roe, Classification of Fluidic Power Supplies, McDonnell Douglas, Titusville, FL, LO244 (21 December 1973).*

General rules of thumb may be applied to compute the flow consumption of laminar devices. A pneumatic device with a nozzle width and a throat length of 0.5 mm operating at a nominal Reynolds number of 120 consumes 0.3 liter/min of air. Flow at constant N_R' is proportional to nozzle width, independent of depth, and flow is proportional to N_R'; hence,

$$Q\left(b_s, N_R\right) = 0.3 \frac{b_s}{0.5} \frac{N_R'}{120} \quad , \tag{103}$$

$$Q\left(b_s, N_R\right)_{air} = 0.005 b_s \text{ (mm)} \; N_R' \left(\frac{\text{liter}}{\text{min}}\right) \quad .$$

With this formula and the number and the size of the elements, one may readily compute the capacity requirements of any pneumatic laminar fluidic system. For hydraulic operation, the same device consumes 6×10^{-6} m^3/s; hence,

$$Q\left(b_s, N_R\right)_{oil} = 10^{-7} b_s \text{ (mm)} \; N_R' \left(\frac{m^3}{s}\right) \quad . \tag{104}$$

In English units, an element consumes 0.1 gpm so that

$$Q\left(b_s, N_R\right) = 0.0017 b_s \text{ (mm)} \; N_R' \left(\text{gpm}\right).$$

For comparison, a typical vortex rate sensor in a tank gun stabilization system consumes 10 times that of a comparable LJARS.[4]

3.8 Noise Effects

Noise can arise from two main places: the power supply or the vents. From either source, common-mode pressure noise changes the operating point. Directed noise at the vents of an LJARS can cause a standing pressure that can cause jet deflection and give rise to a false or offset signal. Directed oscillatory noise may be rectified in the channels and geometry of the vent cavity giving rise to a dc pressure. Directed or preferential noise can occur due to unequal reflections from asymmetrically placed reflecting surfaces in pneumatic fluidic circuits that vent directly into ambient.

---

[4] *K. Chen and V. Neradka, Development of Critical Components, TriTec, Inc., Columbia, MD, DAAG-39-77-C-0173 (July 1978).*

No such noise problems have been encountered in liquid operation since the vent regions are closely coupled and collected. Close coupling and vent collecting in pneumatic circuits also provide satisfactory operation, but often produce other problems such as increased circuit and manifolding complexity.

Sonic isolation[19,22] is one method that has proven successful. In this method, a separate box is provided within which the fluidic package is encased. This box has a sonic orifice bleed to the outside. The fluidic devices are pressurized to give the desired pressure drop across them $(P_s - P_v)$, and the sonic orifice is adjusted to provide a two-to-one pressure ratio from the box to ambient, insuring choked conditions. This, incidentally, causes the density of the air to double. If the box is acoustically insulated, the system should be adequately isolated. More typically, external disturbances such as movement of solid objects may also cause dramatic output changes as shown by Young[37] and reproduced in figure 41. The effects of motion can be eliminated satisfactorily when a foam material covers the vents. The foam also acts as an acoustic baffle and reduces noise input. High-frequency hissing is a typical noise source and is adequately eliminated by foam rubber surrounding the vents. Care should be exercised so that the vent is not adversely affected.

Noise or, more specifically, selected frequency acoustic signals can cause a laminar jet that is near transition to go into transition. Specifically, a pneumatic LJARS operating at $\sigma N_R \sim 1300$ was found to go into transition and develop an offset when subjected to acoustic signals of about 100 dB at between 150 and 250 Hz when a nearby pump was turned on. This action strongly indicates that one must be sure to operate at $\sigma N_R < 1000$ as stipulated in section 3.1. In the above example, when the supply pressure was reduced 20 percent, the effect of the pump noise was eliminated. Its elimination suggests that $\sigma N_R \sim 1000$ is about the limit of absolute laminar jet stability. As the Reynolds number was decreased, as expected, higher frequencies were needed to set off transition until it did not occur at all. Its absence suggests a research area on determination of the stability of confined laminar jets. Regions of stability with frequency (wave number), amplitude of perturbation, and Reynolds number should be

---

[19] *G. Roe, Fluidic Laminar Angular Rate Sensor Research Program, McDonnell Douglas, Titusville, FL, HDL-CR-75-020-1 (November 1975).*

[22] *W. J. Westerman and R. E. Wright, Evaluation Program--Fluidic Laminar Rate Sensor--Final Report, McDonnell Douglas, Titusville, FL, NAVAIR L0252 (8 March 1974).*

[37] *R. Young, Feasibility Investigation of a Laminar Angular Rate Sensor, Phase IV Final Report, General Electric Co. Reentry and Environmental Systems, Schenectady, NY, 73SD2147 (August 1973).*

determined in something akin to neutral stability curves as determined for laminar boundary layers.

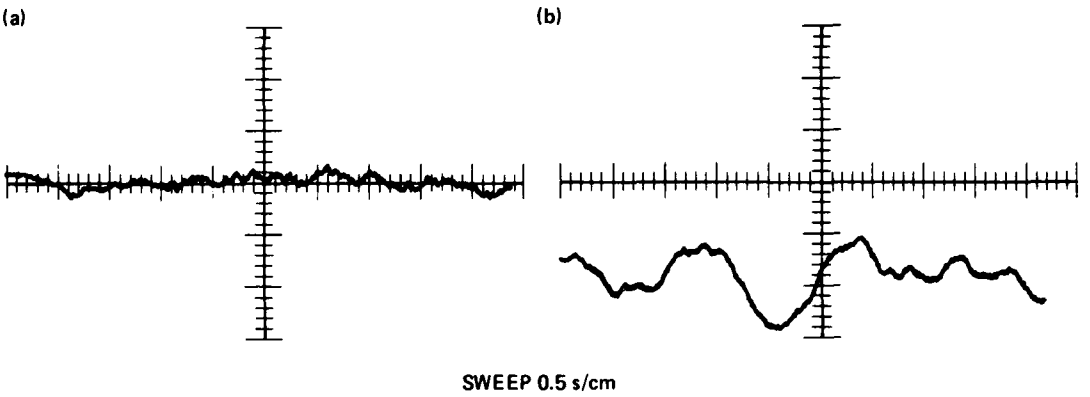

Figure 41. Oscilloscope traces of pneumatic laminar jet angular rate sensor output with uncovered vents: (a) still air and (b) ambient air disturbed by waving of hand; output = 0.025 mm Hg/cm, Pace pressure transducer = 0 to 0.03 psid, and supply pressure = 12 mm Hg (no rotation).

3.9 Operating Fluids

It has been tacitly assumed that the fluids used are Newtonian. Non-Newtonian fluids may be used; however, device operation will be somewhat different. A fluid that shears readily will cause higher pressure recovery; hence, the sensitivity may be greater since frictional losses can be greatly reduced. On the other hand, temperature characteristics of such liquids generally are not well behaved, so it is probably wise to stay clear of these and thixotropic materials.

In general, there is no fundamental difference in the operation of an LJARS when liquids or gases are used. This paper considers the most common fluids, oil and air. Many fluidic circuits are operated with water as well, but water is not advisable for operation over the military temperature range. However, in aqueous environments such as a torpedo guidance system, the local available fluid, sea water, would pose no theoretical limitations.

The big difference in operating with liquid working fluids is the additional manifolding required to return the flow to sump if necessary. Extreme care must be exercised to closely cross couple the vent regions on both sides of the jet to prevent pressure gradients from forming and deflecting the jet. Early attempts to make a hydraulic LJARS resulted in unacceptable offsets that were later relieved when

cross coupling was provided. Figure 42 shows a typical lamination of an LJARS used in this program. Figures 43 and 44 show the plates required to provide cross coupling. The jet bounding plate forms the bounding plane for the jet, and the vent cavity plate couples the vent regions on both sides of the jet.

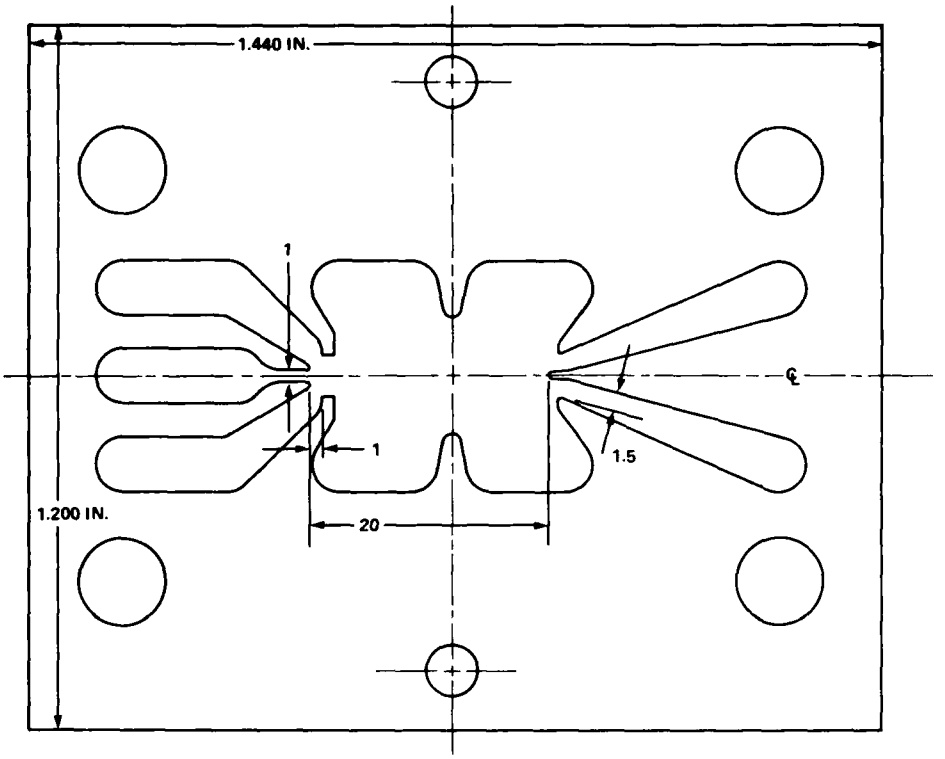

NOTE: RATE SENSOR DIMENSIONS ARE SUPPLY WIDTH (B_s); B_s = 0.020.

Figure 42. Typical laminar jet angular rate sensor horizontal lamination.

The cavity provides a low-impedance, uniform pressure ground that cannot support lateral pressure gradients. This is typically called a floating ground since the vent pressure level depends on the impedance back to sump and the flow through the device. It is usually advantageous to provide this type of venting on both the top and the bottom of the LJARS itself. In this manner, vertical gradients can be minimized; however, coupling on one side only may be adequate for most applications. When vertical laminations are used, the cross coupling is also a practical necessity. Figure 34 shows a vertically laminated device with oval cutouts on top and bottom. These form the cross--coupling cavity, and the outer laminations provide the vent communication to these cavities. The flow returning to sump must be collected

from a point of symmetry so that an asymmetrical flow distribution is not formed. The flow patterns (fig. 45) may indeed deflect the jet, especially since we are expecting to distinguish a jet deflection on the order of 10^{-6} deg. In the asymmetric case (fig. 45), the flow to the lower vent area must be turned upward; hence, a pressure develops that deflects the jet to give a spurious signal. When vertical laminates are used, multiple side outlets must be equally spaced.

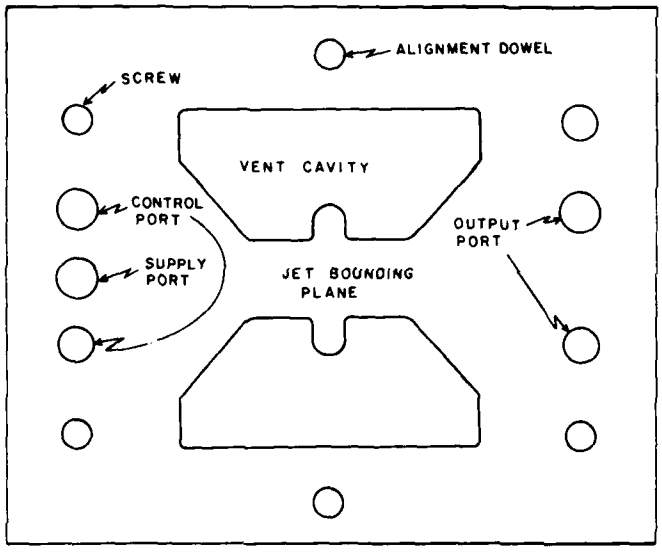

Figure 43. Jet bounding plane plate with vent areas.

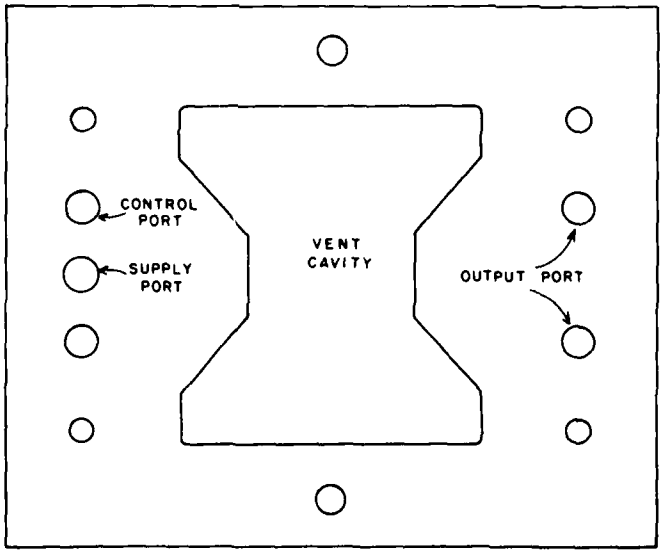

Figure 44. Cross-coupling vent cavity plate.

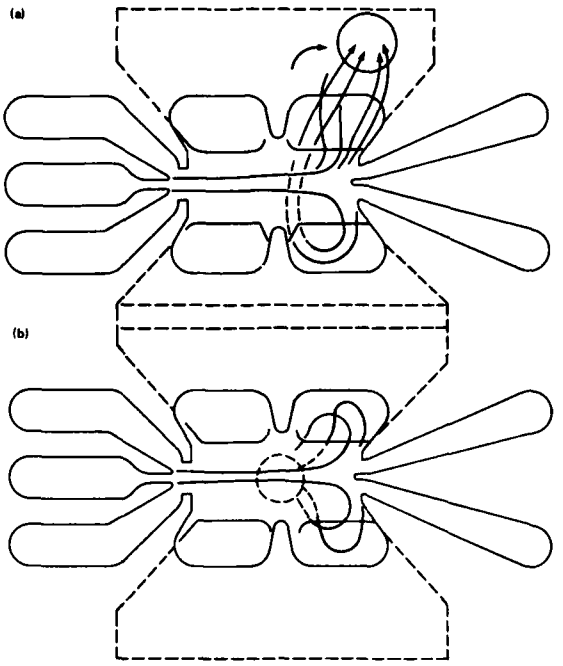

Figure 45. Flow patterns with collected vents.

3.10 Fabrication

Most fluidic devices are made of laminations to provide for a cancellation effect of mechanical errors when they are stacked. Sutton[28] discusses typical industrial methods of photochemical etching. Phillippi[25] discusses fine blanking, which is a high-precision stamping process. It has the great advantage of superior repeatability from laminate to laminate once a die has been custom-tailored to give the desired geometry. Custom-tailoring leads, however, to high die cost. To amortize the die cost so that laminates are competitively priced with those of metal etching, many thousands of pieces must be made. Interestingly, laminations can be thickened so that the cost per unit thickness can quickly be competitive.

---

[25] *R. M. Phillippi, A Study of Fineblanking for the Manufacture of Flueric Laminar Proportional Amplifiers, Harry Diamond Laboratories HDL-TM-77-8 (May 1977).*

[28] *T. Sutton and W. Anderson, Aerospace Fluidics Applications and Circuit Manufacture, Proceedings of HDL Fluidic State-of-the-Art Symposium, V, Harry Diamond Laboratories (October 1974).*

Elements produced by electroforming have the disadvantage of a high cost die and a geometrical limitation on element depth. Normally, devices are limited to an aspect ratio of 1.

Elements may be fabricated in plastic by molding or casting. Normally, military fluidic hardware is not plastic due to lack of ruggedness and dimensional stability. Dimensional accuracy also is more difficult to achieve since the three-dimensional geometry is made at once.

A relatively new fabrication technique is electrical discharge machining (EDM). A wire cuts out the desired shape in a thick piece of material. Tolerance can be maintained by computer control. In this manner, single laminations of the desired aspect ratio can be manufactured. The cost per laminate is prohibitively high, up to $25/laminate or very nearly 100 times more than with etching. This cost is essentially equivalent to that of optical-tracing milling machined elements since the same computer control is required. These techniques are used for small orders and laboratory tests.

Typical costs of production items are $0.25/laminate for metal-etched laminations. For a device of $\sigma = 2.6$, $b_s = 0.5$ mm, and a laminate thickness of 0.1 mm for the LJARS and 0.25 mm for auxiliary manifolds, 13 LJARS laminates are required to make $\sigma = 2.6$. Two bounding plates (fig. 43) are needed, and the cavity depth is twice the height of a device as a rule or 2.6 mm in this case. This depth requires 10 cavity laminations on each side. To complete the device for circuit integration, a cover and a baseplate are required. Thirty-seven laminates cost $9.25 at production prices not including labor and bonding charges. At research prices of up to $2 each, 37 laminates cost up to $74. This is well below $2000 or more than a gyroscope of similar functional properties may cost.

3.11 Testing Procedures

The verification of the operational characteristics of any device is of paramount importance in any practical application. For this reason, we look at the methods required for obtaining valid experimental data. The characteristics of an LJARS are not unlike those of an LPA. Indeed, the pressure gain of the device is one of the quantities required to determine dynamic range as shown in equation (101); hence, the tests must include all those required of an LPA with the addition of

a rate sensitivity test.[19,23,38] This section briefly describes the testing procedures typically conducted on an LJARS.

Eight critical tests are required of an LJARS:

Supply characteristic.--The supply flow is measured against pressure with all ports open and then blocked. Normally if the device is well vented, there is little difference in whether the ports are open or blocked. The supply pressure is the pressure drop from the plenum to the vent cavity (or to ambient if so vented). A supply Reynolds number is defined by this drop, that is,

$$N_R = \frac{b_s \left(\frac{2P_s}{\rho}\right)^{1/2}}{\nu} .$$

Pressure recovery characteristic.--Blocked output pressure is measured versus supply pressure. Five curves are typically taken: one at each of two outputs with the opposite output blocked, one at each of two outputs with the opposite output open, and one with both ports fed together to given an average value. This last is generally used for the pressure recovery. The first four curves give measures of the offset and the load sensitivity. For example, both blocked should not affect jet position. One open may cause jet deflection and gives a measure of loading effects. This test may be repeated for open or blocked controls.

Null offset characteristic.--Differential blocked output pressure is measured versus supply pressure. Curves are taken with open controls, with blocked controls, and with any desired compensation circuitry. These curves give $\Delta P_o/P_s$, which is required for dynamic range, drift, environmental effects, and CMRR computations.

Input resistance characteristic.--Control flow is measured versus control pressure, where control pressure is referenced to the vent cavity. Two sets of curves are taken. The first is called jet centered resistance, which is a measure of the control channel plus the

---

[19] *G. Roe, Fluidic Laminar Angular Rate Sensor Research Program, McDonnell Douglas, Titusville, FL, HDL-CR-75-020-1 (November 1975).*

[23] *M. Cycon, T. Sutton, and H. Gamble, Environmental Test Program for the Evaluation of Fluidic Elements, AiResearch Manufacturing Co. of Arizona, Phoenix, AZ, HDL-CR-75-187-1 (12 December 1975).*

[38] *Fluerics Testing Procedures, Department of Defense MIL-STD-1361 (1971).*

jet edge resistance $(R_c + R_v)$. This is obtained by measuring the total flow through a tee to both controls simultaneously versus the port pressure. A plot is made of half that flow versus pressure. The procedure is repeated for the jet turned off. This curve gives the control channel resistance, R_c, and the difference gives the vent resistance, R_v, required in augmented jet deflection computations. The second set of curves is control flow versus pressure with the opposite side control open to ambient. This with the jet centered curve can be used to get the deflection resistance if necessary.

Output resistance characteristic.--Output flow is measured versus output pressure (referenced to the vent cavity). This is tested in the same manner as the jet centered input characteristic. The outputs are fed together, and the pressure is varied from blocked pressure to zero (or less if one desires to see what happens with a suction load) while the flow is monitored. A plot is made of half this flow (the average of one output) versus output pressure. This test may be repeated for the individual output with opposite outputs open and then blocked to give a measure of load dependence. The inverse slope of the output curve at the operating point gives the operating output resistance, R_o, required to compute the gain (sensitivity) degradation when loading into a circuit. The operating point gives the value of bias into the circuit. The gain is degraded in a circuit by the factor $R_{load}/(R_o + R_{load})$, where R_{load} is the input resistance of the circuit into which the LJARS feeds. The point at which the flow is zero gives the pressure recovery; the point at which the pressure is zero gives the flow recovery.

Pressure gain or pressure transfer characteristic.--Blocked output differential pressure is measured versus differential input pressure with supply pressure held constant. The slope of this curve at zero differential pressure gives the pressure gain, G_p, and the differential output gives the offset. The linear portion of this curve defines the linear range of operation of the LJARS. Also, G_p is required for computation of dynamic range and CMRR.

Sensitivity or rate transfer characteristic.--Blocked output differential pressure is measured versus applied angular rate with supply pressure held constant. This is obtained by use of a rate table to provide input. The slope of this curve is sensitivity.

Frequency response characteristic.--Ratio of amplitudes of blocked output differential pressure to an input rate signal is measured versus frequency. Typically, this is called a Bode plot when the phase shift is included. The phase shift portion is critical because it is used to define the bandwidth of the LJARS. A gain-phase meter and a servo-controlled rate table are generally required to make this measurement with minimum effort.

The last five tests are conducted at various supply pressures or Reynolds numbers within the operating range so that auxiliary curves such as sensitivity versus Reynolds number may be obtained. Figures 46 to 51 show the experimental data for the LJARS shown in figures 42 to 44 operating with air, b_s = 0.75 mm, and σ = 1.67. Not all the curves specified above are presented in these figures; however, all pertinent data are presented. The Bode plot is shown in figure 19 for oil. Since the kinematic viscosities of air and oil are almost the same at room temperature, the frequency response is similar. In figure 51, we have replotted the data of figure 11, for completeness. Figure 50 is the plot of the actual data from which figure 51 was plotted. The uncompensated outputs in figure 50 have a null offset on the order of 2.0 Pa. At a sensitivity of 0.05 Pa/(deg/s), this corresponds to an error rate of 40 deg/s, so the LJARS must be compensated. Figure 52 shows the null offset changed by the negative feedback through valves from output to input. There exists a fairly wide range over which the null can be eliminated. In this range one would operate the LJARS.

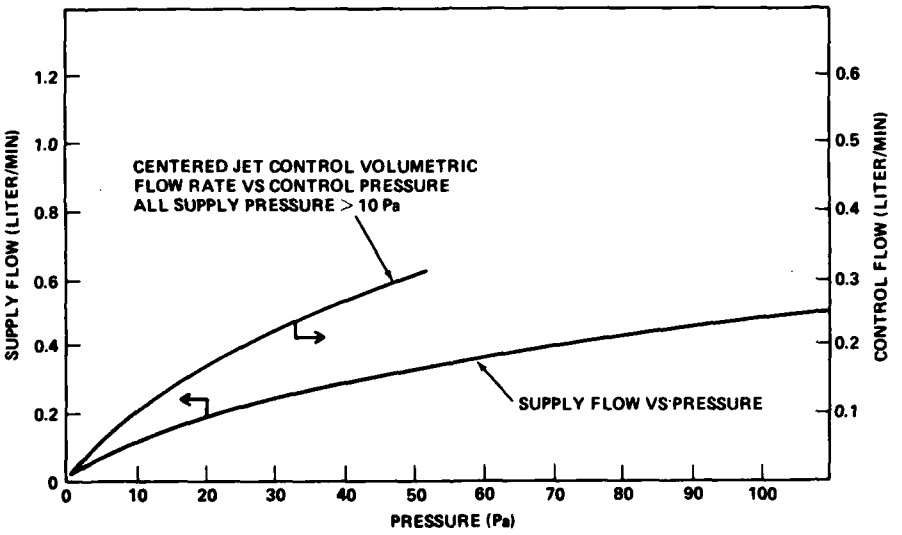

Figure 46. Experimental supply and control characteristics for laminar jet angular rate sensor: normalized splitter length = 20, supply width = 0.75 mm, normalized output width = 1.7, and aspect ratio = 1.667.

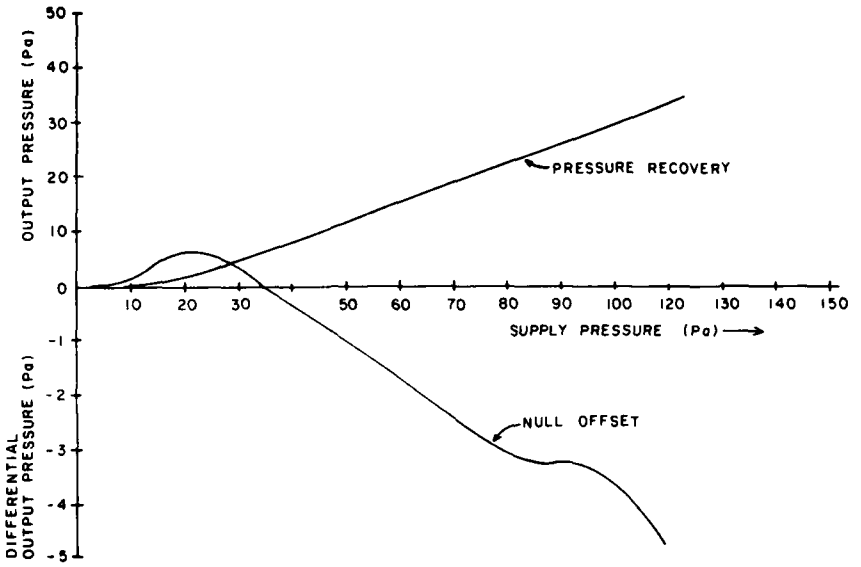

Figure 47. Experimental pressure recovery and null offset for laminar jet angular rate sensor.

Westerman and Wright[22] conducted an optimization program based on the single parameter of sensitivity. Figure 53 shows a sample of silhouettes used in the program, and figure 54 shows their sensitivity. Unit FM4 corresponds with the device of figure 42, and the sensitivity is a good order of magnitude lower than for FM5. In FM5, the positive feedback effect of the control ports is used. Interestingly, the theory developed in section 2 more than adequately predicts the performance of FM4 and the others. However, all the devices using control edge feedback depend on the Reynolds number. We have opted for a trade-off with sensitivity for operating range. If one desires a single high-gain element and is willing to pay the costs of keeping the Reynolds number constant, then FM5 is desirable.

The operating characteristics of the HDL LJARS shown in figures 42 to 44 are given in table 1.

---

[22] *W. J. Westerman and R. E. Wright, Evaluation Program--Fluidic Laminar Rate Sensor--Final Report, McDonnell Douglas, Titusville, FL, NAVAIR LO252 (8 March 1974).*

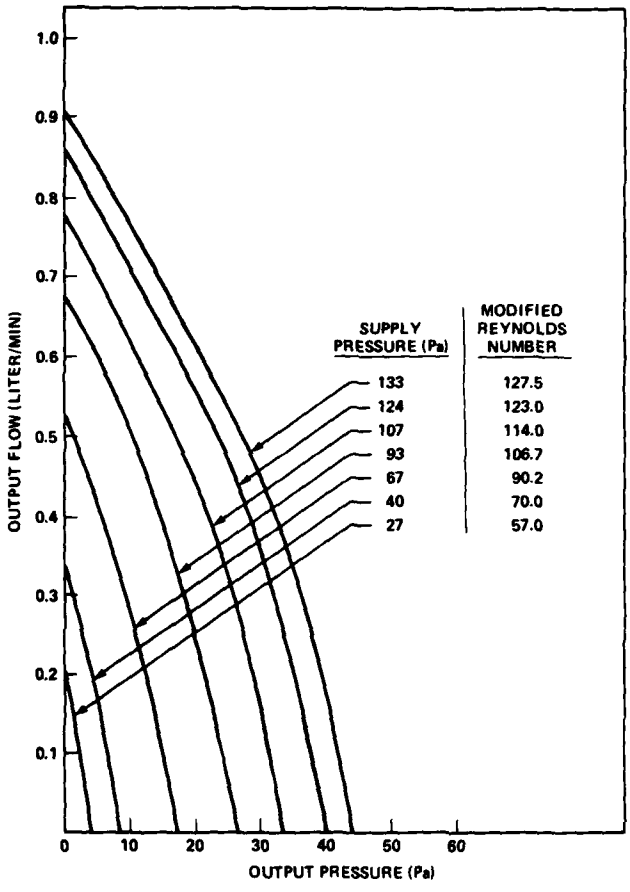

Figure 48. Output characteristic of experimental laminar jet angular rate sensor.

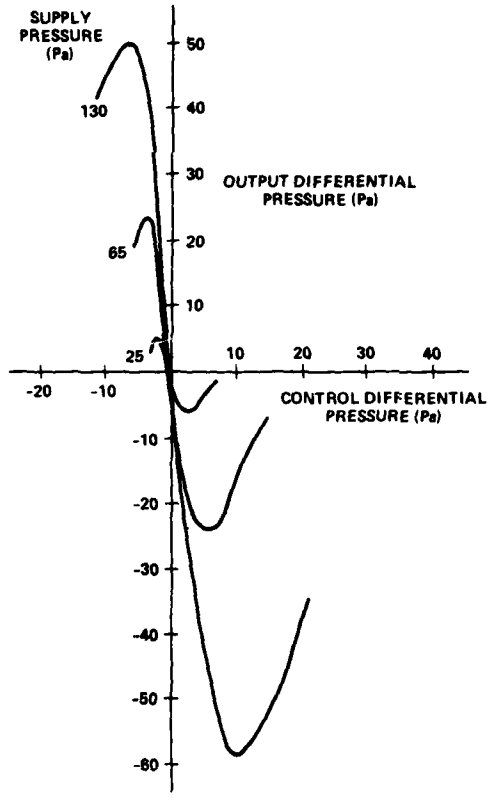

Figure 49. Experimental pressure gain of laminar jet angular rate sensor.

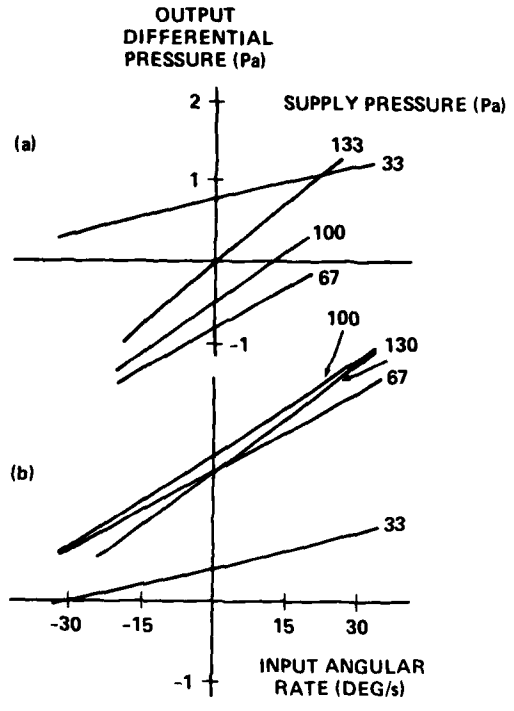

Figure 50. Experimental sensitivity of laminar jet angular rate sensor: (a) blocked controls and (b) open controls.

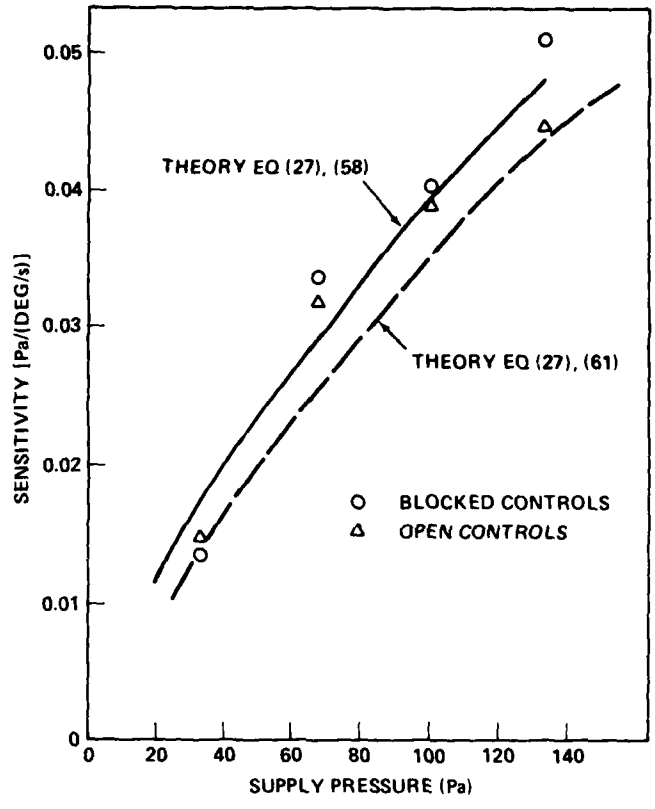

Figure 51. Experimental sensitivity as function of supply pressure.

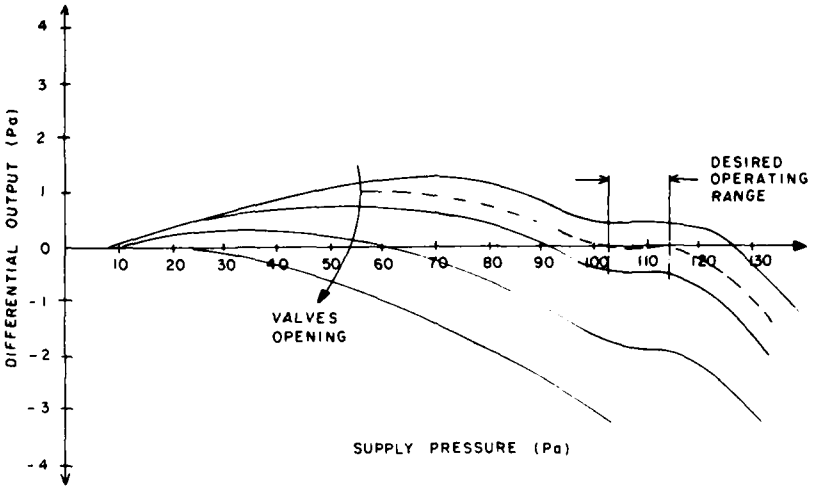

Figure 52. Experimental negative feedback null compensation with valves.

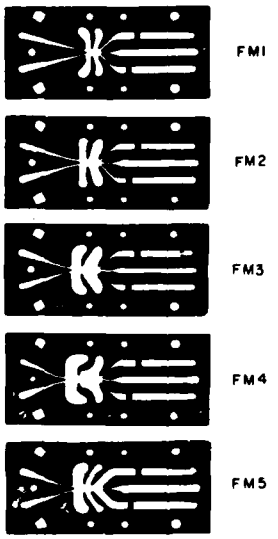

Figure 53. Parametric variations on laminar jet angular rate sensor (from G. Roe, McDonnell Douglas HDL-CR-75-020-1, November 1975).

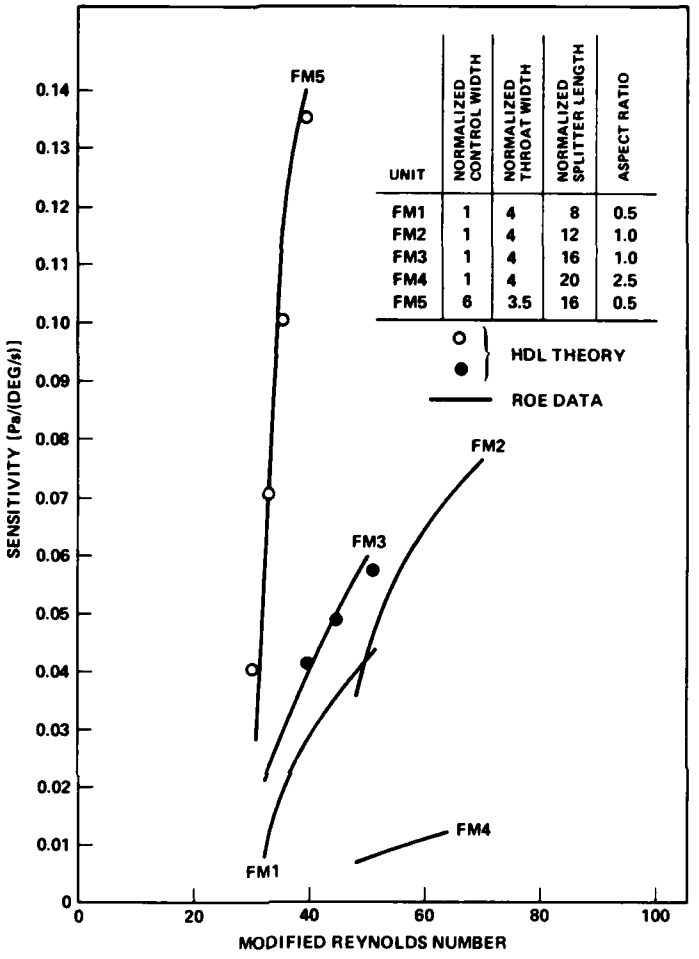

Figure 54. Sensitivity versus Reynolds number of laminar jet angular rate sensors of figure 53 (from G. Roe, McDonnell Douglas HDL-CR-75-020-1, November 1975).

TABLE 1. TECHNICAL DATA FOR LAMINAR JET ANGULAR RATE SENSOR OF HARRY DIAMOND LABORATORIES

Parameter	Pneumatic LJARS	Hydraulic LJARS	Comment
Dimension	b_s = 0.75 mm, h = 1.25 mm	b_s = 0.75 mm, h = 1.875 mm	σ = 1.667 pneumatic σ = 2.5 hydraulic
Supply	$35 \leq P_s \leq 130$ Pa $4 \times 10^{-6} \leq Q_s \leq 8 \times 10^{-6}$ m^3/s	$20 \leq P_s \leq 80$ kPa	±0.1% regulation
Output impedance	1.68×10^6 $Pa/m^3/s$	1.6×10^9 $Pa/m^3/s$	--
Gain	10	10	--
Sensitivity	0.015 to 0.05 Pa/(deg/s)	10 to 30 Pa/(deg/s)	--
Sensitivity temp coeff	1.25×10^{-4} [Pa/(deg/s)]/deg C at 20 C	0.75 [Pa/(deg/s)]/deg C at 60 C	0.3%/deg C pneumatic 5.0%/deg C hydraulic
Null offset	Uncompensated, 10 to 100 deg/s Compensated, 0.1 deg/s	-- --	Pneumatic operating range 100 ± 10 Pa
Null offset supply sensitivity	Uncompensated, 1.5 (deg/s)/Pa Compensated, 0.05 (deg/s)/Pa	-- --	P_s = 100 Pa P_s = 100 ± 5 Pa
Max rate	900 deg/s	550 deg/s	Decreases with supply
Threshold	>0.1 deg/s	0.02 deg/s	Not readily measured with state-of-art instruments
Linear range	75% max rate	75% max rate	Linearity <1%
Dynamic range	25,000	32,000	--
Cross axis sensitivity	--	--	None perceptible when care is taken to align LJARS
Bandwidth ϕ = -90 deg -3 dB	 20 to 40 Hz 300 to 400 Hz	 10 to 20 Hz 100 to 200 Hz	Hydraulic lower because of larger σ
Common mode rejection ratio	>400	>400	Depends on fabrication

Notes: b_s = supply width.
h = height.
P_s = supply pressure.
σ = aspect ratio, h/b_s.

AD-A083 637 HARRY DIAMOND LABS ADELPHI MD F/G 13/7
FLUERICS 40: LJARS, THE LAMINAR JET ANGULAR RATE SENSOR.(U)
DEC 79 T M DRZEWIECKI, F M MANION
UNCLASSIFIED HDL-TM-79-7 NL

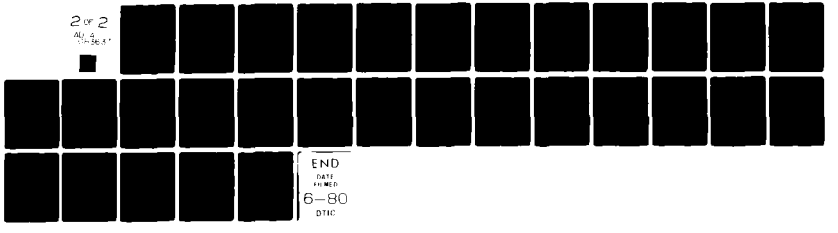

4. DISCUSSION AND CONCLUSIONS

We have presented an analysis and a few rules of thumb for the design of a fluidic LJARS. Throughout this report, most emphasis has been on a single component thought to be representative--namely, the one depicted in figure 42. The raw data for the performance are given in figures 46 to 51. This LJARS is not optimal because optimality is a function of what is desired. Nevertheless, it has most of the good characteristics attributable to an LJARS, such as high sensitivity, low output impedance, ease of compensation for null and temperature, and generally low sensitivity to temperature changes. Although these characteristics are not final or conclusive, they show what can be done with minimum effort. The negative feedback offset compensation yields satisfactory results that depend on the type of feedback resistor. In general, the shape of the offset curve (fig. 52) and the magnitude of the offset may be affected, thus giving considerable flexibility.

Temperature compensation is more dramatically incorporated in a hydraulic LJARS, in which the density does not change, than in a pneumatic LJARS, in which it does. In a hydraulic LJARS, sensitivity can be decreased with an increase in temperature, but in a pneumatic LJARS, the best that can be achieved is a reduction in the increase.

The threshold depends on the available instrumentation and the environmental noise. Open-loop measurements indicate thresholds of less than 0.1 deg/s (as fast as a minute hand turns on a clock). Closed-loop performance on a pneumatic fluidic gun stabilization system for the M60/M48 tank showed disturbance suppression of 40 dB for signals on the order of 1 deg/s, which means that the rate sensor is moving at 0.01 deg/s. Closed-loop operation is less susceptible to common-mode noise.

To facilitate design, the important equations for LJARS operation are these:

Sensitivity:
$$\frac{\Delta P_o}{\dot{\mu}\theta} = \frac{N_R c_\theta X_{sp}^2}{57.3 c_d B_o}\left(1 - \frac{8X_{sp}}{c_\theta N_R \sigma^2}\right)\left[1 - \frac{1.1B_{sp}}{\left(\frac{c_d N_R B_{sp}}{2}\right)^{1/2}}\right],$$

Bandwidth:
$$f_{\theta=-90°} = \frac{c_d N_R \nu}{16 X_{sp} b_s^2},$$

Operating range:
$$500 \leq \sigma N_R \leq 1000,$$

Dynamic range: $$D_R = 4 \left(\frac{P_{rec}}{P_s}\right) \left(\frac{P_s}{\Delta P_s}\right) \frac{CMRR}{G_p} .$$

In conclusion, this report has shown how an LJARS may successfully be modelled and has presented guidelines to build it.

The applications of an LJARS fall into several categories from simple rate limit switches to rate gyroscope replacement. The broadest applications appear to be in guidance and disturbance suppression systems. The overwhelming asset of the LJARS is the low cost. Current production rate costs of $0.25/laminate yield cost estimates between $10 and $100 for an LJARS. A trade-off can be made between accuracy (null offset and drift) and low cost when an LJARS is compared with a gyroscope. The cost of the LJARS increases with the power supply complexity.

Another asset is the instant-on feature. The sensor works as soon as a jet is developed--one jet transport time. Typically, for a pneumatic LJARS with a jet velocity of 10 m/s over a distance of 15 mm, the LJARS starts in only 1.5 ms. This time can be compared with the several seconds required to spin up a mechanical gyroscope. This asset is of particular interest to those who design seat ejection systems that must be on line in less than 10 ms from storage to provide adequate performance.

The LJARS appears to apply to many guidance and control systems. Lest this impression be imprinted too strongly, one must remember this important caveat: The LJARS is only as good as its power supply. Reliable, accurate, fluidic power supplies are more difficult to make with the current state of the art than electronic ones, for which far more research dollars have been expended.

In addition, the problem of interfacing must yet be addressed. Interfacing with electronic systems involves a pressure transducer, which often is the weak link. Interfacing with mechanical systems involves servo actuators or servo valves. Fluidic first-stage servo valves are on the market. Hence, interfacing may not present a big problem, although it involves moving parts.

We suggest that the interfacing and the power supplies be developed. Null offset compensation and dynamic effects need intensive analytical research to go with current results based on the heuristic arguments presented here.

LITERATURE CITED

1. A. Ostdiek, Viscous Vortex Rate Sensor, Harry Diamond Laboratories HDL-TR-1555 (November 1971).

2. J. M. Kirshner, A Survey of Sensors--Part II, Proceedings of HDL Fluidic State-of-the-Art Symposium, II, Harry Diamond Laboratories (October 1974).

3. J. O. Hedeen, Performance and Application of the Vortex Rate Sensor, Proceedings of HDL Fluidic State-of-the-Art Symposium, II, Harry Diamond Laboratories (October 1974).

4. K. Chen and V. Neradka, Development of Critical Components, TriTec, Inc., Columbia, MD, DAAG-39-77-C-0173 (July 1978).

5. H. Ziebolz, Characteristics of Hydraulic and Pneumatic Relays as Energy-Converting Devices, Instruments, 15 (September 1942).

6. T. Reader, Laminar Fluidic Devices, U.S. Patent 3,662,772 (16 May 1972).

7. A. G. Moore, Angular Movement Sensing Device, U.S. Patent 3,500,691 (17 March 1970).

8. T. M. Rankin, A. G. Moore, and W. C. Schuemann, Fluidic Angular Rate Sensor--A Replacement for Rate Gyroscopes? Johns Hopkins Applied Physics Laboratory Technical Digest (March-April 1969).

9. T. Reader, T. Shaffer, J. Goren, and R. Kantola, Feasibility Investigation of a Laminar Rate Sensor (LARS), Phase I Report, General Electric Co. Reentry and Environmental Systems, Schenectady, NY, 69SD698 (June 1969).

10. P. L. Jacobs, Theoretical Analysis of a Two-Dimensional Laminar Jet Rate Sensor, Proceedings of HDL Fluidic State-of-the-Art Symposium, II, Harry Diamond Laboratories (October 1974).

11. R. Young, Development of a Laminar Angular Rate Sensor (LARS), Proceedings of HDL Fluidic State-of-the-Art Symposium, II, Harry Diamond Laboratories (October 1974).

12. F. Manion and T. Drzewiecki, Analytical Design of Laminar Proportional Amplifiers, Proceedings of HDL Fluidic State-of-the-Art Symposium, I, Harry Diamond Laboratories (October 1974).

LITERATURE (Cont'd)

13. T. M. Drzewiecki, D. N. Wormley, and F. M. Manion, Computer-Aided Design Procedure for Laminar Fluidic Systems, J. Dyn. Syst. Meas. Control, 97, Series G (December 1975).

14. T. M. Drzewiecki, Interpretation of Surface Static Pressure Distributions in Fluid Amplifier Applications, Harry Diamond Laboratories HDL-TR-1627 (July 1973).

15. H. Schlichting, Boundary Layer Theory, McGraw-Hill Book Co., New York (1960).

16. T. M. Drzewiecki, Fluerics 38: A Computer Aided Design Analysis for the Static and Dynamic Port Characteristics of Laminar Proportional Amplifiers, Harry Diamond Laboratories HDL-TR-1758 (June 1976).

17. F. M. Manion and G. Mon, Fluerics 33: Design and Staging of Laminar Proportional Amplifiers, Harry Diamond Laboratories HDL-TR-1608 (September 1972).

18. J. O. Hinze, Turbulence, McGraw-Hill Book Co., New York (1959).

19. G. Roe, Fluidic Laminar Angular Rate Sensor Research Program, McDonnell Douglas, Titusville, FL, HDL-CR-75-020-1 (November 1975).

20. T. M. Drzewiecki, Fluidic Resistive Element, U.S. Patent 3,980,103 (14 September 1976).

21. George Mon, Flueric Laminar Gain Blocks and an Operational Amplifier Scaler, Harry Diamond Laboratories HDL-TR-1730 (December 1975).

22. W. J. Westerman and R. E. Wright, Evaluation Program--Fluidic Laminar Rate Sensor--Final Report, McDonnell Douglas, Titusville, FL, NAVAIR L0252 (8 March 1974).

23. M. Cycon, T. Sutton, and H. Gamble, Environmental Test Program for the Evaluation of Fluidic Elements, AiResearch Manufacturing Co. of Arizona, Phoenix, AZ, HDL-CR-75-187-1 (12 December 1975).

24. V. Bravo, Feasibility Investigation of a Laminar Rate Sensor (LARS), Phase III Report, General Electric Co, Schenectady, NY, 71SD2118 (December 1971).

25. R. M. Phillippi, A Study of Fineblanking for the Manufacture of Flueric Laminar Proportional Amplifiers, Harry Diamond Laboratories HDL-TM-77-8 (May 1977).

26. C. D. O'Neal, Stacked Port Fluidic Amplifier, U.S. Patent 3,468,331 (23 September 1969).

27. D. O'Keeffe, Null Offset Compensation of Fluidic Amplifiers Using External Negative Feedback, Proceedings of HDL Student Technical Symposium, Harry Diamond Laboratories (August 1978).

28. T. Sutton and W. Anderson, Aerospace Fluidics Applications and Circuit Manufacture, Proceedings of HDL Fluidic State-of-the-Art Symposium, V, Harry Diamond Laboratories (October 1974).

29. W. Westerman and R. Wright, Fluidic Reliability Program, McDonnell Douglas, Titusville, FL, LO242 (21 December 1973).

30. W. Westerman, R. Wright, and G. Roe, Investigation of the Effectiveness of Cyclone Separators on Fluidic Power Supplies, McDonnell Douglas, Titusville, FL, L0243 (21 December 1973).

31. L. Banaszak and W. Posingies, Hydrofluidic Stability Augmentation System (HYSAS) Operational Suitability Demonstration, Honeywell, Minneapolis, MN, USAAMRDL-TR-77-31 (October 1977).

32 W. Westerman and R. Wright, Reliability Testing of Laminar Jet Fluidic Elements, McDonnell Douglas, Titusville, FL, L0266 (1 June 1974).

33. R. Comparin, H. Moses, and E. Rowell, Contamination Effects in a Laminar Proportional Amplifier, Virginia Polytechnic Institute, Blacksburg, VA, HDL-TR-74-175-1 (June 1974).

34. H. Moses and E. Sancaktar, The Effect of Geometric Changes Due to Contamination on Fluid Amplifier Performance, Virginia Polytechnic Institute, Blacksburg, VA, HDL-CR-75-192-1 (November 1975).

35. R. Martin, J. Denneny, and T. Sutton, Three-Phase Program to Define Requirements for Operation of Fluidics on Compressor Bleed Air, AiResearch Manufacturing Co. of Arizona, Phoenix, AZ, 76-411328 (August 1976).

36. W. Westerman and G. Roe, Classification of Fluidic Power Supplies, McDonnell Douglas, Titusville, FL, L0244 (21 December 1973).

37. R. Young, Feasibility Investigation of a Laminar Angular Rate Sensor, Phase IV Final Report, General Electric Co. Reentry and Environmental Systems, Schenectady, NY, 73SD2147 (August 1973).

38. Fluerics Testing Procedures, Department of Defense MIL-STD-1361 (1971).

NOMENCLATURE

a_1	Net entrainment coefficient
A	Cross-sectional area (m^2)
b	Width dimension (m)
B	Normalized width (b/b_s)
c_d	Flow discharge coefficient = Q_a/Q_i
c_θ	Momentum flux discharge coefficient = J_a/J_i
C	Loss coefficient
D_R	Dynamic range
f	Bandwidth (Hz)
f(x)	Center-line decay function
G	Forward gain
h	Height (m)
H	Feedback gain
J	Momentum flux = ρAU^2
k	Constant
K	Kinematic momentum flux = J/ρ
K_o	Orifice coefficient
$\dot{m}$	Mass flow rate (kg/s)
n	Integer
N_R	Reynolds number = $\rho b_s U_s/\mu$
P	Pressure (Pa)
Q	Volumetric flow rate (m^3/s)

NOMENCLATURE (Cont'd)

r	Radial position (m)
R	Resistance based on Q, $R = \Delta P/Q$ (kg/m^4s)
R'	Resistance based on $\dot{m}$, $R' = \Delta P/\dot{m}$ ($1/m \cdot s$)
S	Normalized angular rate sensitivity
T	Temperature (C or K)
u	x-direction velocity (m/s)
U	Mean or reference velocity (m/s)
v	Lateral velocity
V	Velocity (m/s)
x	Coordinate dimension measured from nozzle exit (m)
X	Normalized length in x-direction
y	Lateral deflection distance (m)
ZO	Half square of effective normalized splitter distance
γ	Angle
δ	Boundary layer thickness
δ^*	Displacement thickness
θ	Momentum thickness
$\dot{\theta}$	Angular rate
λ	Wavelength
μ	Absolute viscosity ($kg/m \cdot s$)
ν	Kinematic viscosity (m^2/s)
ρ	Density (kg/m^3)

σ	Aspect ratio, h/b_s
τ	Transit time (s)
ϕ	Phase angle (deg)
χ	Other causes

Subscripts

a	Augmented
BC	Downstream control edge
BSP	Splitter width
c	Control
cℓ	Center line
core	Pertaining to potential core
d	Delay
e	Entrainment
eff	Effective
enet	Net entrainment
j	Jet
L	Loop
n	Nozzle
o	Output pressure and width for B_o, P_o; orifice for all others
r	Relative

rec	Recovered (block loaded)
s	Supply
sp	Splitter
SB	Spill back
t	Throat
th	Nozzle throat
T	Total
v	Vent
vo	Virtual origin
XSP	At splitter
y	Deflection
$\dot{\theta}$	Due to rotation
0	Reference 0
1	Reference 1
2	Reference 2
3	Reference 3
90	-90 deg of phase lag

Superscripts

$\bar{}$	Average
'	Dimensional quantities in temperature compensation equations

APPENDIX A.—COMPUTER PROGRAMS FOR LJARS

This appendix lists computer programs for the laminar jet angular rate sensor (LJARS) (listings A-1 to A-3), defines the terms (table A-1), and shows a sample printout (fig. A-1) and a standard silhouette (fig. A-2) of the laminar proportional amplifier.

APPENDIX A

LISTING A-1. LJARS

```
10PRINT "IF YOU ARE INTERESTED ONLY IN AN ANGULAR RATE SENSOR AN
SWER NO  FOR PLOTS.":INPUT "TODAYS DATE",C$
20SELECT PLOT 413,PRINT 213(100):PLOT [,,]:SELECT CO 213(100)
30PRINT C$:PRINT "LAMINAR JET DEVICE CHARACTERISTICS"
40DIM V5(56),W5(56),V6(56),W6(56),V7(56),W7(56),G7(55),G1(100),P
4(100),C(25),F0(25)
50INPUT "DO YOU WANT ANGULAR RATE DATA",R$
60INPUT "DOES THIS DEVICE HAVE CENTER DUMP OR OUTPUT VENTS",Y$:I
F Y$="YES"THEN 70:V1=1E-10:V2=1E10:L8=1E10:L9=0
70Y2=0:INPUT "DOES THIS DEVICE HAVE SUDDEN EXPANSION OUTPUTS",Y1
$:IF Y1$[]"YES"THEN 80:Y2=1
80INPUT "MODIFIED(1) OR WIDTH(2) REYNOLDS NO.",Y3
90INPUT "DO YOU WANT RANGES,DO YOU WANT PLOTS",Z3$,Z9$
100IF Z3$="YES"THEN 270:IF Z9$="NO"THEN 120
110INPUT "RESPONSE OTHER THAN SELF-STAGED",Z5$:IF Z5$="NO"THEN 1
20:INPUT "BIAS PRESSURE FOR RESPONSE",J6:INPUT "SELF-LOAD(1),BLO
CKED(2),BOTH(3)",Z2
120INPUT "CONTROL AND THROAT WIDTH",W,B
130IF Y3=1THEN 160
140INPUT "ASPECT RATIO AND REY.NO.",S,N
150GOTO 170
160INPUT "ASPECT RATIO,MOD REY.NO.",S,N9
170INPUT "SPLITTER DISTANCE       ",B6
180INPUT "NOZZLE AND SPLITTER LGTH",L4,C9
190INPUT "OUTPUT LENGTH,AVG.WIDTH ",X3,F8
200IF Y$[]"YES"THEN 220
210INPUT "CNTR DUMP W,L; VENT W,L ",V1,V2,L8,L9
220INPUT "BIAS CONTROL PRESSURE   ",H3
230INPUT "CTRL L,AVG.W,MIN.W,ENT.R",X1,W0,W3,B1
240INPUT "SPLITTER , OUTPUT WIDTH ",B5,E7:PRINT "  "
250IF Z3$="YES"THEN 310
260GOTO 390
270INPUT "RANGE AND STEP OF NR',BC,BT,AR,XSP",N1,N2,N3,Z4,Z5,Z6,
Z7,Z8,Z9,S3,S4,S5,X4,X5,X6
280J=0
290GOTO 180
300REM LOOPS FOR RANGES
310FOR N9=N1TO N2STEP N3
320FOR S=S3TO S4STEP S5
330FOR B6=X4TO X5STEP X6
340FOR W=Z4TO Z5STEP Z6
350FOR B=Z7TO Z8STEP Z9
360IF J=0THEN 390
370SELECT PLOT 413:PLOT [,-395,]:SELECT PRINT 213
380REM CALL DISCHARGE COEFF. ROUTINE
390J=1:IF Y3=1THEN 400:N9=N/(L4+1)/(1+1/S)!2:GOSUB 4020:GOTO 410

400GOSUB 4020:N=N9*(L4+1)*(1+1/S)!2
410IF N*S[1400THEN 430:PRINT "**** W A R N I N G ****":PRINT "MA
X.DYN.RANGE REYNOLDS NO.EXCEEDED...FLOW BECOMING TURBULENT"
420REM COMPUTE 2-D CD,ENTR.FLOW,JET-EDGE SPACE,SPILLBACK FLOW, N
ET ENTR.COEFF.,SPILLBACK LOSS COEFF.
430D=(1-S)/2+SQR((S+1)!2/4-S*(1-C))
440Q=1.651*(.02772+1.32*(W+B1)/(C*N))!(1/3)-.5
450K=1/(C*Q+D/2):Y=K*B/2:B8=.5*(B-(1+W/.021/C/N)!(2/3))
460T1=LOG((1+.5*D*K)/(1-.5*D*K))/2
470K3=4/(EXP(T1)+EXP(-T1))!2:K4=K3/Q/C:R4=0
480Q4=Q*EXP(-K4*B8)/2:A=K4*Q4*2:C3=1-3.0303*K4*Q4!2
490REM IF CONTROL PARAMETERS UNCHANGED BYPASS RV CALC.
500IF W[]M5THEN 560
510IF B[]M6THEN 560
520IF N[]M7THEN 560
530IF S[]M8THEN 560
540GOTO 660
550REM COMPUTE VENT RESISTANCE
560FOR P1=.1TO .5STEP .05
570P=P1!.25:S1=LOG(1/P+SQR(1/P!2-1)):Y0=S1/K:D1=(B/2-Y0)/10:I=0
580FOR Y1=Y0TO B/2STEP D1
590S2=2/(EXP(Y1*K)+EXP(-Y1*K))
600A1=(SQR(S2!4+P1)-S2!2)*D1:I=I+A1:NEXT Y1
610R1=D*P1/I
620ZRV= #.###,NR= ####.#,NR'=###.#,AR= #.###,BC= ##.##,BT=##.##,
XSP=##.##,CD= .###
630R4=R4+R1
640NEXT P1
650R1=R4/10
```

LISTING A-1. LJARS (Cont'd)

```
660M5=W:M6=B:M7=N:M8=S
670REM CHANNEL RESISTANCE CORRECTION AND COEFFICIENTS
680IF W0/S]2THEN 690:K2=.35:GOTO 700
690K2=.5
700T4=24*X1*C*(S/W0+W0/S+K2)/(W0!2*S*N):T5=.95*(C/W3)!2:C2=1.32*
C*C
710IF V1/S]2THEN 750
720IF S/V1]2THEN 750
730K9=.35
740GOTO 830
750K9=.5
760 IF C].5THEN 770:N0=2*C:GOTO 790
770 N0=1
780REM JET CHARACTERISTICS,DISP.TH,EFF.NOZZLE L.,CORE L.,VIRTUAL
 ORIGIN,MOMENTUM LOSS COEFF.,RATE SENSOR EFF.L.,PARTICLE TRANSIT
 TIME
790 D0=(1+S)/4-.5*SQR((1+S)!2/4-(1-C)*S)
800 X=N*(D0*10/3)!2/25*N0
810 X0=X*(.25/(D0*1.4)!2-1)
820 X2=.0155*C*N:PRINT "CORE LENGTH=",X0,"VIRTUAL ORIGIN=",X2,"D
ISPLACEMENT THICKNESS=",D0
825 IF S[1THEN 826:N5=4:N6=5.6:GOTO 830
826 N5=3.00:N6=3.00
830IF X0]=0THEN 850
840 C0=(1+B6/X2)!(-2/3):N0=2*C:Z0=9*X2!2*((1+B6/X2)!(7/3)-1)/28-
.75*B6*X2:F0=1/12/X2/((1+B6/X2)!(4/3)-1):GOTO 900
850 IF X0]B6 THEN 880:IF C].5THEN 860:C0=(1+(B6-X0)/X2)!(-2/3):G
OTO 870
860 C0=(1+(B6-X0)/X2)!(-2/3)*(1-N5*SQR((X+X0)/N)/S)/(1-N6*SQR(X/
N)/S)
870 Z0=X0*(B6-X0/2)-.75*X2*(B6-X0)+9*X2!2*((1+(B6-X0)/X2)!(7/3)-
1)/28:F0=1/16/(X0+.75*X2*((1+(B6-X0)/X2)!(4/3)-1)):GOTO 900
880C0=(1-N5*SQR((B6+X)/N)/S)/(1-N6*SQR(X/N)/S):N0=1:Z0=B6!2/2:F0
=1/16/B6
890REM PRESSURE RECOVERY AT +-1% AND 0
900P2=H3:GOSUB 4330:GOSUB 4280:A3=Q2+.5
910B2=2/(1+B6/.021/C/N)!(2/3):IF B7[B2 THEN 920:B2=B7
920P6=C0*(1-1.1*B5/(SQR(C*N*B5/2)))*C2/B2*(1-SQR(C2*C0)*V1!2*S*N
/(24*V2*(S/V1+V1/S+K9)))*(1+2*C*P1*SQR(ABS(P1))/(R1*C2))*C3
930D6=C0*(1-1.1*B5/(SQR(C*N*B5/2)))*W*W/B2*(1-SQR(C2*C0)*V1!2*S*
N/(24*V2*(S/V1+V1/S+K9)))*C3
940D5=24*L9*C*(S/L8+L8/S+.5)/S/N/L8!2:J9=1+.5*(D5+.95*C*C*.5/L8!
2)/P6
950GOSUB 4330:GOSUB 4190
960E=1:O2=1:O3=1
970REM OUTPUT CHARACTERISTICS
980FOR M=-.01TO .01STEP .01
990IF Z9$="YES"THEN 1000:M=0
1000P5=P6+G*M/2
1010A5=A3*P5/P6
1020R5=24*X3*C*(S/F8+F8/S+K2)/(F8!2*S*N)
1030K5=.95*C!2/B7!2
1040IF M[]0THEN 1090
1050FOR I=1TO 5:PRINT HEX(0A):NEXT I
1060PRINT " CENTERED INPUT AND OUTPUT CHARACTERISTICS"
1070FOR I=1TO 3:PRINT HEX(0A):NEXT I
1080PRINT "    Q      PO     PO*QO     RO      PC      RC"
1090H=0
1100E2=0:E3=0:E4=0:E6=0:E7=0:E8=0:T7=0:A6=0:Z3=1
1110FOR Q0=0TO .5STEP .010:IF A6=1THEN 1170
1120R=D5+.95*C*C*(.5-Q0)/L8!2
1130IF S[2THEN 1140:Z3=2/S
1140P0=P5*(1-2*Q0*C/SQR(P5*B7))/(1-Q0*C/B7/SQR(B7*P5))-R5*Q0-K5*
Q0!2+C*SQR(P5/B7)*Q0*.25*S*Z3+(.5-Q0)*R+(C*Q0/B7)!2*4*Y2
1150R6=C*SQR(P5/B7)/(1-Q0*C/B7/SQR(P5*B7))*(-2+(1-2*Q0*C/SQR(P5*
B7))/B7/(1-Q0*C/B7/SQR(P5*B7)))-R5-2*K5*Q0+C*SQR(P5/B7)*.25*S*Z3
-R-.95*C*C*(.5-Q0)/L8!2+8*(C/B7)!2*Q0*Y2
1160Z=R5+K5*Q0+P0/(Q0+.000001):A4=.5/A5:IF A4[ZTHEN 1180:IF P0/(
A5-Q0)[-R6THEN 1180:A6=1:A7=Q0:A8=P0
1170P0=A8/(A5-A7)*(A5-Q0):R6=-A8/(A5-A7)
1180E1=(P0-E2)*1000+E3
1190E2=P0
1200E3=E1-INT(ABS(E1))*SGN(E1)
1210E4=E4+INT(ABS(E1))*SGN(E1)
1220E5=(Q0-E6)*500+E7
1230E6=Q0
```

APPENDIX A

LISTING A-1. LJARS (Cont'd)

```
1240E7=E5-INT(ABS(E5))*SGN(E5)
1250E8=E8+INT(ABS(E5))*SGN(E5)
1260REM STORE DATA POINTS FOR OUTPUT PLOTS
1270IF M]-.01THEN 1280:V5(E)=E1:W5(E)=E5:L5=E4:Y5=E8:E=E+1:GOTO
1300
1280IF M]0THEN 1290:V6(O2)=E1:W6(O2)=E5:L6=E4:Y6=E8:O2=O2+1:GOTO
1300
1290V7(O3)=E1:W7(O3)=E5:L7=E4:Y7=E8:O3=O3+1
1300IF M[]0THEN 1450
1310Q2=Q0
1320GOSUB 4000
1330GOSUB 4260
1340F=P0-P2
1350IF F]0THEN 1420
1360IF T7=1THEN 1420:T7=1:R7=R6
1370P7=P0
1380R8=R0
1390Q7=Q2
1400 PRINTUSING 1410,Q0
1410%   SELF-STAGED OPERATING FLOW = -#.###
1420IF (H-INT(H))]0THEN 1450
1430PRINTUSING 1440,Q0,P0,Q0*P0,R6,P2,R0
1440%-#.## -#.#### -#.####-##.### -#.### -#.###
1450H=H+.2
1460IF P0[0THEN 1480
1470NEXT Q0
1480IF Z9$="YES"THEN 1490:M=.01
1490NEXT M
1500IF Z9$="NO"THEN 1760
1510REM DRAW AXES AND PLOT OUTPUT
1520SELECT PLOT 413
1530PLOT [500,300,],60[,-5,HEX(27)],100[5,,HEX(2D)],[,,"+"],5[-1
00,,"+"],3[,100,"+"],[,-300,"+"]
1540FOR E9=1TO E-1
1550PLOT [V5(E9),W5(E9),"*"]
1560NEXT E9
1570PLOT [-L5,-Y5,"+"]
1580FOR E9=1TO O2-1:PLOT [V6(E9),W6(E9),"*"]:NEXT E9
1590PLOT [-L6,-Y6,"+"]
1600FOR E9=1TO O3-1:PLOT [V7(E9),W7(E9),"*"]:NEXT E9
1610PLOT [-L7,-Y7,"+"]
1620REM PLOT INPUT
163004=0:O2=0:O3=0
1640C4=INT(100*Q7)/100+.04
1650FOR Q2=0TO C4STEP .002
1660GOSUB 4000
1670GOSUB 4260
168001=(P2-O2)*1000+O3
169002=P2
170003=O1-INT(ABS(O1))*SGN(O1)
171004=O4+INT(ABS(O1))*SGN(O1)
1720PLOT [O1,1,"+"]
1730NEXT Q2
1740PLOT [-O4,-(C4/.002+1),"+"]
1750REM COMPUTE DEFL.RESIST.
1760R0=R8
1770P2=P7
1780Q2=Q7
1790P1=P2-R0*Q2
1800 GOSUB 4190
1810 GOSUB 4130
1820G2=G*R3/(R3-R7)
1830IF Z9$="NO"THEN 1930
1840REM PLOT DEFL.RESIST.
1850PLOT [P7*1000-R3*150,Q7*500-75,HEX(FB)]:I4=0
1860FOR I1=1TO 30:PLOT [R3*10+I3,5,HEX(FB)]:I2=R3*10+I3:I3=I2-IN
T(I2):I4=I4+INT(I2)
1870NEXT I1:PLOT [-P7*1000+R3*150-I4,-Q7*500-75,"+"]
1880REM LABEL AXES
1890PLOT [0,-15,"0"],[80,0,"0.1"],[70,0,"0.2"]
1900PLOT [70,0,"0.3"],[70,0,"0.4"],[70,0,"0.5"]
1910PLOT [-545,15,"0"],[-10,100,"0.2"]
1920PLOT [-30,100,"0.4"],[-30,100,"0.6"],[205,-330,"PRESSURE"],[
-335,305,"FLOW"],[-250,-325,]
1930SELECT PRINT 213:PRINT HEX(0A):PRINTUSING 620,R1,N,N9,S,W,B,
B6,C
```

LISTING A-1. LJARS (Cont'd)

```
1940PRINT " "
1950REM EFFECT OF CONTROLS ON,AND RATE SENSITIVITIES
1960 Z0=Z0+W*W/2*(2/C*SQR(R0*R1/(R0+R1))*(Q-Q4-H3/R0)/SQR(ABS(Q-
Q4-H3/R0))-A)*(2*B6/W-1)/(4*C2*(R0+R1)/W/W/R0/R1-(2/C*SQR(R0*R1/
(R0+R1))*(Q-Q4-H3/R0)/SQR(ABS(Q-Q4-H3/R0))-A))
1970 S7=4*P6*Z0/N0/N/C:S8=2*N*P6*Z0/C/57.3/N0
1980PRINTUSING 2090," SELF-STAGED DEFL. RESIST.=",R3
1990PRINTUSING 2090,"SELF-STAGED OUTPUT RESIST.=",R7
2000PRINTUSING 2090,"BLOCKED GAIN AT SELF-BIAS =",G
2010PRINTUSING 2090,"          SELF-STAGED BIAS =",P2
2020PRINTUSING 2090,"          SELF-STAGED GAIN =",G2
2030IF R$="NO"THEN 2110
2040PRINTUSING 2100,"NORMLIZED RATE SENSITIVITY=",S7
2050PRINTUSING 2100,"DIMNSLESS RATE SENSITIVITY=",S8
2060PRINTUSING 2100,"MILH 5606 RATE SENSITIVITY=",S8*2.2835E-6
2070PRINTUSING 2100,"PNEUMATIC RATE SENSITIVITY=",S8*2.649E-9
2080PRINTUSING 2100,"SENSR-90DEG FREQ,F*BS!2/NU=",F0*C*N:IF Z9$=
"NO"THEN 2960
2090%############################ -###.###
2100%############################ -#.####!!!!
2110PRINT " "
2120PRINT " BIAS PRESS.   P JET      GAIN    DEFL.RES."
2130G6=0
2140REM COMPUTE GAIN VS.BIAS AND STORE DATA
2150G4=0:G8=1:FOR P2=-.05TO .195STEP .005:GOSUB 4330:GOSUB 4280:
GOSUB 4190:G7(G8)=G:G8=G8+1:IF ABS(G)[99THEN 2160:G6=100
2160NEXT P2
2170FOR G8=1TO 49STEP 10:P2=(G8-11)*.005:GOSUB 4330:GOSUB 4280:G
=G7(G8):GOSUB 4130:GOSUB 4300:NEXT G8
2180IF G6[100THEN 2190:SELECT PLOT 413:PLOT [80,-125,]:SELECT PR
INT 213:GOTO 2280
2190IF Z9$="NO"THEN 2960
2200REM DRAW AXES FOR G VS.PCBIAS
2210SELECT PLOT 413:PLOT [120,0,],50[0,-5,HEX(27)]
2220PLOT 80[5,0,HEX(2D)],[,,"+"],5[-100,0,"+"],20[5,0,HEX(2D)]
2230PLOT [0,200,"+"],2[0,-100,"+"],[-110,,]
2240REM PLOT G VS.PCBIAS
2250G9=0:G4=0:FOR G8=1TO 50:J7=(G7(G8)-G4)*10+G5:G5=J7-INT(ABS(J
7))*SGN(J7):G9=G9+INT(ABS(J7))*SGN(J7):PLOT [10,J7,"*"]:G4=G7(G8
)
2260NEXT G8:PLOT [-390,-G9,"+"],[-120,-15,"-.05"],[80,0,"0"],[80
,0,".05"],[70,0,".10"],[70,0,".15"],[70,0,".20"]
2270PLOT [-450,115,"10"],[-20,100,"20"],[70,-230,"CONTROL BIAS P
RESSURE"],[-340,200,"GAIN"]
2280IF Z3$[]"YES"THEN 2290:Z5$="NO"
2290SELECT PLOT 413:T6=0:Z6$="1"
2300IF Z5$="NO"THEN 2310:P2=J6:GOSUB 4330:Q7=Q2:P7=J6:IF Z2=1THE
N 2310:IF Z2=3THEN 2310:X3=0:R7=0
2310C5=W!3/(12*C2)
2320L1=2*C*C*(X1/W0+X3/F8)
2330Q2=Q7
2340GOSUB 4000
2350R9=R0-R7
2360K6=W*W/(4*C2):P1=P7-R0*Q2
2370K1=(1+R9*(A*K6+1/R1+2*K6*P1/(SQR(ABS(P1))*C)))/(2*L1*C5)
2380A0=K1*2*L1*C5
2390A3=(A0-1)*L1/R9
2400A2=2*L1*C5
2410K0=1+R0*(A*K6+1/R1+2*K6*P1/(SQR(ABS(P1))*C))
2420G3=1:P3=0
2430Z3=0
2440GOSUB 4190
2450T8=0
2460FOR L=1TO 100
2470F2=10!(L/50-3)
2480W9=2*#PI*F2
2490G0=G*K0/SQR((A0-A2*W9!2)!2+(A3*W9)!2)
2500F1=SQR(K1)/(2*#PI)
2510G1(L)=20*.432945*(LOG(G0)-LOG(G3))
2520G3=G0
2530P8=ARCTAN(A3/SQR(A2*A0)*F2/F1/(1-(F2/F1)!2))
2540IF P8]0THEN 2560
2550Z3=180
2560P9=P8*180/#PI+B6*F2*360+Z3
2570P4(L)=P9-P3:P3=P9
2580IF P9-45[0THEN 2600
```

LISTING A-1. LJARS (Cont'd)

```
2590IF T8=1THEN 2600:T8=1:F3=F2:G2=G0
2600NEXT L
2610IF T6=0THEN 2620:Z1=G2*F3:GOTO 2670
2620Z=G2*F3
2630SELECT PLOT 413
2640PLOT [500,230,],80[0,-5,HEX(27)],100[5,0,HEX(2D)]
2650PLOT 80[0,5,HEX(27)]
2660PLOT [0,0,"+"],4[0,-100,"+"],2[-250,0,"+"],[120,,"+"],[250,,
"+"],[-370,,],4[0,100,"+"]
2670PLOT [0,-400,"+"]:U2=0:U3=0
2680FOR L=1TO 100
2690U1=G1(L)*10+U2
2700U2=U1-INT(ABS(U1))*SGN(U1)
2710U3=U3+INT(ABS(U1))*SGN(U1)
2720PLOT [5,U1,Z6$]
2730NEXT L
2740PLOT [-500,-U3,"+"]:U5=0:U6=0:PLOT [0,400,"+"]
2750FOR L=1TO 100
2760U4=P4(L)*2+U5
2770U5=U4-INT(ABS(U4))*SGN(U4)
2780IF U6[400THEN 2800
2790GOTO 2830
2800U6=U6+INT(ABS(U4))*SGN(U4)
2810PLOT [5,-U4,Z6$]
2820NEXT L
2830PLOT [-5*(L-1),U6,"+"]:IF Z2=3THEN 2840:PLOT [-40,0,"40"],[-
20,-100,"30"]:GOTO 2850
2840Z2=2:T6=1:Z6$="2":GOTO 2300
2850PLOT [-20,-100,"20"],[-20,-100,"10"],[-10,-100,"0"]
2860PLOT [0,-20,".001"],[85,,".003"],[95,0,".01"],[85,,".03"],[1
05,0,".1"]
2870PLOT [10,20,"-200"],[-40,100,"-150"],[-40,100,"-100"]
2880PLOT [-40,100,"-50"],[-20,100,"0"],[,-150,"PHASE"]
2890PLOT [-440,-290,"NORMALIZED FREQUENCY"]
2900IF Z5$="YES"THEN 2910:PLOT [-450,250,"SELF"],[-40,-15,"STAGE
D"],[-60,-15,"GAIN DB"]:GOTO 2920
2910PLOT [-450,250,"DB GAIN"],[-30,-30,],[100,-145,]:SELECT PRIN
T 213:GOTO 2930
2920PLOT [100,-145,]:SELECT PRINT 213
2930IF Z=0THEN 2940:T7=1:PRINTUSING 2950,T7,Z
2940IF Z1=0THEN 2960:T7=2:SELECT PLOT 413:PLOT [600,,]:SELECT PR
INT 213:PRINTUSING 2950,T7,Z1
2950%GBP(#) =-#.#####
2960IF Z3$="YES"THEN 3020
2970PRINT " ":PRINT " ":PRINT " ":PRINT " ":PRINT " "
2980INPUT "DO YOU WANT TO DO ANOTHER PROBLEM",Z4$
2990IF Z4$="NO"THEN 3040
3000SELECT PLOT 413:PLOT [,-95,]:SELECT PRINT 213
3010GOTO 30
3020NEXT B:NEXT W:NEXT B6:NEXT S:NEXT N9
3030PRINT " ":PRINT " ":PRINT " "
3040SELECT CO 005(64),PRINT 005(64):END
4000R0=T4+T5*Q2
4010RETURN
4020 FOR I0=1TO 25
4030 IF I0]1 THEN 4050
4040 C(I0)=.5:GOTO 4070
4050 IF I0]2 THEN 4070
4060 C(I0)=.6
4070 F0(I0)=2.667/C(I0)*(EXP(6.6*C(I0)!2)-1)-N9
4080 IF I0[2 THEN 4110
4090 C(I0+1)=C(I0)-F0(I0)*(C(I0)-C(I0-1))/(F0(I0)-F0(I0-1))
4100 IF ABS(F0(I0))[.01 THEN 4120
4110 NEXT I0
4120 C=C(I0):RETURN
4130 K7=(W*W)/(4*C2)
4140 IF Q2]0THEN 4150:B2=0:GOTO 4160
4150 B2=3.4242*(1/(1+B/0.1/Q2/C/N)-0.5):IF B2]0THEN 4160:B2=0
4160 D2=(1-((B2*Q2*A)/2)-((B2*Q2*P1)/(SQR(ABS(P1))*C)))/(2*K7+(B
2*Q2)/R1)
4170R3=(D2*(1+R0/R1)+(R0*P1)/(C*SQR(ABS(P1)))+R0*A/2)/(D2*(1/R1)
+A/2+(P1/(SQR(ABS(P1))*C)))
4180RETURN
4190 K7=(W*W)/(4*C2)
4200 IF Q2]0THEN 4210:B2=0:GOTO 4220
4210 B2=3.4242*(1/(1+B/0.1/Q2/C/N)-0.5):IF B2]0THEN 4220:B2=0
```

LISTING A-1. LJARS (Cont'd)

```
4220 D2=(1-((B2*Q2*A)/2)-((B2*Q2*P1)/(SQR(ABS(P1))*C)))/(2*K7+(B
2*Q2)/R1)
4230 J3=1:IF Q2]=0THEN 4240:J3=0
4240G=D6*(1/(D2*2*(1+R0/R1)+R0*A+(R0*2*P1)/(C*SQR(ABS(P1)))))*J9
*1/K7*(2*B6/W/(1+2*Q2*J3)-1)
4250RETURN
4260P2=-(Q-Q4)*R1+(R1+R0)*Q2
4270RETURN
4280P1=(P2/R0-(Q-Q4))*R0*R1/(R0+R1)
4290RETURN
4300PRINTUSING 4310,P2,P1,G,R3
4310%    -#.###     -#.#####  -###.##    -###.###
4320RETURN
4330Q2=-.5*(T4+R1)/T5+SQR(.25*((T4+R1)/T5)!2+(P2+R1*(Q-Q4))/T5):
GOSUB 4000
4340RETURN
:
```

LISTING A-2. COMPUTER PROGRAM FOR SIMPLIFIED LJARS SENSITIVITY

```
5 SELECT PLOT 413,PRINT 213
6 PLOT [,,]
7 SELECT CO 213
10 DIM C(25),F(25)
20 INPUT "ASPECT RATIO",A
30 INPUT "NOZZLE LENGTH",L
35 INPUT "NOZZLE WIDTH IN MM",B3:B3=B3/1000
40 INPUT "OUTPUT WIDTH",B0
50 INPUT "SPLITTER WIDTH",B1
60 INPUT "SPLITTER DISTANCE",X
70 INPUT "INPUT WORKING FLUID",A$:IF A$="AIR" THEN 80:IF A$="OIL
" THEN 90
80 M=1.789E-5:R=1.2059:GOTO 100
90 M=.0155:R=860
100 PRINT " MOD.NR      NR     SIGMA*NR  S(PA/0/S)   S(PSI/0/S)  P
RESSURE(PA)"
110 FOR N=50 TO 150 STEP 10
120 N1=N*(1+L)*(1+1/A)!2
130 GOSUB 1000
140 C2=1.32*C1*C1
150 S=M*N1*C2*X*X*(1-8*X/C2/N1/A/A)*(1-1.1*B1/SQR(C1*N1*B1/2))/5
7.3/C1/B0
160 S1=S/1000/6.89
165 P=R/2*(N1*M/R/B3)!2
170 PRINTUSING 180,N,N1,A*N1,S,S1,P
180 %   ###  #####.## #####.##  ###.#####     #.###!!!!  #######.
###
190 NEXT N
195 SELECT CO 005,PRINT 005
200 END
1000 FOR I=1TO 25
1010 IF I]1THEN 1030
1020 C(I)=.5:GOTO 1050
1030 IF I]2THEN 1050
1040 C(I)=.6
1050 F(I)=2.667/C(I)*(EXP(6.6*C(I)!2)-1)-N
1060 IF I[2THEN 1090
1070 C(I+1)=C(I)-F(I)*(C(I)-C(I-1))/(F(I)-F(I-1))
1080 IF ABS(F(I))[.01THEN 1100
1090 NEXT I
1100 C1=C(I):RETURN
```

APPENDIX A

LISTING A-2. COMPUTER PROGRAM FOR SIMPLIFIED LJARS SENSITIVITY (Cont'd)

```
ASPECT RATIO? 1.6667
NOZZLE LENGTH? 2
NOZZLE WIDTH IN MM? .75
OUTPUT WIDTH? 1.7
SPLITTER WIDTH? .5
SPLITTER DISTANCE? 20
INPUT WORKING FLUID? AIR
```

MOD.NR	NR	SIGMA*NR	S(PA/0/S)	S(PSI/0/S)	PRESSURE(PA)
50	383.99	640.00	0.01509	2.190E-06	34.786
60	460.79	768.00	0.02080	3.020E-06	50.092
70	537.59	896.00	0.02662	3.864E-06	68.180
80	614.39	1024.00	0.03254	4.723E-06	89.052
90	691.18	1152.00	0.03854	5.594E-06	112.707
100	767.98	1280.00	0.04462	6.476E-06	139.144
110	844.78	1408.00	0.05076	7.368E-06	168.364
120	921.58	1536.00	0.05697	8.269E-06	200.368
130	998.38	1664.00	0.06324	9.178E-06	235.154
140	1075.18	1792.00	0.06956	1.009E-05	272.723
150	1151.98	1920.00	0.07592	1.102E-05	313.075

```
ASPECT RATIO? 2.5
NOZZLE LENGTH? 2
NOZZLE WIDTH IN MM? .75
OUTPUT WIDTH? 1.7
SPLITTER WIDTH? .25
SPLITTER DISTANCE? 20
INPUT WORKING FLUID? OIL
```

MOD.NR	NR	SIGMA*NR	S(PA/0/S)	S(PSI/0/S)	PRESSURE(PA)
50	294.00	735.00	11.94935	1.734E-03	21463.823
60	352.80	882.00	15.71710	2.281E-03	30907.905
70	411.60	1029.00	19.56259	2.839E-03	42069.093
80	470.40	1176.00	23.47678	3.407E-03	54947.387
90	529.20	1323.00	27.45065	3.984E-03	69542.787
100	588.00	1470.00	31.47818	4.568E-03	85855.293
110	646.80	1617.00	35.55275	5.160E-03	103884.904
120	705.60	1764.00	39.67135	5.757E-03	123631.621
130	764.40	1911.00	43.82959	6.361E-03	145095.445
140	823.20	2058.00	48.02430	6.970E-03	168276.374
150	882.00	2205.00	52.25240	7.583E-03	193174.409

LISTING A-3. COMPUTER PROGRAM FOR REYNOLDS NUMBER CONTROL

```
5 REM ******* SHUNT RESISTANCE COMPENSATION *******
10 DIM C(25),F(25)
30 INPUT "NOMINAL MODIFIED REYNOLDS NO.",N
40 INPUT "VISCOSITY CHANGE RATIO",V
50 PRINT "NOMINAL R(NOZ)/R(CAP)   NR' AT NEW VISCOSITY   NR/NRO
"
60 FOR R=.0001TO 5.0001 STEP .50
70 N9=N:GOSUB 4010
80 C0=C1:C=C1
90 N9=2.667*(EXP(6.6*C0*C0)-1)/C0/C0*C*(SQR(.25+V*R*(R+1)*C012/C
/C)-.5)/R
100 GOSUB 4010:IF ABS(C-C1)[.0001 THEN 110:C=C1:GOTO 90
110 PRINTUSING 120,R,N9,N9/N
120     ##       -##.##                -###.###          -#.###

130 NEXT R
140 INPUT "DO YOU WANT ANOTHER CASE",A$:IF A$="N"THEN 150:GOTO 3
0
150 END
4010 REM ******* CD SUBROUTINE ********
4020 FOR I=1TO 25
4030 IF I]1THEN 4050
4040 C(I)=.5:GOTO 4070
4050 IF I]2THEN 4070
4060 C(I)=.6
4070 F(I)=2.667/C(I)*(EXP(6.6*C(I)12)-1)-N9
4080 IF I[2THEN 4110
4090 C(I+1)=C(I)-F(I)*(C(I)-C(I-1))/(F(I)-F(I-1))
4100 IF ABS(F(I))[.01THEN 4120
4110 NEXT I
4120 C1=C(I):RETURN
```

```
NOMINAL MODIFIED REYNOLDS NO.? 120
VISCOSITY CHANGE RATIO? .5
NOMINAL R(NOZ)/R(CAP)   NR' AT NEW VISCOSITY   NR/NRO
          0.00                  66.609            0.555
          0.50                  73.509            0.612
          1.00                  76.694            0.639
          1.50                  78.500            0.654
          2.00                  79.656            0.663
          2.50                  80.456            0.670
          3.00                  81.045            0.675
          3.50                  81.495            0.679
          4.00                  81.851            0.682
          4.50                  82.138            0.684
          5.00                  82.375            0.686
```

APPENDIX A

TABLE A-1. COMPUTER VARIABLE NAME DEFINITIONS FOR LAMINAR JET DEVICE PORT CHARACTERISTIC PROGRAM

Term	Definition
A	Net entrainment coefficient, a_1
A0	A_0
A1	Term used in calculation of R_v
A2	A_2
A3	During output computation, A3 is half the sum of the supply and control flows. During dynamic computations, A3 = A_1.
A4	Jet impedance
A5	Total flow available at output when jet is deflected
A6	Switch, 1 or 0, for output resistance calculation past "knee"
A7	Output flow at "knee"
A8	Output pressure at "knee"
B	B_t
B1	Subtrainment radius
B5	B_{sp}
B6	X_{sp}
B7	B_o
B8	B_v
C	c_d
C0	Bounding plate loss coefficient, C_{XSP}
C2	c_θ
C3	Control edge spill-back effect pressure recovery coefficient
C4	Limit of flow for Q_c vs P_c plot
C5	C_j
D	c_{dbs}
D0	Displacement thickness
D1	Δy for R_v integration
G6	Gain limiter = 100

TABLE A-1. COMPUTER VARIABLE NAME DEFINITIONS FOR LAMINAR JET DEVICE PORT CHARACTERISTIC PROGRAM (Cont'd)

Term	Definition
G7	Blocked gain matrix variable
G8	Gain loop counter
G9	Running total of gain plot increments
H	Counter in print cycle of Q_o vs P_o
H3	Bias control pressure for Q_o vs P_o
I	Counter
I1	Counter in deflection resistance plot
I2	Plot increment for Q_c deflection
I3	$\Delta Q_{c_{defl.}}$ truncation error
I4	Running total of Q_c deflection increments
J	Counter
J1	Plate loss coefficient
J6	Control bias pressure for dynamics
J7	Gain plot increment
J9	Increase in gain due to side vent configuration
K	K_1
K0	$(1 + A_4)_{DC}$
K1	A_0/A_2
K2	Control channel empirical coefficient
K3	K_5
K4	K_6
K5	Flow dependent term of R_{oc}
P	$(P_j)^{1/4}$
P0	P_o
P1	P_j
P2	P_c
P3	Last value of phase angle

APPENDIX A

TABLE A-1. COMPUTER VARIABLE NAME DEFINITIONS FOR LAMINAR JET DEVICE PORT CHARACTERISTIC PROGRAM (Cont'd)

Term	Definition
P4	Phase plot increment
P5	$P_r(\delta)$
P6	$P_r(\delta = 0)$
P7	Self-staged output pressure
P8	Phase in radians
P9	Phase in degrees
Q	Q_e
Q0	Q_o
Q2	A_{Qc}
Q4	Q_{SB}
Q5	Flow recovery
Q7	Self-staged output flow
R	Side vent resistance, R_{sv}
R0	R_c
R1	R_v
R3	R_i
R4	R_{ocL}
V2	X_{cd}
V5	$P_o(\Delta P_c = -0.01)$ matrix
V6	$P_o(P_c = 0)$ matrix
V7	$P_o(P_c = +0.01)$ matrix
W	B_c
W0	$\bar{B}_c$
W3	$B_{c_{min}}$
W5	$Q_o(P_c = -0.01)$ matrix
W6	$Q_o(P_c = 0)$ matrix
W7	$Q_o(P_c = +0.01)$ matrix

TABLE A-1. COMPUTER VARIABLE NAME DEFINITIONS FOR LAMINAR JET DEVICE PORT CHARACTERISTIC PROGRAM (Cont'd)

Term	Definition
W9	Normalized radian frequency
X	Virtual nozzle length
X0	Jet potential core length
X1	X_c
X2	Virtual origin
X3	X_o
X4	Starting value of X_{sp}
X5	Ending value of X_{sp}
X6	Step of X_{sp}
Y	Entrainment streamline
Y0	Streamline location
Y1	Lateral distance, Y
Y5	Running total of W5
Y6	Running total of W6
Y7	Running total of W7

```
IF YOU ARE INTERESTED ONLY IN AN ANGULAR RATE SENSOR ANSWER NO  FOR PLOTS.
TODAYS DATE? MON 22 JAN 79
MON 22 JAN 79
LAMINAR JET DEVICE CHARACTERISTICS
DO YOU WANT ANGULAR RATE DATA? YES
DOES THIS DEVICE HAVE CENTER DUMP OR OUTPUT VENTS? NO
DOES THIS DEVICE HAVE SUDDEN EXPANSION OUTPUTS? NO
MODIFIED(1) OR WIDTH(2) REYNOLDS NO.? 1
DO YOU WANT RANGES,DO YOU WANT PLOTS? NO,YES
RESPONSE OTHER THAN SELF-STAGED? NO
CONTROL AND THROAT WIDTH? 1,3.5
ASPECT RATIO,MOD REY.NO.? 2.5,70
SPLITTER DISTANCE      ? 20
NOZZLE AND SPLITTER LGTH? 2,.75
OUTPUT LENGTH,AVG.WIDTH ? 12,2.35
BIAS CONTROL PRESSURE   ? 0
CTRL L,AVG.W,MIN.W,ENT.R? 19,2.75,1,.5
SPLITTER , OUTPUT WIDTH ? .5,1.7

CORE LENGTH=      20.27135454473 VIRTUAL ORIGIN=  4.239552972889 DISPLACEMENT THICKNESS=
 .1293762816
```

CENTERED INPUT AND OUTPUT CHARACTERISTICS

Q	PO	PO*QO	RO	PC	RC
0.00	0.2461	0.0000	-0.309	-0.010	0.091
0.05	0.2297	0.0114	-0.346	0.008	0.112
0.10	0.2114	0.0211	-0.386	0.029	0.133
0.15	0.1910	0.0286	-0.428	0.052	0.154
0.20	0.1685	0.0337	-0.472	0.077	0.175
0.25	0.1432	0.0358	-0.514	0.104	0.196
SELF-STAGED OPERATING FLOW = 0.290					
0.30	0.1175	0.0352	-0.514	0.134	0.217
0.35	0.0918	0.0321	-0.514	0.165	0.238
0.40	0.0660	0.0264	-0.514	0.199	0.259
0.45	0.0403	0.0181	-0.514	0.234	0.280
0.50	0.0146	0.0073	-0.514	0.272	0.301

SELF-STAGED DEFL. RESIST.=	0.440
SELF-STAGED OUTPUT RESIST.=	-0.514
BLOCKED GAIN AT SELF-BIAS =	10.536
SELF-STAGED BIAS =	0.122
SELF-STAGED GAIN =	4.859
NORMLIZED RATE SENSITIVITY=	7.206E-01
DIMNSLESS RATE SENSITIVITY=	1.065E+03
MILH 5606 RATE SENSITIVITY=	2.432E-03
PNEUMATIC RATE SENSITIVITY=	2.822E-06
SENSR-90DEG FREQ,F*BS!2/NU=	8.547E-01

BIAS PRESS.	P JET	GAIN	DEFL.RES.
-0.050	-0.04516	14.60	0.322
0.000	-0.00296	11.24	0.373
0.050	0.02784	8.43	0.401
0.100	0.05335	9.82	0.427
0.150	0.07560	11.02	0.445

```
RV= 0.264,NR=  411.6,NR'= 70.0,AR= 2.500,BC=  1.00,BT= 3.50,XSP=20.00,CD= .664
```

Figure A-1. Printout for HDL LJARS.

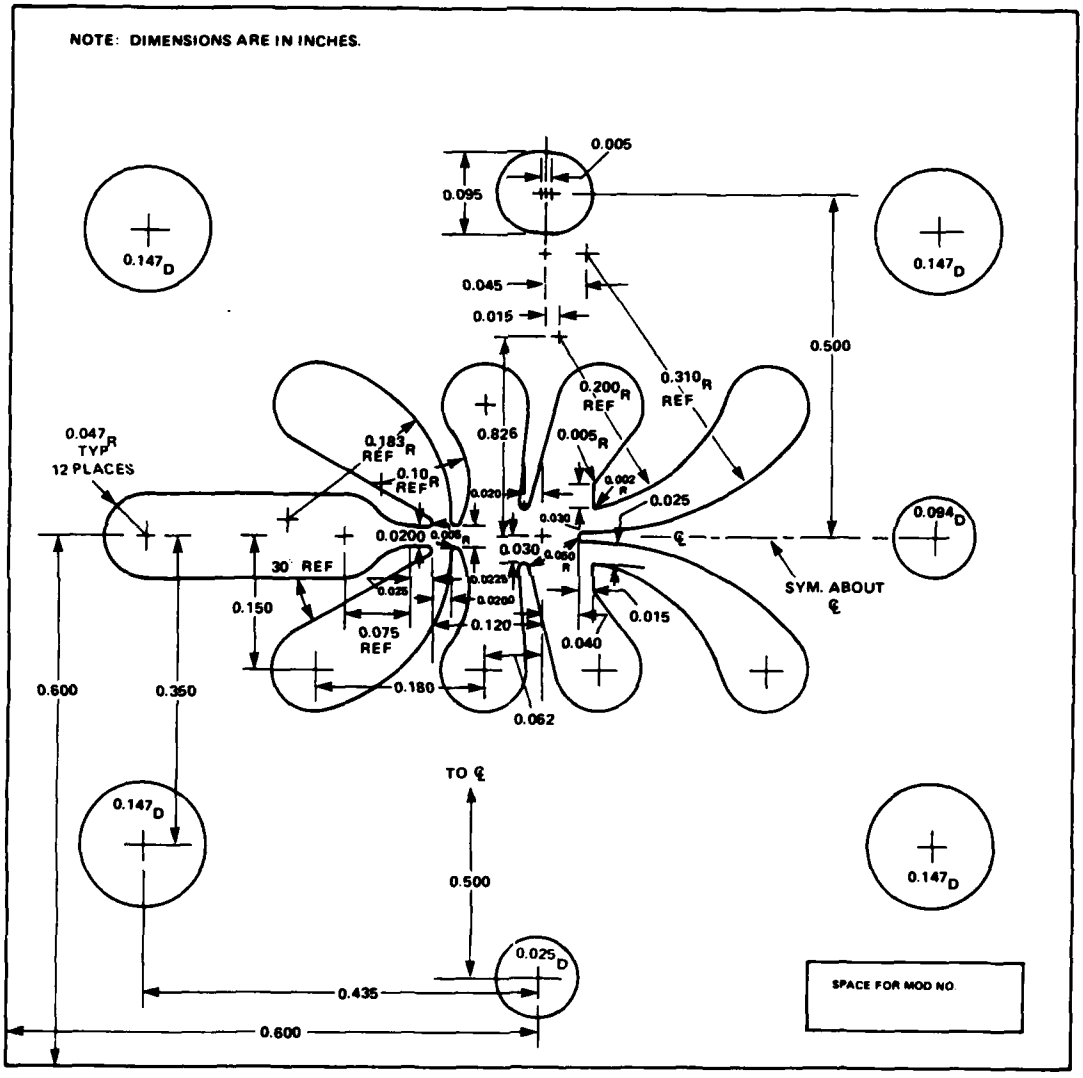

Figure A-2. Standard silhouette of laminar proportional amplifier (model 3.1.1.8).

DISTRIBUTION

ADMINISTRATOR
DEFENSE DOCUMENTATION CENTER
ATTN DDC-TCA (12 COPIES)
CAMERON STATION, BUILDING 5
ALEXANDRIA, VA 22314

COMMANDER
US ARMY RSCH & STD GP (EUR)
ATTN LTC JAMES M. KENNEDY, JR.
CHIEF, PHYSICS & MATH BRANCH
FPO NEW YORK 09510

COMMANDER
US ARMY MATERIEL DEVELOPMENT &
READINESS COMMAND
ATTN DRXAM-TL, HQ TECH LIBRARY
ATTN DRCRD-TP, WILLIAM RALPH
5001 EISENHOWER AVENUE
ALEXANDRIA, VA 22333

COMMANDER
US ARMY ARMAMENT MATERIEL
READINESS COMMAND
ATTN DRSAR-ASF, FUZE &
MUNITIONS SUPPORT DIV
ATTN DRSAR-RDF, SYS DEV DIV - FUZES
ATTN DRSAR-RDG-T, MR. R. SPENCER
ATTN DRSAR-ASF
ATTN DRSAR-LEP-L, TECH LIBRARY
ROCK ISLAND, IL 61299

COMMANDER
US ARMY MISSILE & MUNITIONS
CENTER & SCHOOL
ATTN ATSK-CTD-F
REDSTONE ARSENAL, AL 35809

DIRECTOR
US ARMY MATERIEL SYSTEMS ANALYSIS ACTIVITY
ATTN DRXSY-MP
ABERDEEN PROVING GROUND, MD 21005

DIRECTOR
US ARMY BALLISTIC RESEARCH LABORATORY
ATTN DRDAR-TSB-S (STINFO)
ABERDEEN PROVING GROUND, MD 21005

TELEDYNE BROWN ENGINEERING
CUMMINGS RESEARCH PARK
ATTN DR. MELVIN L. PRICE, MS-44
HUNTSVILLE, AL 35807

COMMANDER IDDR&E
PENTAGON, ROOM 3D 1089
WASHINGTON, DC 20310
ATTN LTC G. KOPESAK

OFFICE OF THE DEPUTY CHIEF OF STAFF FOR
RESEARCH, DEVELOPMENT & ACQUISITION
DEPARTMENT OF THE ARMY
WASHINGTON, DC 20310
ATTN DAMA-ARP-P
ATTN MR. JOHN HILL, ROOM 3D424

US ARMY R&D GROUP (EUROPE)
BOX 15
FPO NEW YORK 09510
ATTN CHIEF, AERONAUTICS BRANCH
ATTN CHIEF, ENGINEERING SCIENCES

US ARMY RESEARCH OFFICE
P. O. BOX 12211
RESEARCH TRIANGLE PARK, NC 27709
ATTN JAMES J. MURRAY, ENG SCI DIV
ATTN R. SINGLETON

BMD ADVANCED TECHNOLOGY CENTER
P.O. BOX 1500
HUNTSVILLE, AL 35807
ATTN J. PAPADOPOULOS

COMMANDER
USA FOREIGN SCIENCE & TECHNOLOGY CENTER
FEDERAL OFFICE BUILDING
220 7th STREET, NE
CHARLOTTESVILLE, VA 22901
ATTN DRXST-SD1
ATTN DRXST-IS3, C. R. MOORE

DIRECTOR
APPLIED TECHNOLOGY LABORATORY
FORT EUSTIS, VA 23604
ATTN GEORGE W. FOSDICK, DAVDL-EU-SYA

COMMANDER
USA MISSILE COMMAND
REDSTONE ARSENAL, AL 35809
ATTN REDSTONE SCIENTIFIC INFORMATION
CENTER, DRSMI-RBD
ATTN DRDMI-TGC, WILLIAM GRIFFITH
ATTN DRDMI-TGC, J. C. DUNAWAY
ATTN DRCPM-TOE, FRED J. CHEPLEN

COMMANDER
USA MOBILITY EQUIPMENT R&D CENTER
FORT BELVOIR, VA 22060
ATTN TECHNICAL LIBRARY (VAULT)
ATTN DRDME-EM, R. N. WARE

COMMANDER
EDGEWOOD ARSENAL
ABERDEEN PROVING GROUND, MD 21010
ATTN SAREA-MT-T, MR. D. PATTON

COMMANDER
US ARMY ARRADCOM
DOVER, NJ 07801
ATTN SARPA-TS-S-#59
ATTN DRDAR-LCN-F, A. E. SCHMIDLIN
ATTN DRDAR-LCW-E, MR. J. CONNOR
ATTN SARPA-ND-C-C, D. SAMPAR

COMMANDER
WATERVLIET ARSENAL
WATERVLIET ARSENAL, NY 12189
ATTN SARWV-RDT-L
ATTN GARY WOODS
ATTN JOHN BARRETT

COMMANDER
USA TANK AUTOMOTIVE RES & DEV COMMAND
ARMOR & COMP DIV, DRDTA-RKT
BLDG 215
WARREN, MI 48090
ATTN T. KOZOWYK
ATTN M. STEELE

COMMANDER
WHITE SANDS MISSILE RANGE, NM 88002
ATTN STEWS-AD-L, TECHNICAL LIBRARY

COMMANDER/DIRECTOR
ATMOSPHERIC SCIENCES LABORATORY
USA ERADCOM
WHITE SANDS MISSILE RANGE, NM 88002
ATTN DELAS-AS (HOLT)

OFFICE OF NAVAL RESEARCH
DEPARTMENT OF THE NAVY
ARLINGTON, VA 22217
ATTN STANLEY W. DOROFF, CODE 438
ATTN D. S. SIEGEL, CODE 211

DEPARTMENT OF THE NAVY
R&D PLANS DIVISION
ROOM 5D760, PENTAGON
WASHINGTON, DC 20350
ATTN BENJ R. PETRIE, JR.
OP-987P4

COMMANDER
NAVAL AIR DEVELOPMENT CENTER
WARMINSTER, PA 18974
ATTN R. MCGIBONEY, 30424
ATTN CODE 8134, LOIS GUISE

COMMANDING OFFICER
NAVAL AIR ENGINEERING CENTER
LAKEHURST, NY 08733
ATTN ESSD, CODE 9314, HAROLD OTT

NAVAL AIR SYSTEMS COMMAND
DEPARTMENT OF THE NAVY
WASHINGTON, DC 20360
ATTN CODE AIR-52022A, J. BURNS
ATTN CODE AIR-52022E, D. HOUCK

COMMANDER
PACIFIC MISSILE RANGE
NAVAL MISSILE CENTER
POINT MUGU, CA 93042
ATTN CODE 3123, ABE J. GARRETT
ATTN CODE 1243, A. ANDERSON

COMMANDER
NAVAL SHIP ENGINEERING CENTER
PHILADELPHIA DIVISION
PHILADELPHIA, PA 19112
ATTN CODE 6772, D. KEYSER

COMMMANDER
NAVAL SURFACE WEAPONS CENTER
WHITE OAK, MD 20910
ATTN CODE 413, CLAYTON MCKINDRA
ATTN DIV 412, C. J. SEWELL

COMMANDER
NAVAL ORDNANCE STATION
INDIANHEAD, MD 20640
ATTN CODE 5123B, J. MORRIS

NAVAL SHIP RES & DEV CENTER
CODE 1619, MR. K. READER
BETHESDA, MD 20084

NAVAL SEA SYSTEMS COMMAND
SEA0331H
WASHINGTON, DC 20362
ATTN A. CHAIKIN

COMMANDER
NAVAL WEAPONS CENTER
CHINA LAKE, CA 93555
ATTN CODE 533, LIBRARY DIVISION
ATTN CODE 3636, C. BURMEISTER

COMMANDER
AF AERO PROPULSION LABORATORY, AFSC
WRIGHT-PATTERSON AFB, OH 45433
ATTN LESTER SMALL 1TBC

COMMANDER
AIR FORCE AVIONICS LABORATORY
WRIGHT-PATTERSON AFB, OH 45433
ATTN RWN-2, RICHARD JACOBS

DIRECTOR
AF OFFICE OF SCIENTIFIC RESEARCH
1400 WILSON BLVD
ARLINGTON, VA 22209
ATTN NE, MR.GEORGE KNAUSENBERGER

COMMANDER
AIR FORCE FLIGHT DYNAMICS LABORATORY
WRIGHT-PATTERSON AFB, OH 45433
ATTN AFFDL/FGL, H. SNOWBALL

COMMANDER
AF WEAPONS LABORATORY, AFSC
KIRTLAND AFB, NM 87117
ATTN SUL, TECHNICAL LIBRARY

COMMANDER
ARMAMENT DEVELOPMENT AND TEST CENTER
EGLIN AIR FORCE BASE, FL 32542
ATTN ADTC (DLOSL), TECH LIBRARY

AIR FORCE FLIGHT TEST CENTER
6510 ABG/SSD
EDWARDS AFB, CA 93523
ATTN TECHNICAL LIBRARY

AF INSTITUTE OF TECHNOLOGY, AU
WRIGHT-PATTERSON AFB, OH 45433
ATTN LIBRARY AFIT(LD),
BLDG 640, AREA B
ATTN AFIT(ENM), MILTON E. FRANKE (3 COPIES)

AEROSPACE MEDICAL DIVISION
BROOKS AFB, TX 78235
ATTN AMD/RDN, CPT G. JAMES

DIV. OF REACTOR RES & DEV
F-309 USERDA
WASHINGTON, DC 20545
ATTN FRANK C. LEGLER

OAK RIDGE NATIONAL LABORATORY
CENTRAL RES LIBRARY, BLDG 4500N, RM 175
P. O. BOX X
OAK RIDGE, TN 37830
ATTN E. HOWARD

DEPT OF HEW
PUBLIC HEALTH SERVICE
NATIONAL INSTITUTE OF HEALTH
BLDG 13, RM 3W-13
BETHESDA, MD 20014
ATTN C. J. MCCARTHY

DEPARTMENT OF COMMERCE
NATIONAL BUREAU OF STANDARDS
WASHINGTON, DC 20234
ATTN DR. JAMES SCHOOLEY, CHIEF,
TEMPERATURE SECTION
ATTN DR. T. NEGAS, MATERIALS DIVISION

DEPARTMENT OF COMMERCE
BUREAU OF EAST-WEST TRADE
OFFICE OF EXPORT ADMINISTRATION
WASHINGTON, DC 20230
ATTN WALTER J. RUSNACK

SCIENTIFIC LIBRARY
US PATENT OFFICE
WASHINGTON, DC 20231
ATTN MRS. CURETON

NASA AMES RESEARCH CENTER
MOFFETT FIELD, CA 94035
ATTN MS 244-13, DEAN CHISEL

NASA LANGLEY RESEARCH CENTER
HAMPTON, VA 23665
ATTN MS 494, H. D. GARNER
ATTN MS 494, R. R. HELLBAUM
ATTN MS 185, TECHNICAL LIBRARY

NASA LEWIS RESEARCH CENTER
21000 BROOKPARK ROAD
CLEVELAND, OH 44135
ATTN VERNON D. GEBBEN

NASA SCIENTIFIC & TECH INFO FACILITY
P. O. BOX 8657
BALTIMORE/WASHINGTON INTERNATIONAL
AIRPORT, MD 21240
ATTN ACQUISITIONS BRANCH

UNIVERSITY OF ALABAMA
CIVIL & MINERAL ENGINEERING DEPT.
P. O. BOX 1468
UNIVERSITY, AL 35486
ATTN DR. HAROLD R. HENRY

UNIVERSITY OF ARKANSAS
TECHNOLOGY CAMPUS
P. O. BOX 3017
LITTLE ROCK, AR 72203
ATTN PAUL C. MCLEOD

UNIVERSITY OF ARKANSAS
MECHANICAL ENGINEERING
FAYETTEVILLE, AR 72701
ATTN JACK H. COLE, ASSOC PROF

CARNEGIE-MELLON UNIVERSITY
SCHENLEY PARK
PITTSBURGH, PA 15213
ATTN PROF W. T. ROULEAU, MECH ENGR DEPT

CASE WESTERN RESERVE UNIVERSITY
UNIVERSITY CIRCLE
CLEVELAND, OH 44106
ATTN PROF P. A. ORNER
ATTN PROF B. HORTON

THE CITY COLLEGE OF THE CITY
UNIVERSITY OF NY
DEPT OF MECH ENGR
139th ST. AT CONVENT AVE
NEW YORK, NY 10031
ATTN PROF L. JIJI
ATTN PROF G. LOWEN

CLEVELAND STATE UNIVERSITY
FENN COLLEGE OF ENGINEERING
CLEVELAND, OH 44115
ATTN PROF R. COMPARIN

DUKE UNIVERSITY
COLLEGE OF ENGINEERING
DURHAM, NC 27706
ATTN C. M. HARMAN

ENGINEERING SOCIETIES LIBRARY
345 EAST 47TH STREET
NEW YORK, NY 10017
ATTN HOWARD GORDON
ATTN ACQUISITIONS DEPARTMENT

FRANKLIN INSTITUTE OF THE STATE
OF PENNSYLVANIA
20TH STREET & PARKWAY
PHILADELPHIA, PA 19103
ATTN KA-CHEUNG TSUI, ELEC ENGR DIV
ATTN C. A. BELSTERLING

HUGHES HELICOPTERS
DIVISION OF SUMMA CORPORATION
CENTINELA & TEALE STREETS
CULVER CITY, CA 90230
ATTN LIBRARY 2/T2124

IIT RESEARCH INSTITUTE
10 WEST 35th STREET
CHICAGO, IL 60616
ATTN DR. K. E. MCKEE

JOHNS HOPKINS UNIVERSITY
APPLIED PHYSICS LABORATORIES
LAUREL, MD 20810
ATTN MR. MAYNARD HILL
ATTN MR. THOMAS RANKIN
ATTN MR. JOSEPH WALL

LEHIGH UNIVERSITY
DEPARTMENT OF MECHANICAL ENGINEERING
BETHLEHEM, PA 18015
ATTN PROF FORBES T. BROWN

LINDA HALL LIBRARY
5109 CHERRY STREET
KANSAS CITY, MO 64110
ATTN DOCUMENTS DIVISION

MASSACHUSETTS INSTITUTE OF TECHNOLOGY
77 MASSACHUSETTS AVENUE
CAMBRIDGE, MA 02139
ATTN ENGINEERING TECHNICAL REPORTS,
RM 10-408
ATTN DAVID WORMLEY, MECH ENGR DEPT,
RM 3-146

MICHIGAN TECHNOLOGICAL UNIVERSITY
LIBRARY, DOCUMENTS DIVISION
HOUGHTON, MI 49931
ATTN J. HAWTHORNE

UNIVERSITY OF MISSISSIPPI
201 CARRIER HALL, DEPT OF MECH ENGR
UNIVERSITY, MS 38677
ATTN DR. JOHN A. FOX

MISSISSIPPI STATE UNIVERSITY
DRAWER ME
STATE COLLEGE, MS 39672
ATTN DR. C. J. BELL, MECH ENG DEPT

UNIVERSITY OF NEBRASKA LIBRARIES
ACQUISITIONS DEPT, SERIALS SECTION
LINCOLN, NE 68508

UNIVERSITY OF NEW HAMPSHIRE
MECH ENGR DEPT, KINGSBURY HALL
DURHAM, NH 03824
ATTN PROF CHARLES TAFT (3 COPIES)

DEPARTMENT OF MECHANICAL ENGINEERING
NEWARK COLLEGE OF ENGINEERING
323 HIGH STREET
NEWARK, NJ 07102
ATTN DR. R. Y. CHEN

OHIO STATE UNIVERSITY LIBRARIES
SERIAL DIVISION, MAIN LIBRARY
1858 NEIL AVENUE
COLUMBUS, OH 43210

OKLAHOMA STATE UNIVERSITY
SCHOOL OF MECH & AEROSPACE ENGR.
STILLWATER, OK 74074
ATTN PROF KARL N. REID

MIAMI UNIVERSITY
DEPT OF ENG TECH
SCHOOL OF APPLIED SCIENCE
OXFORD, OH 45056
ATTN PROF S. B. FRIEDMAN

PENNSYLVANIA STATE UNIVERSITY
215 MECHANICAL ENGINEERING BUILDING
UNIVERSITY PARK, PA 16802
ATTN DR. J. L. SHEARER

PENNSYLVANIA STATE UNIVERSITY
ENGINEERING LIBRARY
201 HAMMOND BLDG
UNIVERSITY PARK, PA 16802
ATTN M. BENNETT, ENGINEERING LIBRARIAN

PURDUE UNIVERSITY
SCHOOL OF MECHANICAL ENGINEERING
LAFAYETTE, IN 47907
ATTN PROF. VICTOR W. GOLDSCHMIDT
ATTN PROF. ALAN T. MCDONALD

ROCK VALLEY COLLEGE
3301 NORTH MULFORD ROAD
ROCKFORD, IL 61101
ATTN KEN BARTON

RUTGERS UNIVERSITY
LIBRARY OF SCIENCE & MEDICINE
NEW BRUNSWICK, NJ 08903
ATTN GOVERNMENT DOCUMENTS DEPT
MS. SANDRA R. LIVINGSTON

SYRACUSE UNIVERSITY
DEPT OF MECH & AEROSPACE ENGINEERING
139 E. A. LINK HALL
SYRACUSE, NY 13210
ATTN PROFESSOR D. S. DOSANJH

UNIVERSITY OF TENNESSEE
DEPT OF MECHANICAL ENGINEERING
KNOXVILLE, TN 37916
ATTN PROF G. V. SMITH

UNIVERSITY OF TEXAS AT AUSTIN
DEPT OF MECHANICAL ENGINEERING
AUSTIN, TX 78712
ATTN DR. A. J. HEALEY

THE UNIVERSITY OF TEXAS AT ARLINGTON
MECHANICAL ENGINEERING DEPARTMENT
ARLINGTON, TX 76019
ATTN DR. ROBERT L. WOODS

TULANE UNIVERSITY
DEPT OF MECHANICAL ENGINEERING
NEW ORLEANS, LA 70118
ATTN H. F. HRUBECKY

UNION COLLEGE
MECHANICAL ENGINEERING
SCHENECTADY, NY 12308
ATTN ASSOC PROF W. C. AUBREY
MECH ENGR DEPT, STEINMETZ HALL

VIRGINIA POLYTECHNIC INSTITUTE OF STATE UNIV
MECHANICAL ENGINEERING DEPARTMENT
BLACKSBURG, VA 24061
ATTN PROF H. MOSES

WASHINGTON UNIVERSITY
SCHOOL OF ENGINEERING
P. O. BOX 1185
ST. LOUIS, MO 63130
ATTN W. M. SWANSON

WEST VIRGINIA UNIVERSITY
MECHANICAL ENGINEERING DEPARTMENT
MORGANTOWN, WV 26505
ATTN DR. RICHARD A. BAJURA

WICHITA STATE UNIVERSITY
WICHITA, KS 67208
ATTN DEPT AERO ENGR, E. J. RODGERS

UNIVERSITY OF WISCONSIN
MECHANICAL ENGINEERING DEPARTMENT
1513 UNIVERSITY AVENUE
MADISON, WI 53706
ATTN FEDERAL REPORTS CENTER
ATTN NORMAN H. BEACHLEY, DIR,
DESIGN ENGINEERING LABORATORIES

WORCESTER POLYTECHNIC INSTITUTE
WORCESTER, MA 01609
ATTN GEORGE C. GORDON LIBRARY (TR)
ATTN TECHNICAL REPORTS

AIRESEARCH
P. O. BOX 5217
402 SOUTH 36th STREET
PHOENIX, AZ 85034
ATTN DAVID SCHAFFER
ATTN TREVOR SUTTON
ATTN TOM TIPPETTS

AVCO SYSTEMS DIVISION
201 LOWELL STREET
WILMINGTON, MA 01887
ATTN W. K. CLARK
ATTN R. LIMPAECHER (2 COPIES)

BELL HELICOPTER COMPANY
P. O. BOX 482
FORTWORTH, TX 76101
ATTN MR. R. D. YEARY

BENDIX CORPORATION
ELECTRODYNAMICS DIVISION
11600 SHERMAN WAY
N. HOLLYWOOD, CA 90605
ATTN MR. D. COOPER

BENDIX CORPORATION
RESEARCH LABORATORIES DIV.
BENDIX CENTER
SOUTHFIELD, MI 48075
ATTN C. J. AHERN

BOEING COMPANY, THE
P. O. BOX 3707
SEATTLE, WA 98124
ATTN HENRIK STRAUB

BOWLES FLUIDICS CORPORATION
9347 FRASER AVENUE
SILVER SPRING, MD 20910
ATTN VICE PRES./ENGR.

DR. RONALD BOWLES
2105 SONDRA COURT
SILVER SPRING, MD 20904

CHAMBERLAIN MANUFACTURING CORP
EAST 4TH ESTHER STS
WATERLOO, IA 50705
ATTN W. WESTERMAN

CONTINENTAL CAN COMPANY
TECH CENTER
1350 W. 76TH STREET
CHICAGO, IL 60620
ATTN P. A. BAUER

DISTRIBUTION (Cont'd)

CORDIS CORPORATION
P. O. BOX 428
MIAMI, FL 33137
ATTN STEPHEN F. VADAS, K-2

CORNING GLASS WORKS
FLUIDIC PRODUCTS
HOUGHTON PARK, B-2
CORNING, NY 14830
ATTN R. H. BELLMAN

CHRYSLER CORPORATION
P.O. BOX 118
CIMS-418-33-22
DETROIT, MI 48231
ATTN MR. L. GAU

JOHN DEERE PRODUCT ENGINEERING CENTER
WATERLOO, IA 50704
ATTN V. S. KUMAR

EMX ENGINEERING, INC
BOX 216 - 216 LITTLE FALLS RD
CEDAR GROVE, NJ 07009
ATTN ANTHONY P. CORRADO, PRESIDENT

FLUIDICS QUARTERLY
P. O. BOX 2989
STANFORD, CA 94305
ATTN D. H. TARUMOTO

GENERAL ELECTRIC COMPANY
SPACE/RESD DIVISIONS
P. O. BOX 8555
PHILADELPHIA, PA 19101
ATTN MGR LIBRARIES, LARRY CHASEN

GENERAL MOTORS CORPORATION
DELCO ELECTRONICS DIV
MANFRED G. WRIGHT
NEW COMMERCIAL PRODUCTS
P. O. BOX 1104
KOKOMO, IN 46901
ATTN R. E. SPARKS

GRUMMAN AEROSPACE CORPORATION
TECHNICAL INFORMATION CENTER
SOUTH OYSTER BAY ROAD
BETHPAGE, L. I., NY 11714
ATTN C. W. TURNER, DOCUMENTS
LIBRARIAN

HAMILTON STANDARD
DIVISION OF UNITED AIRCRAFT CORPORATION
WINDSOR LOCKS, CT 06096
ATTN MR. PHILIP BARNES

HONEYWELL, INC.
1625 ZARTHAN AVE
MINNEAPOLIS, MI 55413
ATTN J. HEDEEN

HUGHES AIRCRAFT CO
MAIL STOP 6/D131
CULVER CITY, CA 90230
ATTN WILLIAM GRIFFIN

JOHNSON CONTROLS, INC
507 E. MICHIGAN
MILWAUKEE, WI 53201
ATTN WARREN A. LEDERMAN

MOORE PRODUCTS COMPANY
SPRING HOUSE, PA 19477
ATTN MR. R. ADAMS

MARTIN MARIETTA CORPORATION
AEROSPACE DIVISION
P. O. BOX 5837
ORLANDO, FL 32805
ATTN R. K. BRODERSON, MP 326
ATTN VITO O. BRAVO, MP 326

MCDONNELL AIRCRAFT COMPANY
GUIDANCE AND CONTROL MECHANICS DIVISION
ST. LOUIS, MO 63166
ATTN MR. LOYAL GUENTHER

NATIONAL FLUID POWER ASSOCIATION
3333 NORTH MAYFAIR ROAD
MILWAUKEE, WI 53222
ATTN JOHN R. LUEKE
DIR OF TECH SERVICES

PLESSEY AEROSPACE LTD
1700 OLD MEADOW ROAD
MCLEAN, VA 22102
ATTN A. ROSENBERG

RICHARD WHITE & ASSOCIATES
ELECTRO/MECHANICAL ENGINEERS
77 PELHAM ISLE ROAD
SUDSBURY, MA 01776
ATTN RICHARD P. WHITE

ROCKWELL INTERNATIONAL CORPORATION
COLUMBUS AIRCRAFT DIVISION, P. O. BOX 1259
4300 E. 5TH AVENUE
COLUMBUS, OH 43216
ATTN MR. MARVIN SCHWEIGER

SANDIA CORPORATION
KIRTLAND AFB, EAST
ALBUQUERQUE, NM 87115
ATTN WILLIAM R. LEUENBERGER, DIV 2323

STEIN ENGINEERING SERVICES, INC
5602 E. MONTEROSA
PHOENIX, AZ 85018

TIMEX
WATERBURY, CT 06720
ATTN ERIK HERZLICH

DISTRIBUTION (Cont'd)

TRITEC, INC
P.O. BOX 56
COLUMBIA, MD 21045
ATTN L. SIERACKI

UNITED TECHNOLOGIES RESEARCH CENTER
400 MAIN STREET
E. HARTFORD, CT 06108
ATTN R. E. OLSON, MGR FLUID
DYNAMICS LABORATORY

US ARMY ELECTRONICS RESEARCH
& DEVELOPMENT COMMAND
ATTN TECHNICAL DIRECTOR, DRDEL-CT
ATTN MANION, F. M., (2 COPIES)

HARRY DIAMOND LABORATORIES
ATTN 00100, COMMANDER/TECH DIR/TSO
ATTN CHIEF, DIV 10000
ATTN CHIEF, DIV 20000
ATTN CHIEF, DIV 30000
ATTN CHIEF, DIV 40000
ATTN RECORD COPY, 81200
ATTN HDL LIBRARY, (3 COPIES) 81100
ATTN HDL LIBRARY, (WOODBRIDGE) 81100
ATTN TECHNICAL REPORTS BRANCH, 81300
ATTN CHAIRMAN, EDITORIAL COMMITTEE
ATTN CORRIGAN, J., 00240
ATTN CHIEF, 13000
ATTN CHIEF, 13400 (10 COPIES)
ATTN DRZEWIECKI, T., 13400 (10 COPIES)
ATTN COX, L. S., 00210
ATTN LANHAM, C., 00210
ATTN MON, G., 13400
ATTN DEADWYLER, R., 13400
ATTN GOTO, J., 13400
ATTN TENNEY, S., 13400
ATTN TODA, K., 13400
ATTN JOYCE, J., 13400
ATTN POPE, G. E., 00210
ATTN LANHAM, C., 00210
ATTN LOKERSON, D., 15100 (4 COPIES)
ATTN GLEASON, T., 15400 (2 COPIES)
ATTN PHILLIPPI, R. M., 13400